The future of engineered timber dry joints

A comparative analysis of the efficacy of timber dry joints in embodied carbon reduction

R.D.H. Post

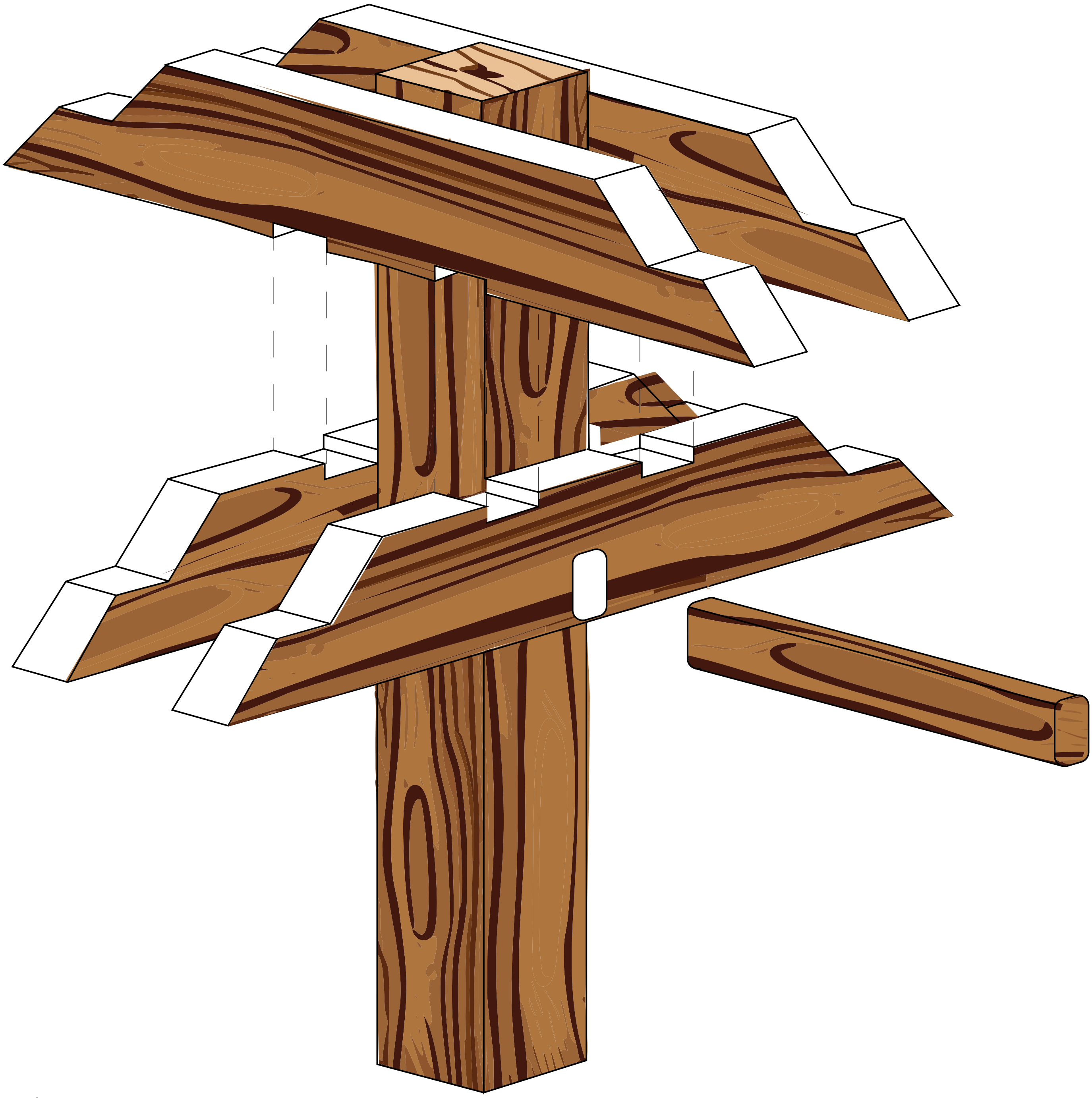

TU Delft Delft University of Technology

The future of engineered timber dry joints

A comparative analysis of the efficacy of timber dry joints
in embodied carbon reduction

Thesis Report

by

R.D.H. Post

To obtain the degree

Master of Science
in Building Engineering

Faculty of Architecture and the Built Environment
Delft University of Technology
to be defended publicly on June 26, 2024

Graduation committee:

Prof. dr. M. Overend
Dr.ing. M. Bilow
Dr. A.J. Oxenaar

Preface

This master thesis concludes my studies at the Delft University of Technology, fulfilling the requirements of my Master of Science in Architecture, Urbanism and Building Sciences, specializing in Building Technology.

I would like to express my sincere appreciation to my primary mentor, Prof. Dr. M. Overend, for useful guidance throughout the progression of my thesis and contributions to structural design. Additionally, I thank my secondary mentor, Dr. Ing. M. Bilow, for expertise in wood and woodworking techniques.

I am thankful for the guidance and expertise provided by both mentors throughout this process. Their knowledge has been valuable in shaping my research. I am especially grateful for their feedback and suggestions during our progress meetings, which have been motivating and enlightening. I always got a lot of new energy after those meetings to dive deeper into the topic, and setting a clear direction of further research.

Bob Post
Delft, June 2024

Abstract

Building construction accounts for roughly 36% of global energy consumption and emits about 39% of CO_2 from energy use [9]. Consequently, there is a growing push to adopt sustainable construction methods and utilize materials with low embodied energy [10]. As buildings stand as major contributors to CO_2 emissions, the focus is shifting towards timber as a building material choice. Timber is renewable, stores carbon, and boasts low embodied carbon from production [11]. However, while high-rise timber frames represent a significant step in integrating timber at a larger scale, their connections often rely on steel, contributing to increased embodied carbon.

This thesis explores the resurgence of interest in wood-to-wood connections as a response to sustainability imperatives in modern construction. It examines the historical significance of timber joinery, the current state of sustainable construction, and the potential of engineered timber products in reducing carbon emissions. Furthermore, the thesis investigates modern innovations in timber connections, focusing on the development of ductile and eco-friendly alternatives to steel fasteners. Through theoretical frameworks, experimental studies, and structural validations, this research aims to understand the impact of implementing timber dry joints on the embodied carbon of high-rise timber building frames.

Results reveal that while timber dry joints offer potential in reducing embodied carbon, their effectiveness varies. While they can reduce the need for steel fasteners, their impact on lowering embodied carbon is limited. Conversely, the integration of continuous beams and multiple-span floor systems proves to significantly reduce embodied carbon in timber building frames.

Overall, the findings underscore the importance of holistic approaches in optimizing timber building frames for sustainability, highlighting the potential of innovative design strategies in achieving carbon reduction goals.

Key words

Timber dry joints, rotational embedment, rotational stiffness, timber building frames, sustainability, novel connections

Table of contents

List of graphs

List of tables

List of symbols

A	Area
a	Distance from centre of rotation to edge of material
$a(\theta)$	Moment arm at rotation angle
a_f	Moment arm for friction
B_d	Beam depth
b	Beam width
B_w	Beam width
β	Rotation angle
C_d	Column depth
d	Depth
Δ	Embedment depth
Δ_y	Yield embedment depth
Δ_{max}	Maximum deflection
Δ_{rigid}	Rigidly connected beam deflection
$\Delta_{semi-rigid}$	Semi-rigidly connected beam deflection
δ	Displacement
e	Natural logarithm
ε	Strain
ε_y	Yield strain
E	Materials Youngs modulus
E_0	Youngs modulus of timber parallel to grain
E_{90}	Youngs modulus of timber perpendicular to grain
$E(\theta)$	Youngs modulus at rotation angle
$f_{h,1,d}$	Design value of embedment strength
h	Beam height
I	Moment of inertia / second moment of area
k_0	Characteristic splitting strength of wood parallel to grain
k_{90}	Characteristic splitting strength of wood perpendicular to grain
K_1	Elastic stiffness
K_2	Plastic stiffness
l	Beam length
L	Beam length
L_c	Elastic embedment length of continuous beam end
L_e	Elastic embedment length of short beam end
$L_{p,e}$	Plastic embedment length of short beam end
$L_p(\theta)$	Plastic embedment length
$L_{p,c}$	Plastic embedment length of continuous beam end
M_{max}	Maximum occurring moment
M_{sr}	Moment of semi-rigid connection
M_{Rigid}	Moment of rigid connection
$M(\theta)$	Moment at rotation angle
$M_{el}(\theta)$	Moment at elastic region at rotation angle
$M_{pl}(\theta)$	Moment at plastic region at rotation angle
N	Normal force
$N(\theta)$	Force at rotation angle
μ	Connection rigidity factor

PR_{90}	Plastic stiffness reduction factor for compression perpendicular to grain
q	Uniformly distributed load
R_d	Force applied
σ	Stress
t	Thickness
(θ)	Rotation angle
θ_y	Yield rotation angle
θ_{pin}	Rotation angle of pinned connection
V	Volume
$V(\theta)$	Volume at rotation angle
$V_{d,el}(\theta)$	Direct embedment volume in elastic region
$V_{e,el}$	Short beam end embedment volume in elastic region
$V_{c,el}$	Continuous beam end embedment volume in elastic region
$V_{d,pl}(\theta)$	Direct embedment volume in plastic region
$V_{e,pl}(\theta)$	Short beam end embedment volume in plastic region
$V_{c,pl}(\theta)$	Continuous beam end embedment volume in plastic region
w	Beam width
W_E	Mechanical work
W_I	Dissipated energy
x	Point of interest in length
x_1	First point of contraflexure
x_2	Second point of contraflexure
Z_0	Original depth
$Z_0(\theta)$	Original depth at rotation angle

01

Introduction

Introduction

Wood has been a key material throughout history and across cultures. With the emergence of civilization came the cutting and shaping of wood, from the felling of trees to building structures [1]. For centuries carpenters across developing civilizations refined the practice of shaping wood into timber structural elements with interconnecting parts to build countless structures [2]. From the natural evolution of standardization, distinct regional carpentry styles arose through trial and error. This enabled craftsmen to create better structures. Local artisans inherited and refined skills and knowledge across generations. This trove of understanding in materials, tools, and techniques resulted in buildings that endured for centuries. However, much of this technical expertise has vanished with the craftspeople who possessed it. Presently, only a few carpenters focus on wood-to-wood connections [2].

As civilization progressed and expanded its capabilities to work with materials, the resulting market pressures led to a demand for more cost-effective technology. This drive ushered in the era of metal fasteners, which eventually decreased the need for highly skilled tradespeople almost to the point of non-existence. Similarly, timber, once a prevalent building material in China, saw reduced usage due to resource depletion. Consequently, this decline led to a decreased demand for expertise in traditional timber construction and engineering [3]. In today's building codes, there is an abundance of information on bolted or adhesive connections, while carpentry joints receive limited to no coverage. As a result, the majority of contemporary joints rely on steel fasteners and brackets for construction. As the construction sector faces growing pressure to meet higher sustainability standards, the imperative to utilize eco-friendly materials as a response to climate change has sparked a renewed fascination with wood-to-wood connections [4]. In the early 21st century, the pursuit of creating both environmentally friendly and visually appealing buildings has led to a rise in timber structures, reigniting interest in innovative adaptations of traditional techniques [5].

In many situations experienced by architects and engineers, there is a need for the provision of a corrosion resistant timber structure [6]. To address these challenges, adhesive connections have been utilised. Despite offering corrosion resistance and improved fire safety performance [7], these bonded connections necessitate precise off-site fabrication under controlled conditions. Consequently, their size is constrained due to transport limitations, and they exhibit limited capacity perpendicular to the grain. Furthermore, their non-demountable nature presents a significant drawback in contemporary structures [8]. In addition to these shortcomings of adhesive and steel connections, and the growing need for better alternatives, their CO_2 emissions fall short of the purely timber counterparts. With changes in technology and demands for sustainability, the idea of reintroducing wooden joints into modern construction is increasingly appealing [2]. In the context of structural connections, this term "Wooden or traditional joints" refers to wood-wood connections that are linked together by geometries that can provide interlocking and friction necessary to transfer loads between elements while maintaining rigidity.

1.1 Sustainability

Building construction accounts for roughly 36% of global energy consumption and emits about 39% of CO_2 from energy use [9]. Consequently, there is a growing push to adopt sustainable construction methods and utilize materials with low embodied energy [10]. As buildings stand as major contributors to CO_2 emissions, the focus is shifting towards timber as a building material choice. Timber is renewable, stores carbon, and boasts low embodied carbon from production [11]. Engineered timber products like plywood, cross-laminated timber (CLT), laminated veneer lumber (LVL), and glue laminate (glulam) are increasingly preferred for tall modern buildings aiming for sustainability objectives. They offer increased strength and design flexibility compared to traditional sawn timber, while still retaining carbon-storing properties. Although the Mass Timber building movement, featuring large engineered timber structures, began in the 1990s, there has been a global surge in the late 2010s [12]. A study examining the potential impact of replacing concrete with engineered timber suggested a notable decrease in greenhouse gas emissions, ranging from 34% to 84% [13].

A life cycle analysis of tall Mass Timber structures highlighted a substantial decrease in greenhouse gas emissions, estimating an overall reduction of about 69.5% by transitioning from concrete to engineered timber [14].Yet, a drawback emerges in the increased embodied energy and CO_2 resulting from the extensive transformation of natural timber into engineered timber [15]. Often, the comparison between stored carbon and embodied carbon in products remains less apparent. An additional sustainable approach involves replacing metal fasteners with interlocking wood-wood connections. The production of steel involves mining and fabrication, both processes consuming large amounts of energy. Comparatively, the embodied energy from primary production of cut Sitka spruce ranges around 10.5–11.6 MJ/kg, while structural grade steel utilizes more than twice that amount [16]. In a proposal by Feng (2020), the integration of wood Nuki beams with Nuki joints serves as an alternative to timber beams with metal joist hangers and steel beams with steel connectors in modern construction, presenting a substantial reduction in embodied CO_2 emissions [4]. (see Fig. 1).

1.2 Timber joinery in history

There are countless ways to connect wooden structural elements together in buildings, bridges, structures and furniture using interlocking shapes. While wood-wood connections share commonalities, historical structures worldwide showcase hundreds of distinct carpentry joint types [17]. Despite large cultural differences, European and East Asian building challenges have not been tackled fundamentally different [18]. Four main categories of joints can be found in van Nimwegen et al. (2023) consisting of: (A) Mortise tenon joint (Classic western timber framing mortise tenon), (B) Notched joint (Western roof truss single step joint), (C) Lap joint (Dovetailed corner joint), and (D) Scarf Joint. (See Fig. 2)

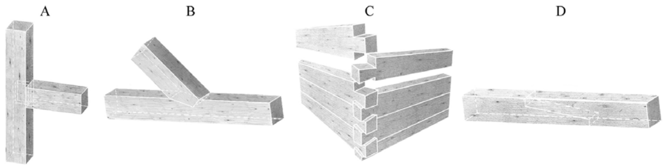

Fig. 2. Four examples of common joint types [2].

The remaining part of this thesis will focus on examining the connections between beams and columns (Fig. 2A). Consequently, the other three types will not be further addressed. The connection between beams and columns, specifically the type shown above, employs the mortise and tenon joint. Mortise and tenon connections are most used in post to beam and roof structure connections, among others. In fact, mortise and tenon joints are one of the most common connections in historic carpentry, and are characterized by interlocking joint that connects two or more elements in a "L" or "T" shape configuration [19]. This joint functions similar to a key in a hole, where the key piece (tenon) slots into the hole (mortise). While a mortise and tenon can take on square, rectangular, or round shapes, it might also incorporate a tapered design. For instance, adopting shapes like a goose neck, dovetail, or partial dovetail enhances interlocking capabilities, addressing potential

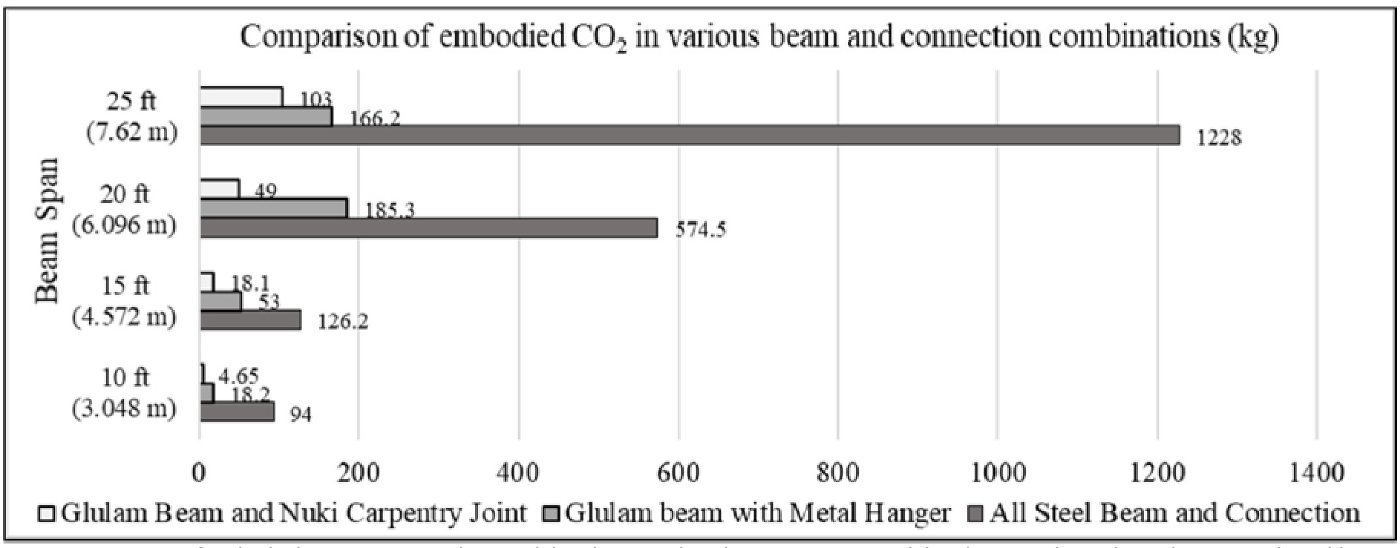

Fig. 1. Comparison of embodied CO2 emissions data in glulam beam with Nuki carpentry joint, glulam beam and metal joist hanger, and steel beam and steel connection [4].

structural limitations of a simple mortise and tenon in transferring tensile forces or resisting rotation. Given the extensive historical use of the mortise and tenon in connection design, current research heavily focuses on evaluating different iterations of this joint. Recent research has delved into numerous variations of this joint, particularly emphasizing the utilization of dowel-type fasteners. By creating a hole through which the two elements can be connected, this approach effectively mitigates a common issue with these joints: pull-out. This however, created a new failure mode where pegs closer to the end of the beam exhibited brittle and catastrophic failures [20]. Most mortise and tenon joints, when accurately fabricated show semi-rigid properties, or an intermediate between an idealized moment connection and an idealized pin connection [21].

1.3 Modern engineered carpentry joints

Most of the modern research in timber connections are about practical ways to connect elements in Mass Timber buildings, making use of steel connectors. These types of connectors have therefore been excluded from this study. Only a small portion of current research is focused on modern wood-wood or all-wood connections. Chang et al. introduced a novel method for connecting all-wood beams using oak pins and plywood slot-in plates within heavy timber structures [22]. Similarly, Kromoser et al. integrated robotics into the production of trusses, employing timber structural elements and all-wood joints made of plywood and wooden pegs to achieve sustainability goals while keeping expenses low [23]. Despite industry standards favouring rectangular sections with pinned plate connections, very recent innovations are stepping away from conventions and are reinventing wood-wood connections to economically address sustainability. Extensive research has been performed on shell-like structures, including various case studies on shell structures made from plates with interlocking edges [24][25][26].

Rezaei Rad et al. describes a modern experimental study exploring the tensile performance of plate elements utilizing through-tenon joints to secure LVL. This investigation demonstrates the potential application of plate elements with steel-free connections [24]. Nguyen et al. introduced a framework incorporating both the design and structural analysis of free-form structures constructed from plates featuring interlocking wood-wood through-tenons along their edges to create a shell structure [25]. Building upon this, Rezaei Rad et al. Utilised the same case study structure as Nguyen et al. , automating a design framework for digitally fabricated free-form shell structures. These structures utilize plates connected through interlocking through-tenons [26]. Furthermore, Gamerro et al. conducted a comparative analysis between Eurocode 5 design equations and experimental tests on compressive and shear connections. They evaluated three variations of digitally fabricated modern mortise tenons crafted from five distinct engineered timber products. These connections were designed for prefabricated residential structural elements, featuring joints specifically configured for in-plane loading [27]. This area diverts from traditional architectural carpentry connections, ushering in contemporary aspects of wood-wood joinery within architecture and engineering. Although the Eurocode has not yet established comprehensive guidelines for calculating wood-wood connections, the initial evidence of their possibilities has been demonstrated. Through the utilization of joinery solvers and CNC machines alongside current manufacturing methods, the qualities of ancient craftsmanship are being revived in a digital form. Additionally, the superior sizing capabilities of engineered wood compared to traditional standard wood offer opportunities to reintroduce old carpentry style joints in modern wood engineering.

1.4 Ductile connections

"A structure is a constructed assembly of joints, separated by members" stated McLain [28]. This could not be any more true for timber structures, where connections greatly influence the overall structural performance. Connections are often intended to act as potential ductile elements, contributing significantly to overall ductility and energy dissipation in case of overloading [29]., and allow for safe load paths when design tolerances are exceeded. Ductility is related to the possibility to attain large displacements without losing too much strength in a material specimen/joint/member/structure loaded in displacement control. Without reinforcement, this can hardly be obtained for timber members in bending, tension and/or shear. However, large displacements are possible for timber loaded in compression parallel and perpendicular (bearing) to the grain, for example carpentry joints with timber loaded in compression at an angle to the grain [30]. Since timber fails brittle in tension, plasticization in bending requires a tensile strength considerably higher than the compression strength. For clear wood this is certainly the case. However, for structural timber containing defects, this is only the case when the defects are located mainly in the compression zone. Consequently, it is possible to construct statically indeterminate systems made of brittle timber members connected with ductile connections that behave in a ductile fashion. The brittle members, however, must be designed to account for the over-strength relative to the strength of the ductile connections, ensuring that the ductile failure mechanism occurs before the brittle members fail [30]. This approach provides sufficient warning through noticeable deformations before catastrophic brittle failure happens, thereby making the ductile element the "weakest link" [29][31][32].

1.5 Rigid and braced framing systems

When constructing structural frames, two primary types stand out: (i) Rigid frames, made from beams and columns with rigid connections, providing stiffness. These frames, often used in steel or reinforced concrete buildings, excel in resisting lateral deformations. One advantage lies in their force diagrams, revealing lower mid-span bending moments and deflections, allowing for smaller beam heights. (ii) Braced frames or pin joint frames offer enhanced efficiency against lateral loads such as wind or earthquakes. However, due to their pinned connections, the resulting bending moment in the beam increases, necessitating larger beam heights. Yet, the absence of a moment in the connection facilitates simpler connections.

1.6 Potential gains and possibilities

Considering the information gathered on the behaviour of ancient carpentry joints, the imperative for a more carbon-neutral/positive built environment, and the potential offered by steel- and adhesive-free connections, there is an opportunity for further optimizing overall framing structures. This includes ensuring wood-wood connections exhibit ductile behaviour, enhancing safety margins. This thesis's primary question emerges:

What is the effect of implementing timber dry joints on the embodied carbon of high-rise timber building frames?

This could result in structural beams requiring less height, thus providing additional floor height or accommodating smaller levels. This not only reduces the weight of an already lightweight timber building but also augments its sustainability, lowering embodied carbon. Moreover, with the advent of new machining techniques and the shaping possibilities afforded by engineered wood, there is enhanced potential to engineer precisely crafted connections. These advancements in machining technology, coupled with the versatile shaping capabilities of engineered wood, offer opportunities to optimize structural integrity while fostering innovative design possibilities within wooden constructions.

1.7 Thesis outline

Throughout the remainder of this thesis, the central inquiry—What is the effect of implementing timber dry joints on the embodied carbon of high-rise timber building frames?—will be explored.
To address this, the following sub-questions will be answered:

(I) How to construct a timber dry joint with a rotational stiffness matching the stiffness of a rigid connection?

(II) How effective are timber dry joints in reducing beam height?

(III) How can timber dry joints exhibit ductile behaviour?

Supporting the research of these questions, this thesis will comprise a structured approach including a theoretical framework establishing the theoretical ground for the research. Additionally, it will include the experimental design of a timber dry joint, a theoretical assessment and a structural validation. Thereafter, a different construction approach is explored, seeking simpler yet effective solutions for reducing the embodied carbon of timber building systems. Including the second set of sub questions:

(IV) What is the effect of utilizing a continuous beam on the embodied carbon?

(V) What is the effect of utilizing different floor span systems on the embodied carbon?
(VI) What is the effect of timber dry joints on the embodied carbon compared to steel fasteners?

Ultimately, the thesis will conclude by presenting the findings and offering further recommendations based on the outcomes.

02

Theoretical framework

Theoretical Framework

This chapter contains an overview of existing literature, laying down a theoretical groundwork that explores the structural characteristics of wood and its behaviour in connections.
As a significant part of this thesis focuses on enhancing the rotational stiffness of an all-wood joint, the theoretical framework primarily centres on this objective. *Existing literature* is categorized into three sections: Analytical methods utilising wood mechanics to calculate rotational stiffness; Structural frame mechanics to understand the potential advantages of the increased rotational stiffness; The resulting effect on material use.

2.1 Fibre directions

Due to woods anisotropic characteristics its strength varies in different fibre directions, E_0 represents the Young's modulus parallel to the grain and E_{90} represents the materials Young's modulus perpendicular to the grain. If both of these values are known, the Young's modulus at any angle of the grain can be calculated using Hankinsons equation [33]:

$$E(\beta) = \frac{E_0 * E_{90}}{E_0 \cos^n \beta + E_{90} \sin^n \beta} \tag{1}$$

Where $\mathrm{n} = 2$ [33].

2.2.1 Embedment theory

The stiffness of a joint will be largely determined by the partial compression of the wood elements against each other. To calculate this compression the principle of mechanical work[1] is Utilised. In a single axis load path the following Nuki can be used:

$$W_E = R_d \delta \tag{2}$$

Where W_E is the work in Joules, R_d is the force applied in Newtons and δ is the displacement in mm. The energy dissipated by the timber in compression is then:

$$W_I = f_{h,1,d} t\ d\ \delta \tag{3}$$

Where W_I is the dissipated energy in the wood, $f_{h,1,d}$ is the design value of the embedding strength, t is the thickness of the material, d is the diameter of the piercing object and δ is the displacement. As this Nuki is meant for dowelled fasteners and not rectangular pierced trough beams, the Nuki can be rewritten as eq. 4, As the diameter is taken as a projected object and curvature is not taking into account.

$$W_I = f_{h,1,d} t\ w\ \delta \tag{4}$$

Where w is the width of the pierced trough object.

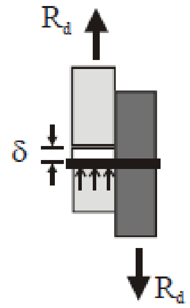

Fig. 3. Failure mode *a* of dowelled wood connection [34].

Apart from these direct failure mechanisms, rotational failure can also occur as shown in Fig. 4.

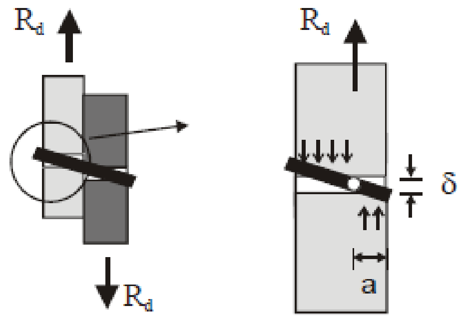

Fig. 4. Failure mode *c* of dowelled wood connection [34].

In this failure mode the dissipated energy is:

$$W_I = f_{h,1,d} w\ a \left(\frac{\delta}{2}\right) + f_{h,1,d} w(t-a) \left(\frac{\delta}{2}\right)\left(\frac{t-a}{2}\right) \tag{5}$$

Where a is the distance from the centre of rotation to the edge of the material. These procedures help determine the resistance in various scenarios related to these principles, like examining connections between different graded materials. Considering Hankinsons equation, eq. 1, the embedding strength is a systems property, owing to its correlation with the timber's grain angle and can be found in the EC5 as:

$$f_{h,a,k} = \frac{f_{h,0,k}}{k_{90} \sin^2 a + cos^2 a} \tag{6}$$

Where K_0 is the characteristic strength against splitting parallel to the grain, K_{90} is the characteristic strength against splitting perpendicular to the grain and a is the angle of the load applied.

1 In physics, work is the energy transferred to or from an object via the application of force along a displacement.

2.2.2 Additional indirect embedment

To later capture the rotational stiffness of the connection, in addition to the direct embedment of two (or more) wooden elements against each other, the additional indirect embedment stress is experienced by the exposed portion just outside of the direct contact region. If the embedment is acting in the z-direction, the additional indirect stress occurs in both the x- and y-directions of the element. This indirect embedment shapes can be approximated as an exponential function. "Having an exponential-shaped additional length" [35]. (Fig. 5)

The indirect embedment takes the form of:

$$f(x) = \delta e^{-ax} \tag{7}$$

Where δ represents the linear compression depth at the end of the direct triangular embedment and a represents the decay coefficient. Which is taken to be $1.5/Z_0$, where Z_0 is the initial depth of the compressed element. Roche [36] provides further documentation on literature investigating decay coefficients in section 2.2. When combining the direct $\delta(x)$ and indirect embedment $f(x)$ along the x- and y-axes, the compressed volume V can be obtained. The compressed volume can be used to calculate the energy needed for the compression and thus the resultant contact force N using the structural-mechanics' basics of stress and strain:

$$N = \sigma A = \varepsilon E A = (\varepsilon A)E = \frac{V}{Z_0}E \tag{8}$$

Where $V = \delta_h A$, δ_h is the transverse displacement and A is the area of the directly loaded surface. In case of the indirect embedment, the volume is calculated by integrating the area of the deformed section.

$$A(x_i) = \int f(x)dx = \frac{\delta}{a_e}(1 - e^{-a_e x_i}) \tag{9}$$

Transforming the equation as a function of rotation angle θ:

$$N(\theta) = \frac{V(\theta)}{Z_0(\theta)}E(\theta) \tag{10}$$

At yield depth $\delta_y = \varepsilon_y Z_0$ the wood has entered its plastic region, where ε_y represents the yield strain, for embedment depth beyond δ_y, A reduced E must be used. As forces are not applied perpendicular to the object pressing into the wood, moment forces can occur. When the contact forces N and associated lever arms a are determined, the moment M can be calculated. For elastic and plastic regions the relationship can be stated as:

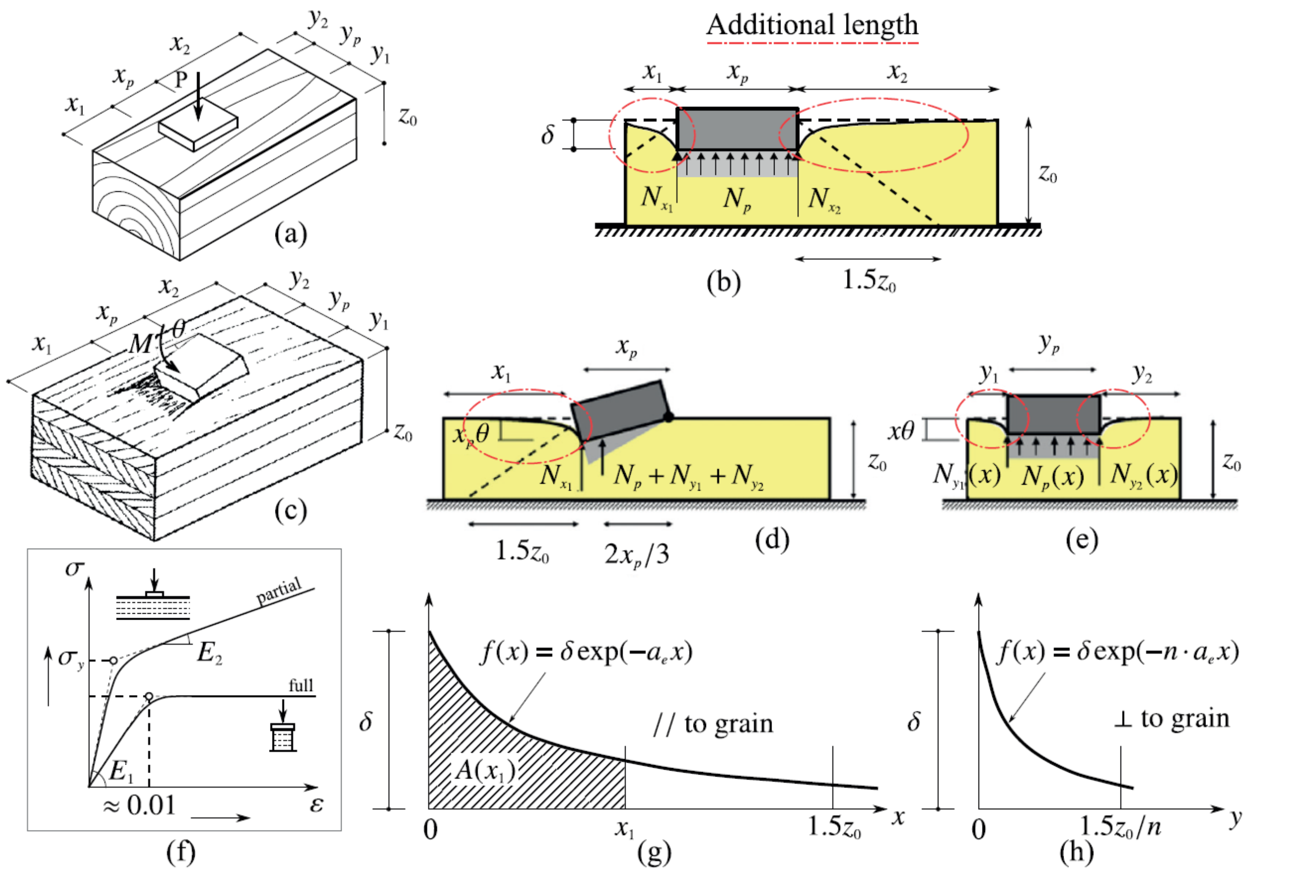

Fig. 5. (a) Equal embedment model, (b) Section of equal embedment model with x_1 as ended beam end, and x_2 as continuous beam end taken to be $1.5Z_0$, (c) Rotational embedment model, (d) Section on x axis of rotational embedment model, (e) Section on y axis of rotational embedment model, (f) Stress-strain curve of full and partial embedment showing effects of additional embedment lengths, (g) Graph of additional length's area parallel to grain, (h) Graph of additional length's area perpendicular to grain angle [35], enhanced by [36].

$$M(\theta) = \sum N_i(\theta) a_i(\theta) \qquad (11)$$

2.2.3 Rotational embedment

Due to the occurring of bending when beams are loaded, beam to column connections experience rotational forces. Expanding upon previously stated theory, rotational embedment is introduced in the connection. As the existing literature containing rotational embedment theories only provide examples using Traditional Japanese joinery, shape-dependent theory will be extracted and transformed into shape-independent fundamentals using elastoplastic material behaviour theories.

2.2.3.1 Elastic embedment.

Fig. 6 illustrates the elastic case where $\Delta<\Delta_y$, both the direct and indirect compressed area are in the elastic region, identifiable by the blue colour. Light blue indicates the direct contact and the darker tone the indirect embedment. Due to the unsymmetrical shape of the connection, there is a short beam-end and a continuous beam-end, set to be 1.5 times the height B_d of the beam to be considered continuous. To calculate the compressed volume the following combination of equations can be made:

$$V_{tot} = V_d + V_e + V_c \qquad (12)$$

Where V_{tot} is the total compressed volume and V_d is the direct compressed volume, V_e is the short beam-end and V_c is the continuous beam-end. B_w is the beam width.

$$V_{d,el}(\theta) = B_w * \frac{1}{2}\Delta(\theta) \qquad (13)$$

$$V_{e,el}(\theta) = B_w * \int_{x=0}^{L_e} f(\theta, x)dx \qquad (14)$$

Where L_e is the distance the beam end extends beyond the column. If L_e=0 then V_e=0.

$$V_{c,el}(\theta) = B_w * \int_{x=0}^{L_c} f(\theta, x)dx \qquad (15)$$

With L_c = 1.5B_d.To transform the volumes back to force, eq. 10 is used. Substituting eq. 1 in eq. 10 where $\beta = \theta$ finds the corresponding E value. Consequentially the moment arm for each moment arm needs to be calculated to determine the rotational stiffness.

$$a_{d,el}(\theta) = \frac{C_d}{2} \qquad (16)$$

The direct embedment a_d is the distance perpendicular to the associated force between the centre of rotation and the centroid of the compressed volume. This is the same for the continuous- and short beam-end:

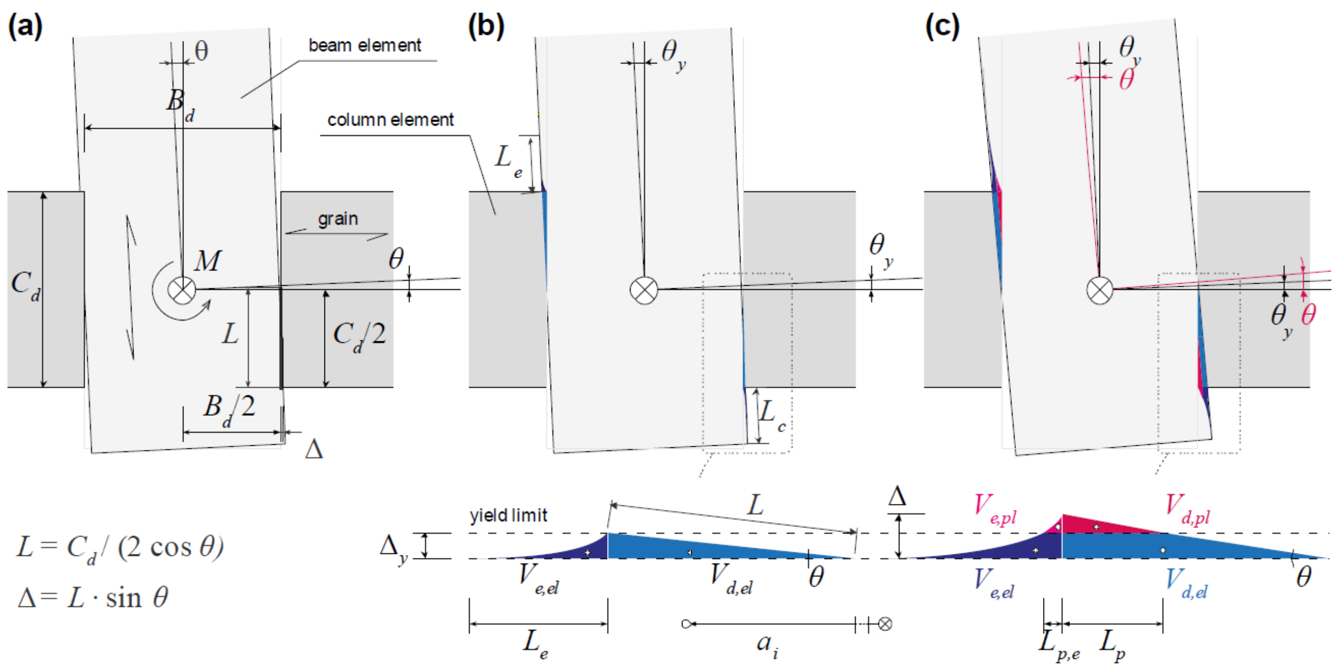

Fig. 6, Analytical model (as a cut section down the middle of the prototype width): (a) joint geometry dimensions, (b) elastically compressed volumes, and (c) compressed volumes for an elastoplastic material behaviour. Elastically compressed volumes are shown in blue tones; plastic volumes are given in magenta tones. The boxed diagrams in (b) and (c) represent the contact at the ended beam end and thus the subscripts e are used; the diagrams are analogous for the continuous beam end, where subscripts e would be replaced with subscripts c. Note that the Nuki for L has been updated since the original published study. Adapted from original illustration by collaborator Jan Brütting. By [4].

$$a_{e,el}(\theta) = \frac{C_d}{2} + \frac{1}{V_{e,el}} * \int_{x=0}^{L_e} x * f(\theta, x) dx \tag{17}$$

$$a_{c,el}(\theta) = \frac{C_d}{2} + \frac{1}{V_{c,el}} * \int_{x=0}^{L_c} x * f(\theta, x) dx \tag{18}$$

With $L_c = 1.5B_d$.

2.2.3.2 Plastic embedment.

When the wood is compressed beyond the yield strain $\Delta > \Delta_y$ it enters its plastic region, identifiable by the magenta tones in Fig. 6. These volumes needs to be calculated separately due to the different characteristics of the wood applying to these volumes. The length along the axis of the beam needs to be identified to distinguish the transition from the elastic to the plastic volume. This length can be identified by:

$$L_p(\theta) = \frac{Cd}{2} * (1 - \frac{\Delta_y}{\Delta_y}) \tag{19}$$

Additionally the length along the x-axis of the additional embedment length, at which the shape matches the yield embedment depth Δ_y can be stated as:

$$L_{p,e} = L_{p,c} = f^{-1}(\Delta_y) \tag{20}$$

The directly compressed volumes then can be defined, some volumes are split into two parts for an easier centroid calculation. Eq. 21 is describing the blue part underneath the magenta area in Fig. 6c. Eq. 22 is the connecting volume on the right side.

$$V_{d,el,1}(\theta) = B_w * \frac{1}{2}\Delta_y * (L(\theta) * \cos\theta - L_p(\theta) \tag{21}$$

$$V_{d,el,2}(\theta) = B_w * \Delta_y L_p \tag{22}$$

The direct plastic embedment volume is then:

$$V_{d,pl}(\theta) = B_w * \frac{1}{2}\big(\Delta(\theta) - \Delta_y\big) L_p(\theta) \tag{23}$$

Analogously, the volumes for the ended beam ends can be calculated:

$$V_{e,el,1} = B_w * L_{P,e}\Delta_y \tag{24}$$

$$V_{e,el,2}(\theta) = B_w * \int_{L_{p,e}}^{L_e} f(\theta, x) dx \tag{25}$$

$$V_{e,pl}(\theta) = B_w * \int_0^{L_{p,e}} f(\theta, x) - \Delta_y dx \tag{26}$$

And for the continuous beam the same procedure applies:

$$V_{c,el,1} = B_w * L_{P,e}\Delta_y \tag{27}$$

Other volumes can be calculated in the same way as eq. 24 & 25 tuned to the continuous embedment lengths. The next step consists of converting the volumes to resultant contact forces again. To do so the relationship given in eq. 10 can be used again. However, this time a bilinear material model is assumed where PR_{90} represents the factor by which the Young's modulus of the wood is reduced to obtain the Young's modulus in the plastic region. Contact force in the elastic region is defined by:

$$N_{d,el,i}(\theta) = \frac{V_{d,el,i}(\theta)}{Z(\theta)} E(\theta) \tag{30}$$

Where i represents the different obtained volumes. Contact force in the plastic region:

$$N_{d,pl}(\theta) = \frac{V_{d,pl}(\theta)}{Z(\theta)} (PR_{90} * E(\theta)) \tag{31}$$

Finally the moment arms can be determined:

$$a_{d,el,1}(\theta) = \frac{3}{2}(\frac{C_d}{2} - L_p(\theta)) \tag{32}$$

For all other volumes eq. 17 & 18 can be used when tuned to the corresponding volume.

2.3 Rotational stiffness

2.3.1 Friction

The moment carrying capacity of timber dry joints is a combination of embedment and friction. The contribution of friction is calculated using the material's static coefficient of friction. The friction force is the sum of the normal forces from direct contact between the wooden elements and can be defined as follows:

$$F_f(\theta) = \mu * \sum_{i \in d} N_i(\theta) \tag{33}$$

Where $F_f(\theta)$ is the force of friction, and μ the static friction coefficient. The associated moment arm, a_f, can be defined as:

$$a_f = B_d \tag{34}$$

Where in the case of Fig. 6 this is equivalent to the beam depth. This can be later used to determine the contribution of friction for the rotational stiffness.

2.3.2 Determining rotational stiffness

The final relationship between moment and angular displacement can be stated as:

$$M(\theta) = \sum_{i \in (d \cup e \cup c \cup f)} N_i(\theta) a_i(\theta) \tag{35}$$

Where d represents the direct contact of embedment, e represents the additional embedment along the ended beam-end, c represents the additional embedment for the continuous beam-end and f represent the friction. As the volume calculations were dependent on whether the embedment has reached it plastic state or not, there are two equations summarising and combining all previous steps explained above. 1) Where the plastic state is not reached ($\theta < \theta_y$) and 2) where the plastic state is reached ($\theta > \theta_y$). These result in the two following combination of equations. Where M_{el} is the relationship in elastic state.

$$\begin{aligned} M_{el}(\theta) = \; & 2\left(N_{d,el}(\theta)a_{d,el}(\theta)\right) \\ & + N_{e,el}(\theta) + a_{e,el}(\theta) \\ & + N_{c,el}(\theta) + a_{c,el}(\theta) \\ & + \mu N_{d,el}(\theta)a_f \end{aligned} \tag{36}$$

And where M_{pl} is the relationship in plastic state.

$$\begin{aligned} M_{el}(\theta) = \; & 2\left(N_{d,el}(\theta)a_{d,el}(\theta)\right. \\ & \left.+ N_{d,pl}(\theta)a_{d,pl}(\theta)\right) \\ & + N_{e,el,1}(\theta) + a_{e,el,1}(\theta) \\ & + N_{e,el,2}(\theta) + a_{e,el,2}(\theta) \\ & + N_{c,el,1}(\theta) + a_{c,el,1}(\theta) \\ & + N_{c,el,2}(\theta) + a_{c,el,2}(\theta) \\ & + N_{e,pl}(\theta) + a_{e,pl}(\theta) \\ & + N_{c,pl}(\theta) + a_{c,pl}(\theta) \\ & + \mu(N_{d,el}(\theta)a_f \\ & + N_{d,pl}(\theta)a_f) \end{aligned} \tag{37}$$

Where equations are defined in section 2.2. The final equation can then be written as eq. 35 where the total moment M per rad θ can be stated as:

$$M(\theta) = \begin{cases} M_{el}(\theta) & When\ \theta{<}\theta_y \\ M_{pl}(\theta) & When\ \theta{<}\theta_y \end{cases} \tag{38}$$

Due to the plastic characteristics of wood when compressed, and described in the equations above, a bilinear model was used. To find the associated rotational stiffness the following relation: ∂M/∂θ can be used to find the regression of the corresponding line segment. Depicted in Fig. 7, as K_1 and K_2 for elastic and plastic stiffness respectively.

To identify the embedment depth at the point of yielding, the materials yield strain E_y can be used. With the yield embedment depth as:

$$\Delta_y = \varepsilon_y B_d \tag{39}$$

With ε_y as the material strain value and B_d the beam depth subjected to embedment. Subsequently the yield angle can be stated as:

$$\theta_y = tan^{-1}\left(\frac{\varepsilon_y B_d}{Cd/2}\right) \tag{40}$$

With these yield limits, elastic and plastic Young's moduli can be assigned to the compressed volumes, allowing for the determination of the different rotational stiffnesses in both the elastic and plastic regions. This is demonstrated in Fig. 7 with *k1* the elastic and *k2* the plastic stiffness.

The equitations outlined in sections 2.2 and 2.3 are specifically tailored for the Nuki

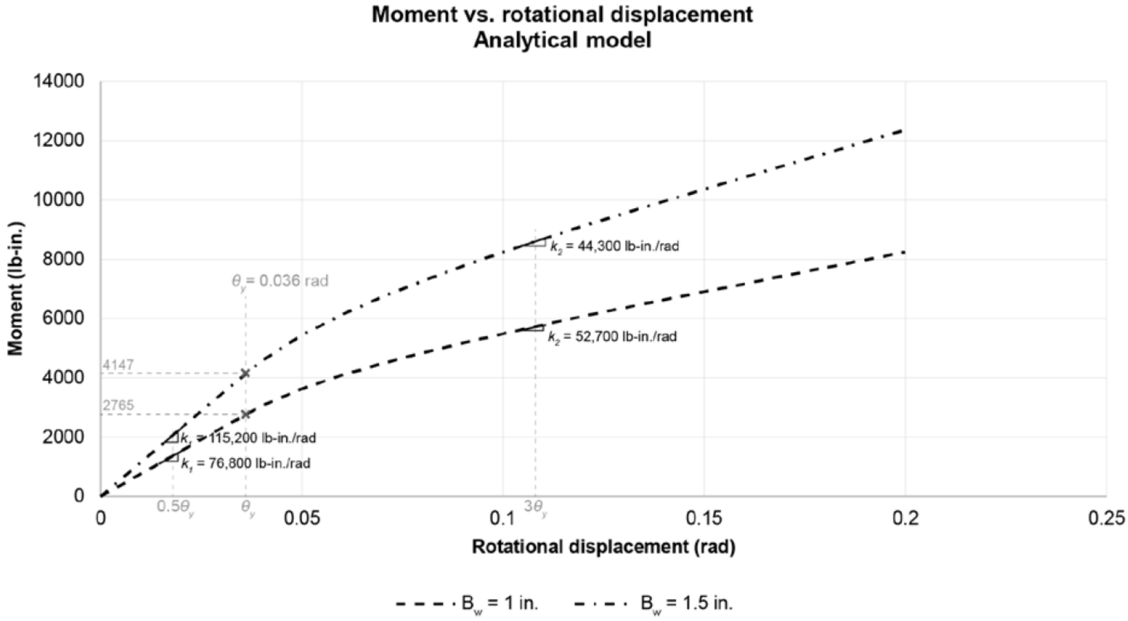

Fig. 7. Moment vs. rotational displacement showcasing different stiffness's k_1 and k_2 [37].

joint shown in Fig. 8. Nevertheless, their applicability extends to virtually any joint shape or configuration. The primary variable that may vary is the amount of contacts of direct embedment, while adjustments for additional embedment in different beam-ends may be required, dependent upon the presence or absence of a beam-end.

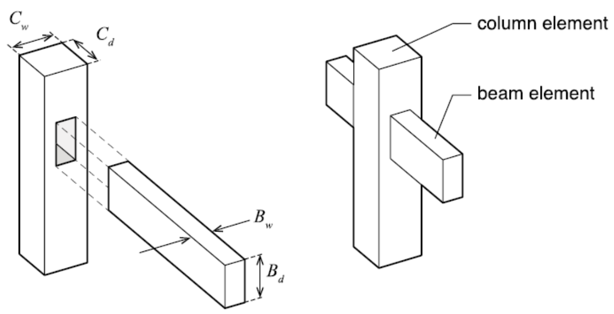

Fig. 8. Typical Nuki joint [37].

2.4 Structural behaviour of existing joints

Several joints and principles have already been tested in existing literature following previously shown calculations and physical testing. Experiments performed by Fang et al [37] show tests of the traditional Japanese mortise and tenon joint named the Nuki joint. Additional experiments were done by comparing three different interlocking wood to wood connections [21]. The experiments were executed using the same principles of theoretical prediction, numerical analysis en physical testing. In experiments performed regarding the Nuki joint [21], physical tests were performed first where after theory was calibrated searching for the right decay coefficient. Fang [37][21] was able to calibrate the results in a 20% accuracy window. All of the experiments' theoretical calculations were done using the same embedment theory from Inayama [35]. using a complementary elastoplastic Pasternak model of embedment [36]. Calculations en theoretical background were thoroughly executed in [21].

Three different joints were assessed, where T* emerged to be the most favourable option. To completely understand the behaviour of this connection all force influences were considered. Given the fact that in addition to the rotational embedment, the wood is cantilever-shaped in the interlocking connection the rotational stiffness lessened as these forces acted in series. In comparison to the Nuki Joint this T* connection performed significantly less.

With a joint rotational stiffness of 4160 Nm/rad this connection exhibits a stiffness less than halve of the Nuki joint performed by Fang [37]. This is assuming that the scaling of this compound is linear. Since the size differed slightly between experiments. The T* joint was 70% of the length of Nuki joint. Which therefore affects the moment arm. The width of both beams was the same at 3.81 cm. Fang [21] has shown with experiments that the width scaling of the beam is linear. Here, a width increase of 50% meant a force increase of 50%.

Four more geometries are tested by Moradei et al [38] joint A is located at the roof level of buildings, where beams are inserted into the column from above to form a so called

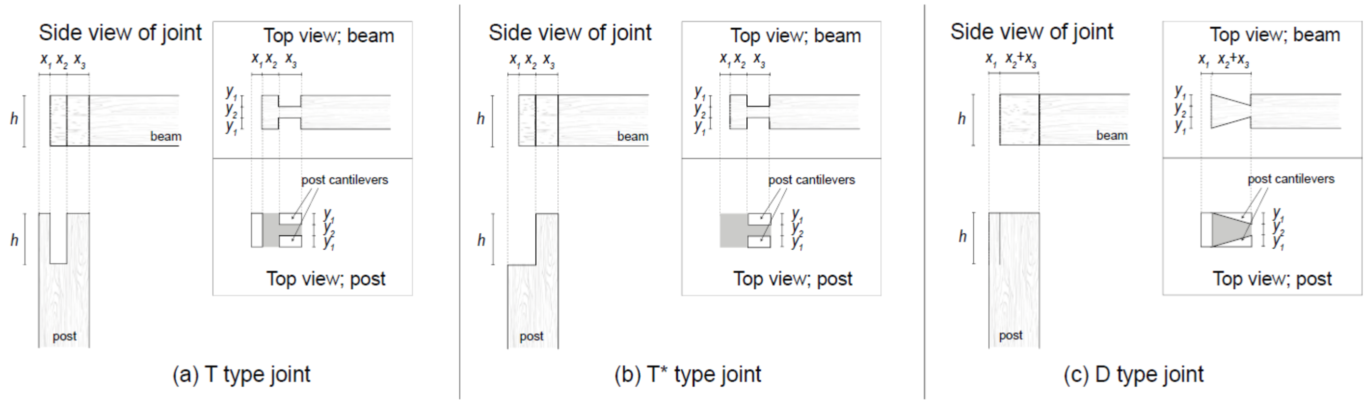

Fig. 9. Different geometries tested [21].

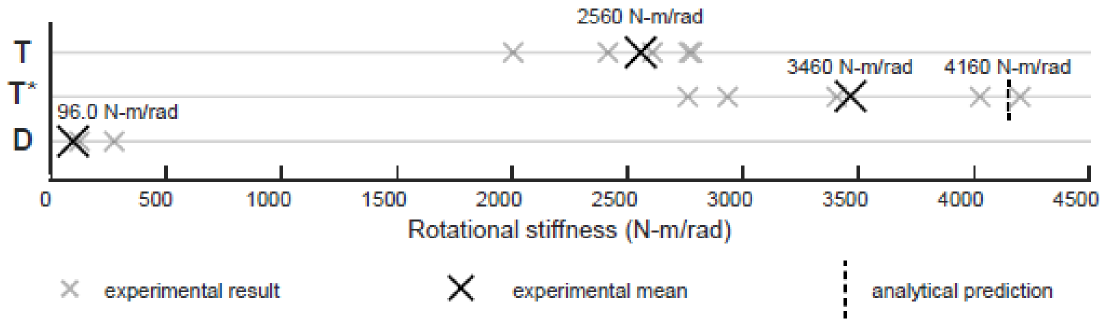

Fig. 10. Test results of the experiments performed by [21].

"bridle joint". The two beams connected at joint A are halved and create a cross lap-joint. Additionally, two typical Japanese connection details for through-type frames are examined. In Fig. 11B, a Nuki joint is shown, where a beam continuously runs through the column. Two wedges facilitate continuous contact between the column and the beam, ensuring rotational stiffness [39]. Joint C connects two beams with a long tenon passing through the column opening. The tensile connection at the beam top allows for rotational stiffness [40]. Joint C is Utilised when building dimensions exceed available beam lengths. In Europe, an equivalent connection topology is entirely unfamiliar and would necessitate the use of steel fasteners [40]. Nevertheless, rounded, CNC-cut versions of such long tenon connections between two beams are commonly used in contemporary building construction in Japan [40, 41]. The dovetail joint D illustrates the typical connection of secondary beams to girders or a column head [42]. This connection detail is widely used in Chinese, Japanese, and European timber construction. Due to variations in the sizes of the tested elements, a direct comparison between the previously demonstrated connections cannot be made. However, failure principles and comparisons among these joints are valuable for understanding their behaviour. To compare the stiffness, the bending moment is plotted against the rotation of the beams, shown in Fig. 12.

Joint B exhibits the stiffest moment-rotation behaviour, characterized by the steepest slope. This behaviour is a result of the continuity of the beam passing through the column opening without any weakening. In contrast, joint

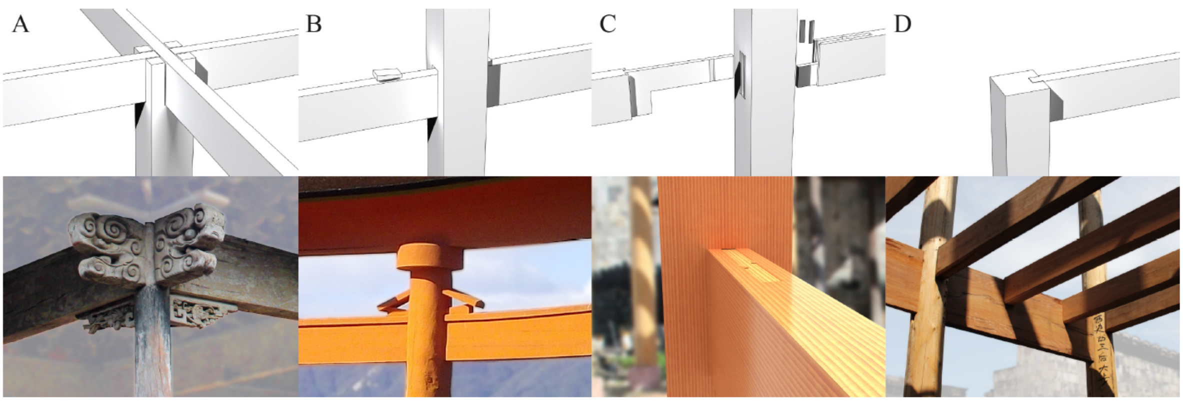

Fig. 11. Selection of commonly used Japanese joints [38].

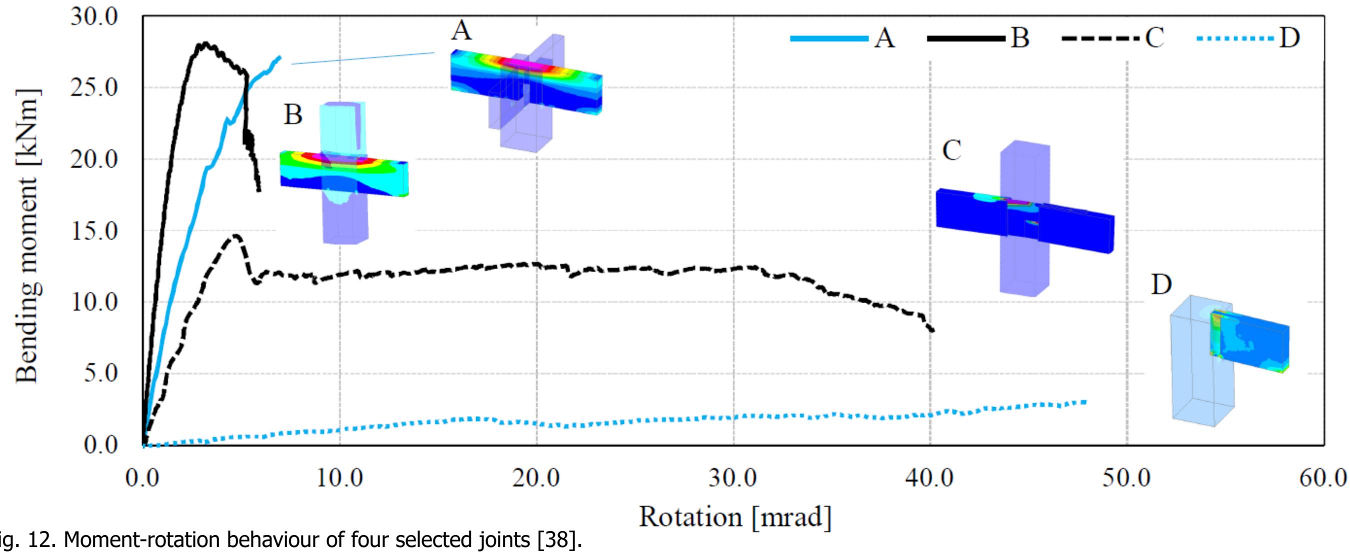

Fig. 12. Moment-rotation behaviour of four selected joints [38].

A experiences a reduction in cross-section height due to the halved lap joint, resulting in compressive forces being transmitted through the secondary beam perpendicular to its fibre direction, leading to a less stiff behaviour. The diminished cross-section of Joint A further contributes to a brittle failure, which dominates its behaviour as depicted in Fig. 12. Nonetheless, both Joints A and B demonstrate nearly equivalent ultimate bending moments. Joint C shows some initial stiffness but then opens up and displays zero stiffness upon further rotation. The dovetail Joint D exhibits a limited moment capacity and undergoes significant rotations due to the small contact area between the pieces and loading perpendicular to the grain inside the dovetail pocket, functioning as pin joint.

Concluding these observations, the stiffest geometry is achieved by leveraging the flexural rigidity of the beam without reducing its cross-sectional area. While this principle does not depend on the embedment strength of the connection but rather on the beam's rigidity, questions could arise regarding the fairness of this comparison.

2.4.2 Initial stiffness

The joints previously shown are made using either press-fitting or highly precise machining techniques. However, this presents a challenge for scaling up these principles, as press-fitting large girders at the construction site would be problematic. Building margins are an given aspect of modern construction practices. The variability of wood, influenced by changes in humidity and temperature over time, prevents precise connection fits. This poses a significant obstacle to up-scaling, as construction margins significantly impact the initial rotational stiffness of the joint. This phenomenon is illustrated by Chang et al [43]. Where the rotational stiffness of the Nuki joint with an initial gap between the beam and column is documented, mirroring the influence of building margins on joint performance.

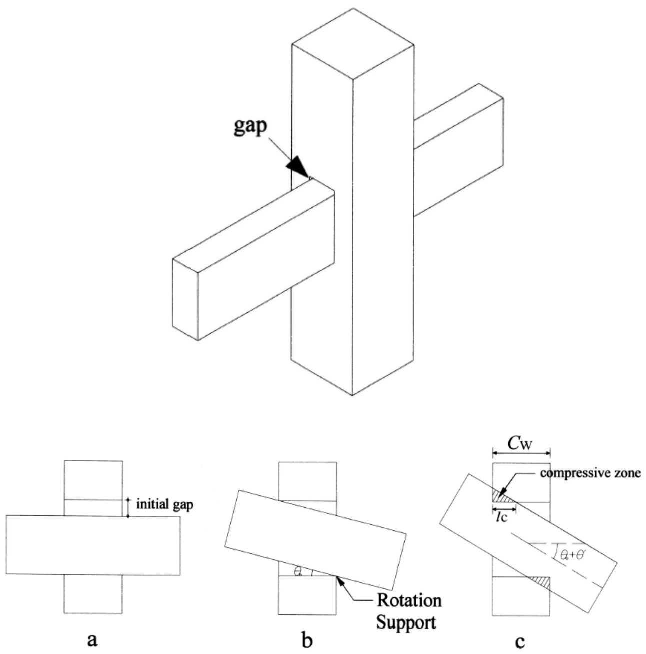

Fig. 13. Nuki joint with gap [43].

The sizing of the initial gap has a large influence on the stiffness of the connection where demonstrate the initial slip stage should be regarded as a pin connection in the early stage[43]. The size of the initial gap not only has an effect on the initial rotation but also on the overall rotational stiffness as the potential embedment volume lessens when the embedment starts at a higher initial angle as shown in Fig. 14.

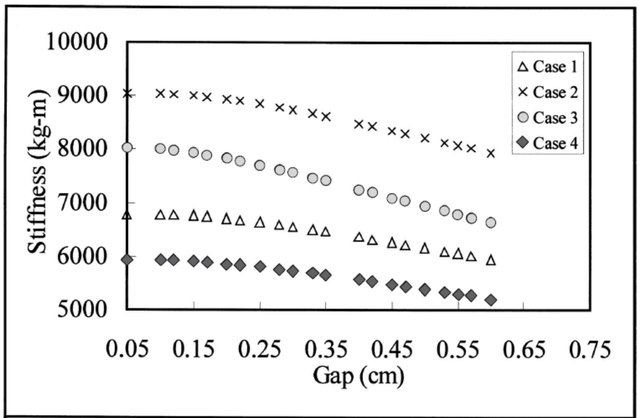

	Cw (cm)	Bw (cm)	Bd (cm)	$E_{\perp}$(kg/cm²)
Case 1	18	6	18	4000
Case 2	18	8	18	4000
Case 3	18	6	15	4000
Case 4	18	6	18	3500

Fig. 14. Effect of gap size on rotational stiffness [43].

With Cw as the column width and Bd as the beam depth an initial gap of only 3% of the beam height (6 mm) the stiffness lessens by nearly 17%. This would largely impact the performance of the joint and consequently the beam depth needed. (explained in chapter 2.5).

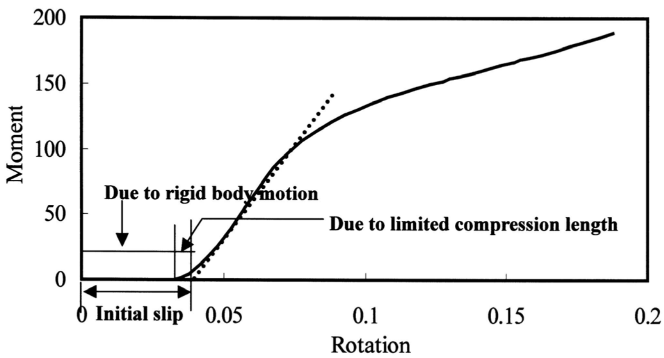

Fig. 15. Typical moment-rotation relationship of timber joint [43].

Fig. 15 illustrates a difference in behaviour between the stiffness characteristics of the in 2.4.1 showcased joint behaviour, and the more probabilistic behaviour of an all wooden Nuki joint, taking construction margins into account.

2.5 Structural-frame mechanics

When designing a structural frame, engineers typically have two main stability principles to chose from. 1) A moment frame where the connections between beams and columns are rigid and 2) a braced frame where the stability is rigid trough a core or bracing, allowing for pinned connections throughout the rest of the frame.

2.5.1 Rigid frame characteristics

Constructing a fully moment-rigid frame within traditional timber dry carpentry poses a significant challenge. Given the slip-out failure mechanics inherent in most Nuki-like connections, resisting translational forces proves difficult for such frames. Nonetheless, these moment-rigid connections offer a notable advantage: the beam depths are considerably reduced compared to a pin joint frame. Following structural principles, the maximum midspan moment experienced in a rigid beam is:

$$M_{max} = \frac{ql^2}{24} \tag{41}$$

While the maximum moment experienced by the connection is:

$$M_{max} = \frac{ql^2}{12} \tag{42}$$

Derived from these equations, it can be observed that the majority of the force is concentrated in the beam at the place of the joint, thereby accentuating the critical role of the joint in the overall design. In conventional wood-steel systems, this is addressed by utilizing numerous steel elements capable of bearing significant loads. However, given the absence of steel in a fully wooden joint, it necessitates the design to accommodate these forces, requiring additional material (wood). Consequently, this requires a larger spatial footprint to achieve a secure connection, complicating the design process.

2.5.2 Braced frame characteristics

In a braced frame, the lateral forces are absorbed by the core or bracing, resulting in the connections to be 'simply supported'. This results in the connections being unable to bear any forces other than vertical load, causing all the bending forces to be transferred onto the beam, this is seen in the following Nuki:

$$M_{max} = \frac{ql^2}{8} \tag{43}$$

Where the maximum occurring moment in the beam is: 24 / 8 = 3 times greater than that in a rigid beam. This also impacts the deflection of the beam, which, in contemporary construction standards, is the decisive factor in determining the required beam height. The relation in beam height between simply supported and rigid beams can be seen in eq. 44: midspan deflection of simply supported beam with a uniformly distributed load (UDL) and eq. 45: midspan deflection of a rigid beam with UDL:

$$\Delta_{max,pin} = \frac{5\, ql^4}{384\, EI} \tag{44}$$

$$\Delta_{max,rigid} = \frac{ql^4}{384\, EI} \tag{45}$$

A simply supported beam can also experience a midspan deflection trough a bending moment applied at both beam ends:

$$\Delta_{max} = \frac{Ml^2}{8\, EI} \tag{46}$$

The comparison of the eq. 44 & 45 indicates that the deflection of a simply supported beam is five times larger than that of a rigid beam, consequently requiring larger beam dimensions for the simply supported configuration. This occurs because the simply supported beam is able to rotate freely at its connections, hence the name "pinned" connection. This rotational freedom at the connections can be quantified using eq. 47.

$$\theta = \frac{ql^3}{24\, EI} \tag{47}$$

2.5.3 Spring supported beam characteristics

Semi-rigid connections can be conceptualized as rotational spring-supported connections, as they can be characterized by a specific rotational stiffness. This stiffness lies intermediate to that of pinned and rigid connections. The magnitude of this stiffness determines the extent to which the beam behaves as a rigid beam or a pinned beam; higher stiffness values result in behaviour closer to that of a rigid beam, whereas lower values induce characteristics more reminiscent of a pinned beam. This stiffness can be expressed as $K_1 = M / \theta$. With K_1 as the stiffness in the elastic region, M the applied moment and θ the rotation in radians.

The beam-line equation shows the relation between the rotational behaviour of a pinned beam connection and the moment that would be exerted on the connection assuming it were rigid. By locating the point where this line intersects with the stiffness curve representing the connection's behaviour, a ratio of stiffness relative to both pinned and rigid connections is found.

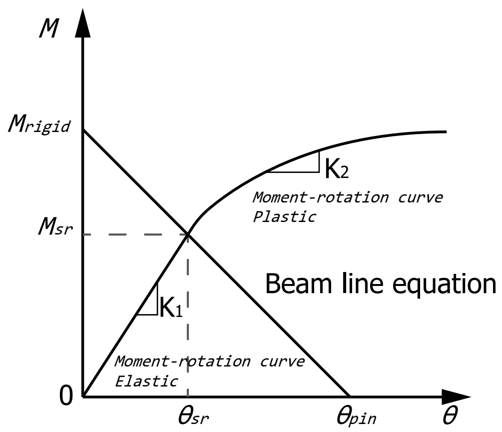

Fig. 16. Semi-rigid connection stiffness [By author].

In further detail, Wang [44]. presents the following equation. :

$$M_{sr} = \frac{M_{Rigid}}{1 + \dfrac{M_{Rigid}}{\theta_{pin} K_1}} \tag{48}$$

With M_{sr} as the moment experienced by the semi-rigid connection.

Following this equation , a dimensionless factor μ is defined to characterize the connection rigidity:

$$\mu = M_{sr} \,/\, M_{rigid} \tag{49}$$

With μ = 0 for pinned, 0 < μ < 1 for semi-rigid and with μ = 1 for a rigid connection.

The deflection of a pinned beam is shown in eq. 44, with the deflection of a rigid beam rewritten to:

$$\Delta_{rigid} = \frac{5\, ql^4}{384\, EI} - \frac{M_{rigid} l^2}{8\, EI} \tag{50}$$

The deflection of a semi-rigid beam can be stated as:

$$\Delta_{semi-rigid} = \frac{5\, ql^4}{384\, EI} - \frac{M_{sr} l^2}{8\, EI} \tag{51}$$

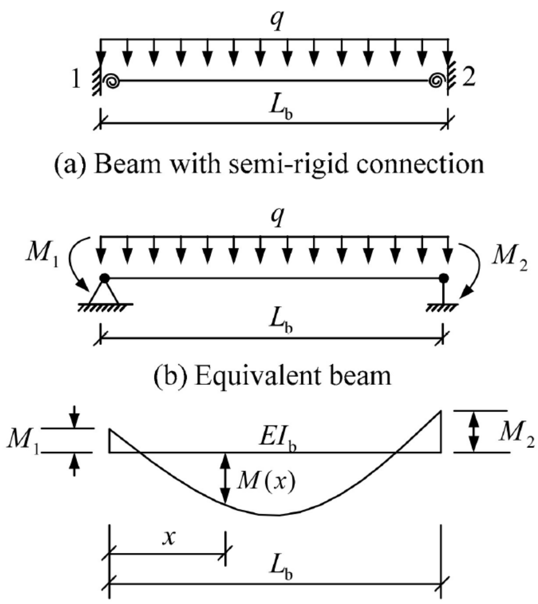

Fig. 17. Semi-rigid beam with UDL [44].

Derived from Fig. 17b, to find the maximum midspan deflection of a semi-rigid beam. The influence of a semi-rigid connection can be visualized as a pinned beam subjected to a UDL along with opposing applied bending moments at each end.

2.6 Effect of midspan deflection on overall material use

Reducing midspan deflection through the use of a rigid connection facilitates the design of beams with smaller dimensions. All deflection equations (eq. 44, 45, 46, 50, and 51) incorporate the flexural rigidity factor of the beam, denoted by EI, where the Young's modulus (E) is material-dependent and the second moment of area (I) is shape-dependent, as defined by eq. 52 for a rectangular cross-section.

$$I = \frac{bh^3}{12} \tag{52}$$

With b for beam width and h for beam height. Because the I is in the denominator (eq 44, 45, 50, 51), increasing its value will decrease the occurring deflection of the beam. Deflection is (mostly) the governing threshold when designing beams in serviceable limit state (SLS). Therefore, when the beam is stiffer than needed to satisfy these deflection limits, the needed I value decreases allowing for designing with smaller beam cross-sections.

03

Timber dry joints

Design exploration

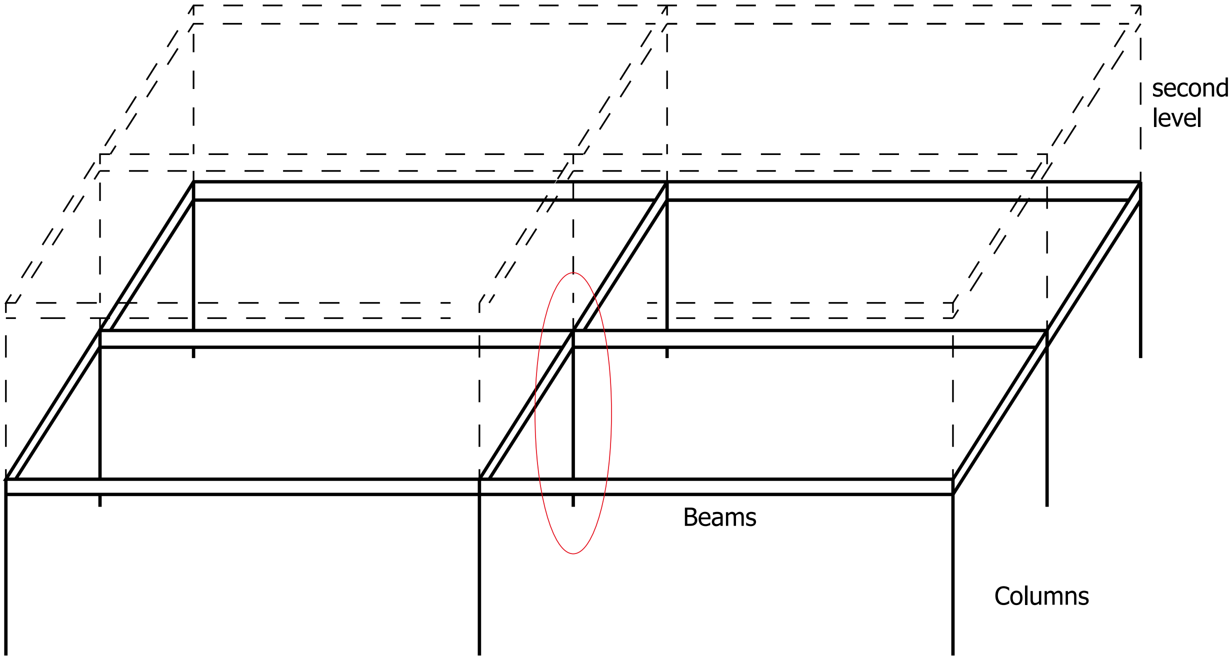

Fig. 18. Building frame principle [By author].

In this chapter multiple designs are evaluated and compared. Previous illustrations primarily showed connection principles that are not directly applicable in structural framing scenarios, typically featuring only one beam per column or unidirectional beam configurations. However, as depicted in Fig. 18, such connections are absent in structural frames. The aim of this chapter is to assess and compare the structural behaviour and material efficiency of a two-directional timber dry joint positioned at the centre of the frame, denoted by the red marking in Fig. 18. Efficiency is measured by the midspan deflection experienced by a beam connected via both pinned and rigid joints. To ascertain the effectiveness of the joint's rotational stiffness, the designed joints are compared to the Nuki joint.

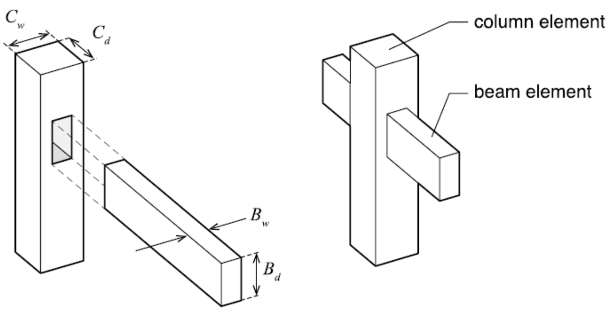

Fig. 19. Typical Nuki joint [37].

3.1 Nuki joint

The Nuki joint, already researched by Fang [37] and elaborated in section 2.2.3, serves as a benchmark. The Nuki joint showed to be the most effective design for a unidirectional connection, maximizing the column depth and showing ductile behaviour resulting in the highest rotational stiffness from the researched joints.

A limitation of the geometry of this joint is the significant cut-out area required for the beam to pass through the column. This leads to a reduction in the column's cross-sectional area, thereby weakening it. Consequently, an oversized column is necessary, as the beam's fibre direction is too weak to withstand the normal force exerted by the column.

Tuned to the new specimen size described in table 1, recalculations are made to create a direct comparison to the newly designed joints. Ensuring to have the same dimensions and strength properties between all tested connections.

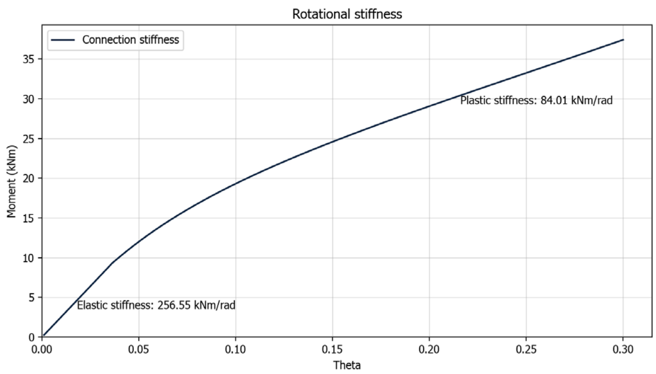

Fig. 20. Rotational stiffness of typical Nuki joint [37].

As shown in Fig. 20, the rotational stiffness curve takes the same shape as described in section 2.3, Fig. 7. This observation indicates that increasing the beam size does not impact the trajectory of the stiffness curve. The effectiveness of the joint in reducing midspan deflection is depicted in Fig. 21, where the midspan deflection is compared against the deflection of the same beam in two other scenario's; 1) a regular simply supported beam (pinned) and 2) a perfectly rigid connection.

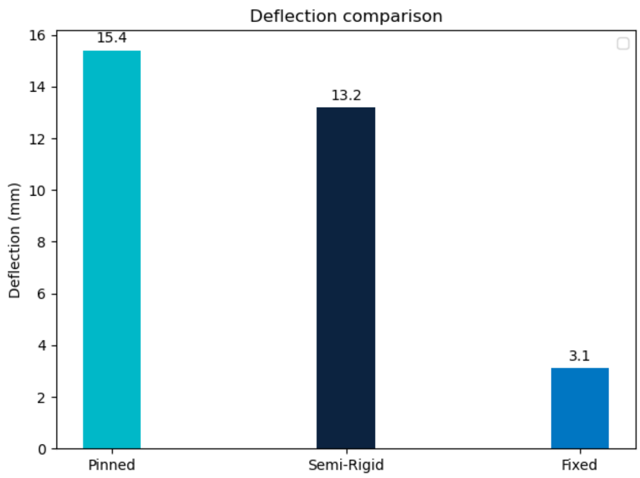

Fig. 21. Midspan deflection of beam connected by typical Nuki joint [By author].

As depicted in Fig. 21, where the Nuki joint is described as semi-rigid, the rotational stiffness generated by the connection geometry does not exhibit the anticipated effectiveness in reducing midspan deflection. As suggested by the theory in section 1.1 larger savings should be made, looking at the embodied carbon saved in the framing system. However, the midspan deflection is not the only factor influencing the emissions, the absence of steel in the connection is another large contributor to the overall reduction in emissions. Further elaboration on this point will be provided later in the discussion.

Table 1. Used material properties for all specimens [By author].

Properties	Value	Source
Mean MOE parallel to grain, E_0	13700 N/mm^2	SAMS lecture notes, EN 1 408016
Mean MOE perp. to grain, E_{90}	420 N/mm^2	SAMS lecture notes, EN 1 408016
Yield strain, ε_y	0.017	From [37]
Plastic stiffness Youngs mod. reduction factor	PR90 = 0.018	From [37]
Static coefficient of friction	$\mu = 0.2$	From [37]
Beam height	200 mm	-
Beam width	100 mm	-
Column depth	200mm	-

Fig. 22 shows the comparison in beam stiffness under three different support conditions. In the case of the beam connected by the Nuki joint, marked as semi-rigid, it initially exhibits a greater stiffness than the pinned connection. However, as it approaches its plastic embedment, the joint's resistance gradually decays, transitioning into a stiffness similar to that of a pinned beam configuration. This pattern is similarly observed in the rigid connection, where the beam initially demonstrates almost 'infinite' rigidity; yet, as the connection begins yielding, it shifts

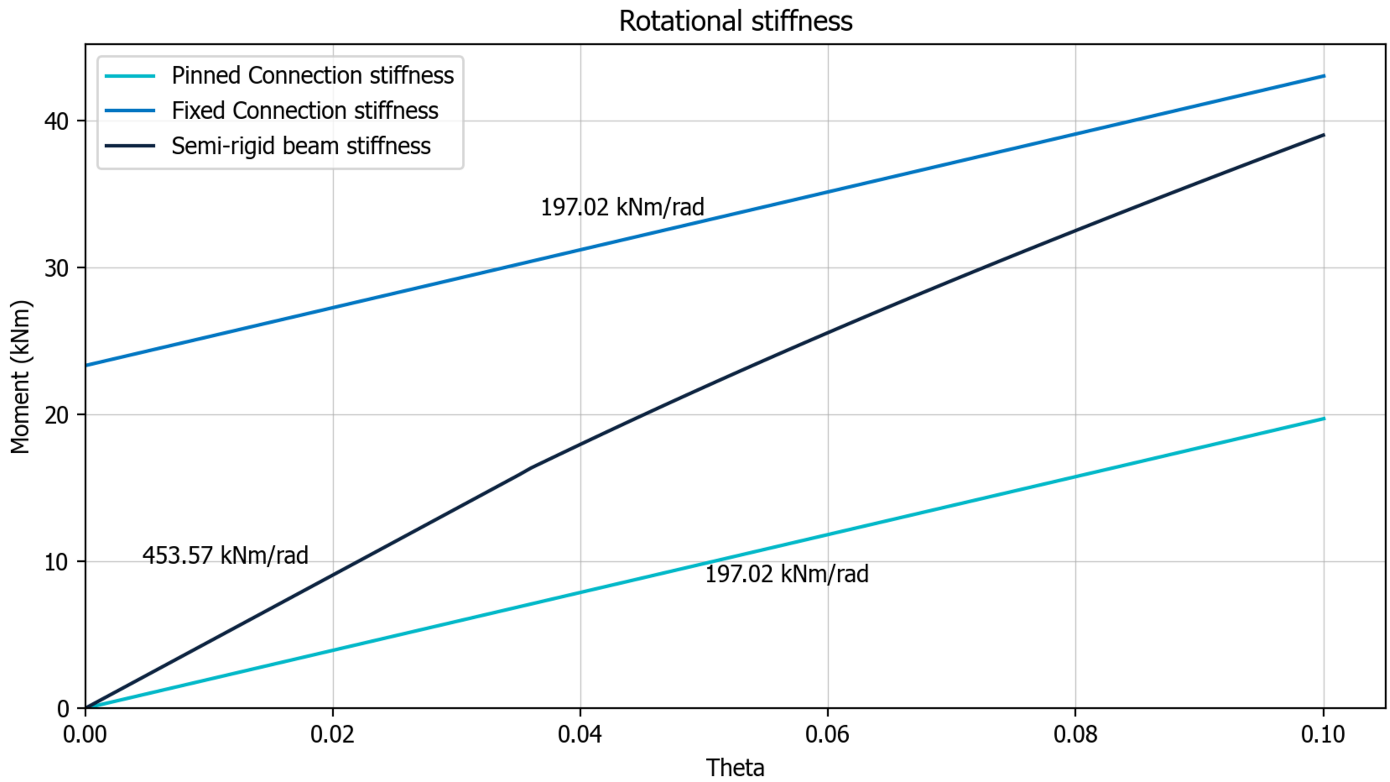

Fig. 22. Beam stiffness comparison Nuki joint [By author].

towards a pinned behaviour, relying solely on the flexural rigidity of the beam itself. Although the elastic stiffness is more than twice the stiffness of the pinned configuration, the effect on the deflection is still closely related to that of the pinned connection, leaving room for improvement and further exploration to closely match the stiffness of a rigid connection.

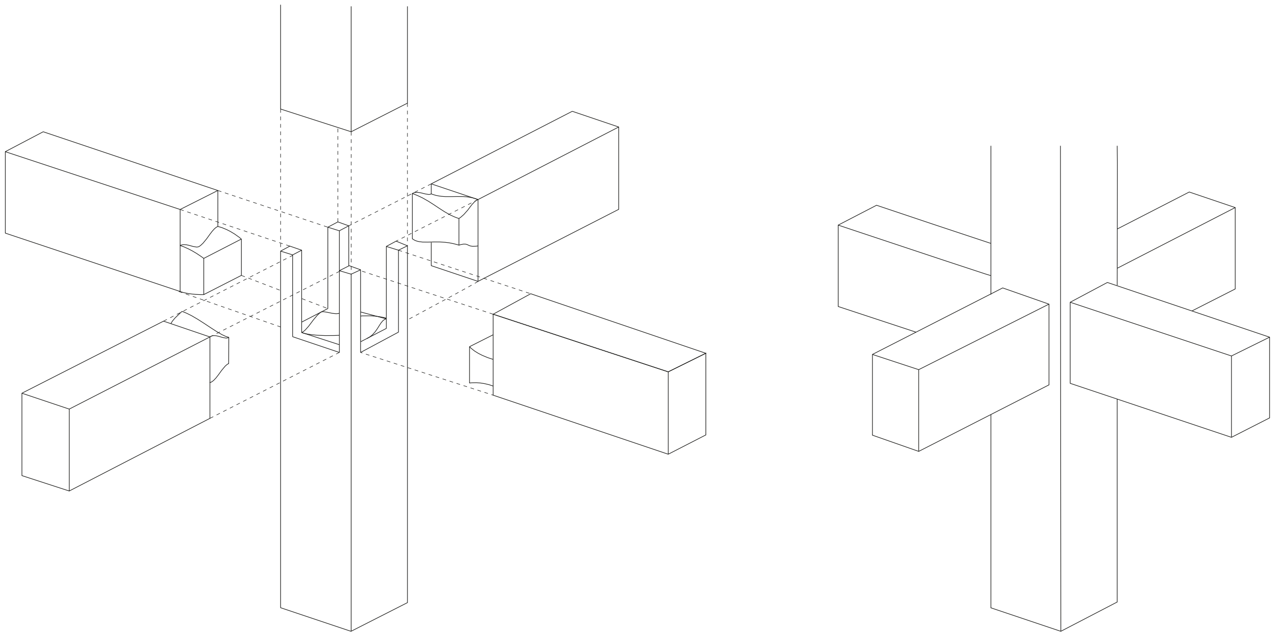

Fig. 23. Interlocking joint 1 [By author].

3.2 Interlocking joint 1

By creating an interlocking design inspired by the configuration of the interlocking glass bricks from Oikonomopoulou et al [45]. A design resistant to the pull-out failure mechanism is created. The vertically and horizontally interlocking shapes requires the beams to be inserted from above, as opposed to the sideways insert as observed in the Nuki joint. This poses a advantage in constructibility eliminating an initial gap on top of the beams causing a free rotation as described in section 2.4.2 Initial stiffness. This improvement in rotational stiffness is achieved because the column is positioned on top of the beams during construction, preventing the necessity for a construction-margin to accommodate beam insertion within the cut-out volume. However, despite the gains in rotational stiffness, the non-continuous nature of the column presents challenges in construction logistics as the beam top is fragile due to its shape, and the transmission of vertical loads is concentrated on small areas.

The wavy profile of the interlocking shape is a complex form and requires a lot of CNC-milling capacity. This intensive machining and pre-treatment needed to construct this joint raises questions regarding the cost-effectiveness and feasibility of implementing such a joint design.

Looking at the section of the joint (Fig. 24), it is notable that the effective depth is only halve that of the column depth, resulting in a reduction in embedment area and effective moment arm. Furthermore, the vertical division of the joint at its point of maximum stress imposes limitations in rotational stiffness. Although the beams placed at a 90-degree angle maintain the effective fiber directions, thereby preserving strain depth as per eq. 39, the introduction of a cantilever induces a rupture mode at point A (Fig. 24). This results in a deflection acting in series to the embedment rotation, decreasing the rotational stiffness as seen in experiments done by Fang [21]. and Fig. 9b.

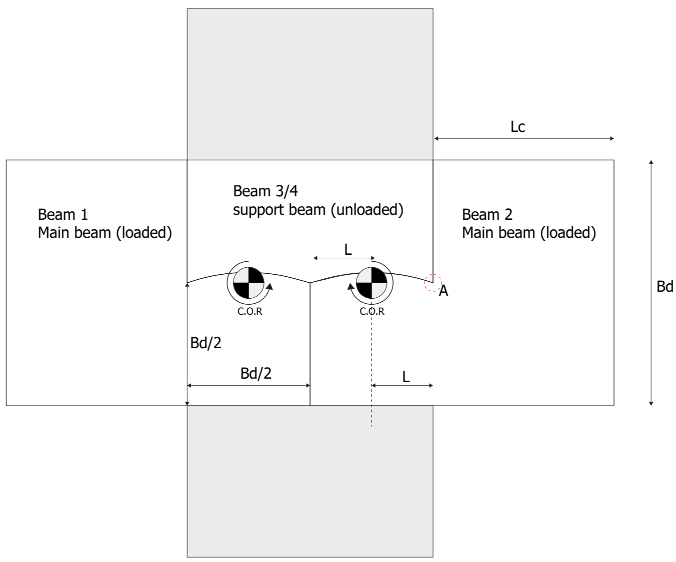

Fig. 24a. Interlocking joint 1 properties [By author].

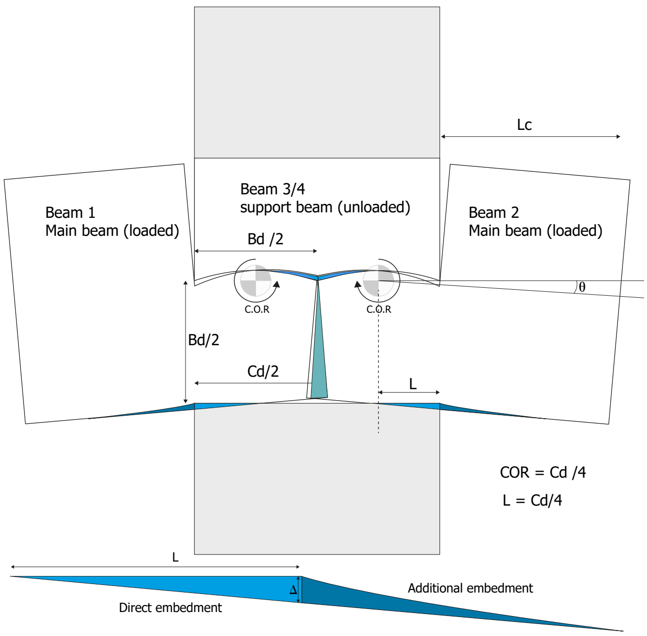

Fig. 24b. Interlocking joint 1 properties [By author].

The inserted depth $Cd/2$ and the shifted Center of Rotation ($C.O.R$) contribute to reducing the embedment length (L) to only one-fourth of the column depth (Cd). Consequently, this division results in the area of the triangle, which is the embedment area, being quartered in comparison to having an L of $Cd/2$. Additionally, with the moment arm being halved compared to the Nuki joint, the elastic stiffness is weakened by a factor of six. As seen in Fig. 25, this results in the connection behaving closely related to a pinned connection. The beam stiffness gained from the connection is barely notable, the elastic stiffness is increased by 18% where after in the plastic zone, it decreases to the same stiffness as the rigid and pinned beams' stiffness.

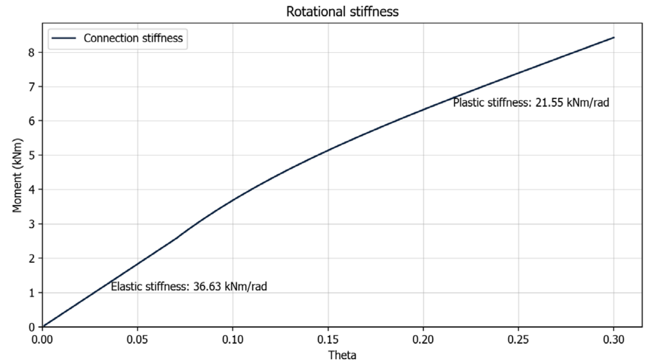

Fig. 26. Interlocking joint 1 rotational stiffness [By author].

This behaviour is also visible in the maximum midspan deflection, calculated using the equation sequence listed in section 2.5.3. and showcased in Fig. 27, where the connection is described as semi-rigid. The importance for a decrease in midspan deflection by connection stiffness, is the smaller cross section needed to satisfy deflection limits, and thus less material use, decreasing embodied carbon

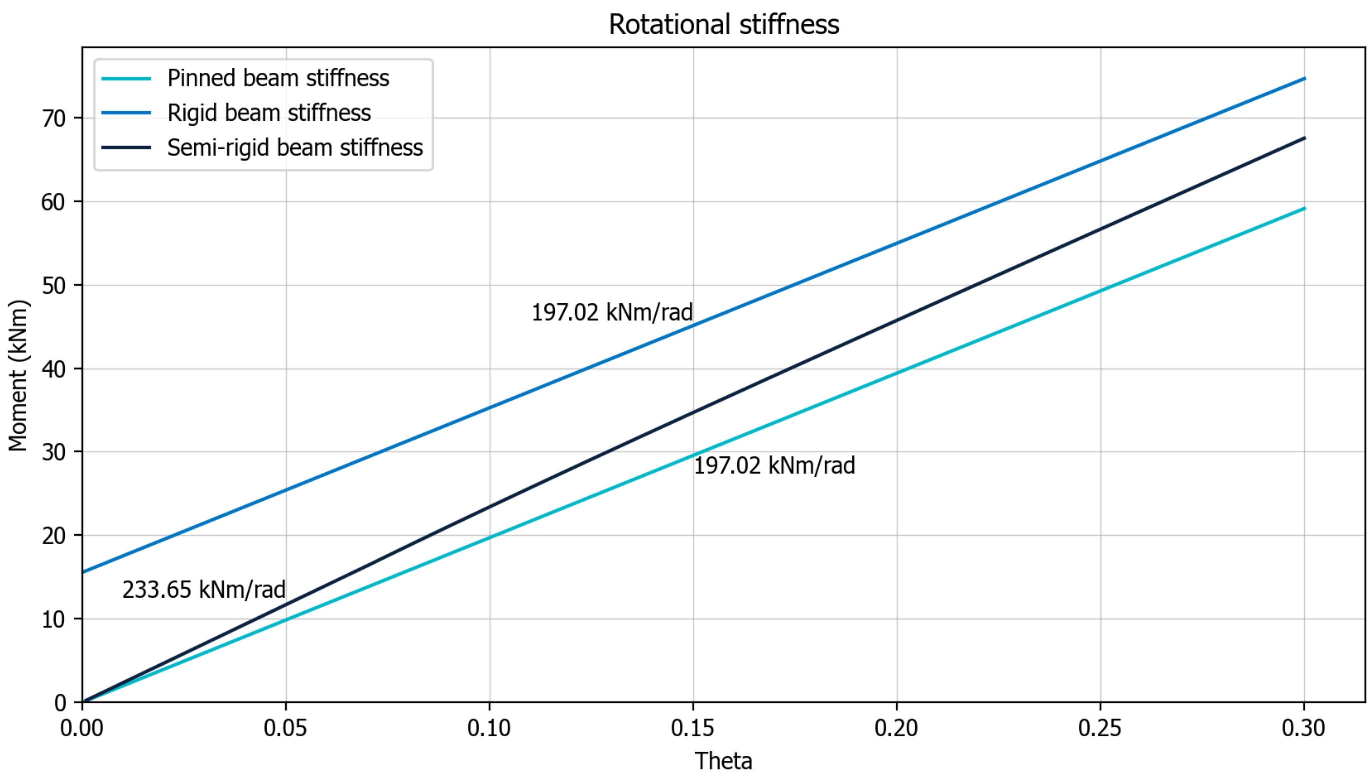

Fig. 25. Interlocking joint 1 beam stiffness [By author].

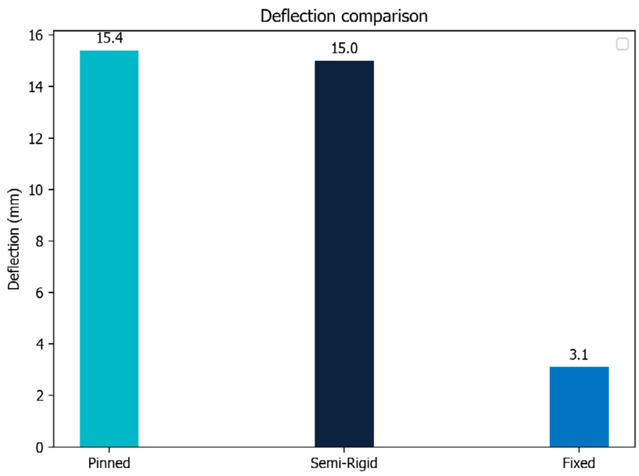

Fig. 27. Interlocking joint 1 midspan deflection [By author].

3.3 Interlocking joint 2

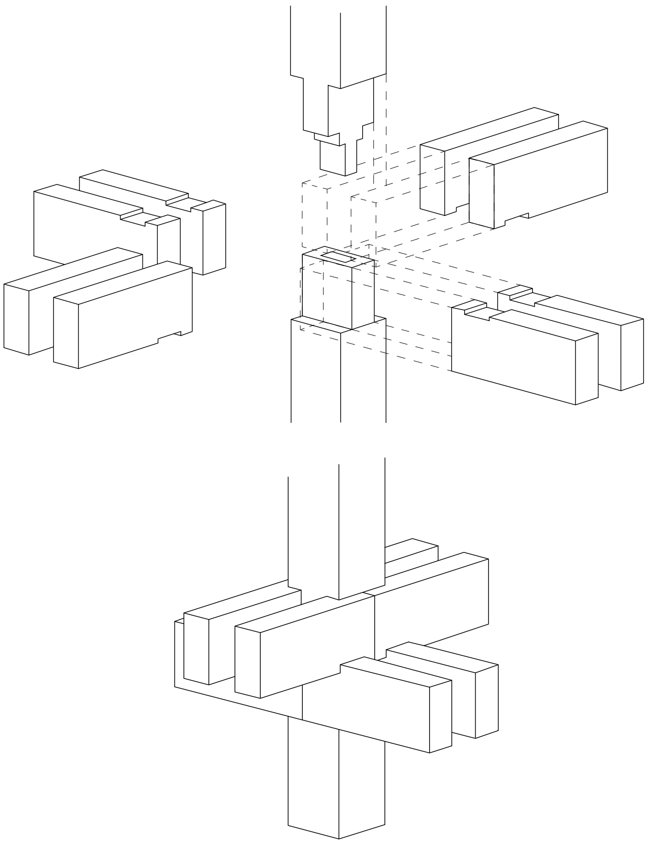

Fig. 28. Interlocking joint 2 [By author].

Joint 2 consists of multiple beams that are partially inserted into the column and partially extend outwards. With notches on all beams, they interlock with each other, forming an interlocking, self-locking mechanism when assembled. The column fits into a slot on the column placed below, thereby securing the beams vertically. Due to the column's fibre directions pressing on the weak fibre direction of the beam, a slight initial embedment of the column in to the beam is created. This geometry allows for the prevention of an initial gap and tightens the connection during assembly.

The rectangular cut-outs of the beam can be achieved either through CNC machining or by leaving out this section of laminate during the manufacturing process of the glulam beam, minimizing wood loss. However, the geometry of the column requires more pre-processing.

A challenge of this geometry is the small contact surface area from column to column. Again, due to the strong and weak fibre directions of the wood, all the vertical forces will be transferred through the small element of the column to the next column. This reduction of cross-sectional area to 1/4 of the original column cross-section will become a critical point, where either the rest of the column must be over dimensioned to accommodate the forces in the smaller cross-section, or the smaller cross-section will fail due to excessive pressure.

The structure of this geometry is based on 1) a loaded main beam, which would be the upper beam, and 2) a secondary unloaded beam that would function as a tie beam in the structural frame and adding support to the loaded main beam. By having this extra width for the main beam to rest on, as the secondary beam is partly extending outwards of the column, additional embedment length and an longer moment arm are created.

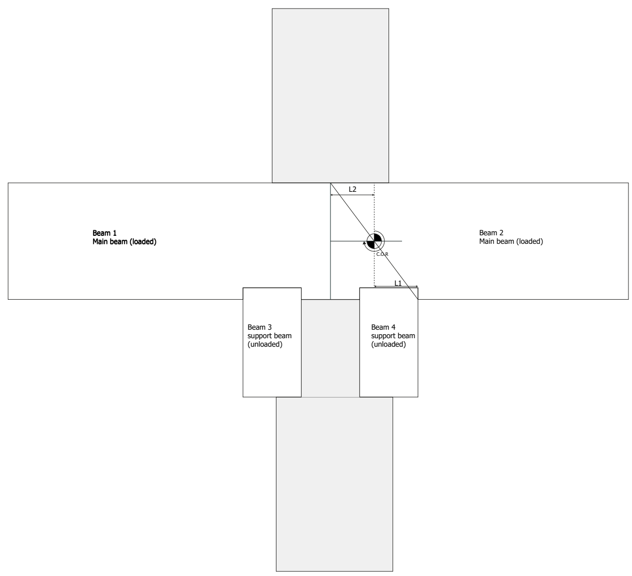

Fig. 29. Interlocking joint 2 properties [By author].

Because the beam is not continuous over the joint, the C.O.R is shifted from the centre of the beam, leading to a smaller embedment length than the Nuki joint. However, the wider base width created by the secondary beams, results in a longer moment arm, which then results in

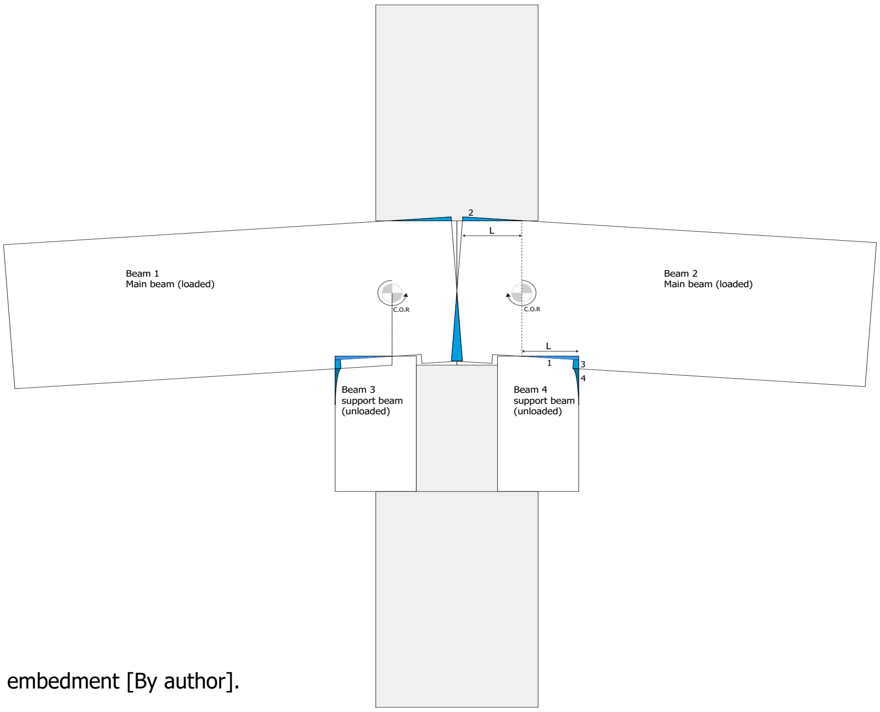

Fig. 30. Interlocking joint 2 embedment [By author].

a higher rotational stiffness Eq. (35). Additionally, the secondary beam experiences extra additional-embedment through the rotation of the main beam, contributing to an increase in rotational stiffness (Appendix A). The interaction between the two beams creates a stiffness curve marked by three phases. Initially, there is the elastic region, exhibiting a stiffness slightly greater than that of the Nuki joint. Secondly there is the first plastic embedment forming in the secondary beam do to the embedment marked with a 3 in Fig. 30. Finally, the third phase exists of the plastic embedment of the main beam into the column.

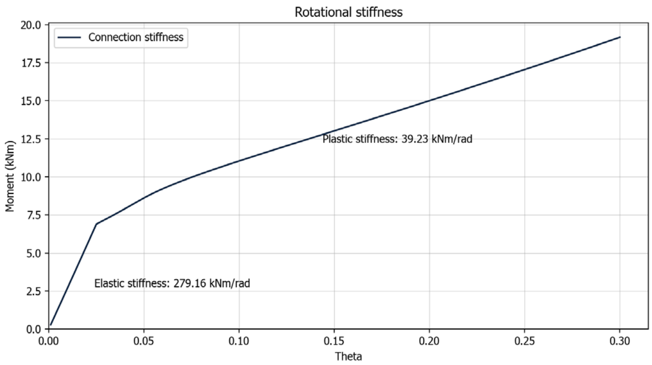

Fig. 31. Interlocking joint 2 rotational stiffness [By author].

The elastic rotational stiffness is twice as great as of joint 1, as illustrated in Fig. 32. The midspan deflection more closely resembles that of a pinned connection rather than a rigid connection. Although the joints have managed to reduce deflection by a few millimetres, their performance still falls short of justifying the pre-processing required for their construction.

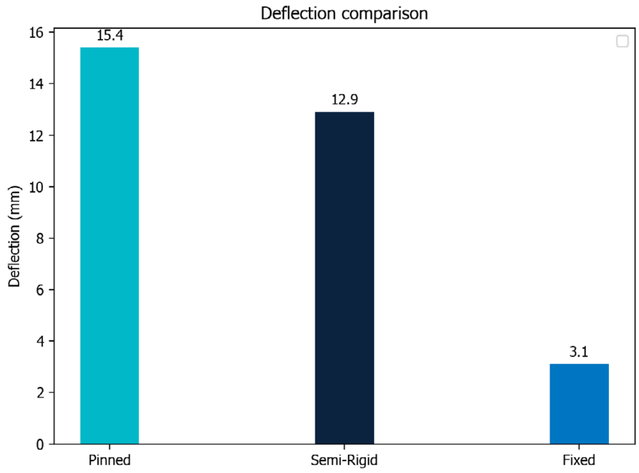

Fig. 32. Interlocking joint 2 midspan deflection [By author].

The midspan deflection is slightly less than the deflection of the Nuki joint. This observation is also evident from the slightly higher stiffness of the beam, as depicted in Fig. 33. However, this connection is still under-performing when aiming to create a rigid timber dry joint.

Dry joint conclusions

Previous approaches did not satisfy the aim to create a rigid timber dry joint. Additionally, there is an effect of scaling. The beam stiffness increases more per unit height added than the rotational stiffness of the connection. This results in the connection becoming less effective as the size of the structural frame increases. Where in small frames like houses, relatively larger savings could be made compared to large structural frames, while these larger frames have more potential in reducing the embodied carbon due to their size. This poses

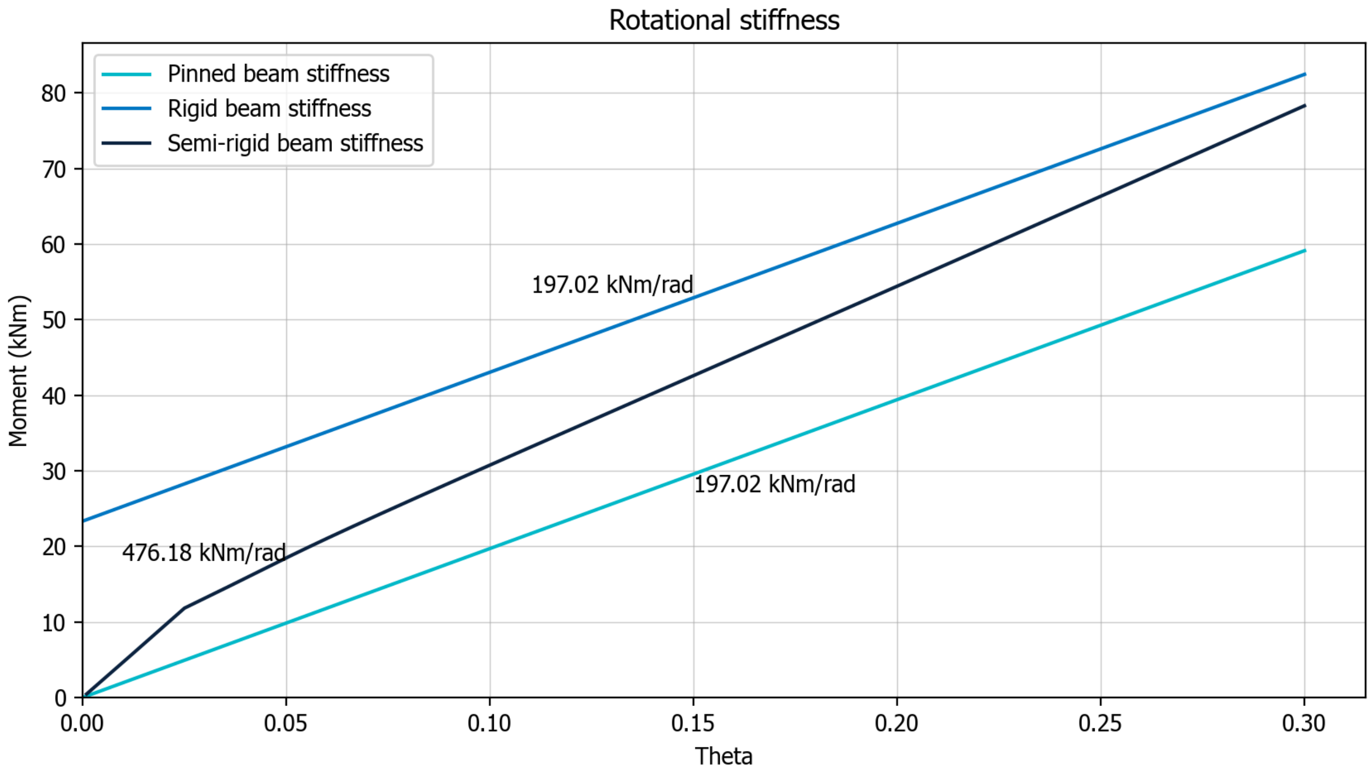

Fig. 33. Interlocking joint 2 beam stiffness [By author].

the need for an alternative approach to design a timber dry joint able to compete with a rigid joint using steel connectors.

The effect of the increasing beam size in relation to the stiffness is shown in Fig. 34. The relation between the flexural rigidity of the beam and the connection stiffness is also derivable from comparing Fig. 33 and Fig. 35, where in Fig. 33 the ratio between the elastic stiffness and the pinned beam stiffness is $476/197\ kNm/rad = 2.42$ and in Fig. 35; $7412/4804\ kNm/rad = 1.54$ showing a decrease in the effect of the connection's rotational stiffness on the resulting beam stiffness and thus midspan deflection.

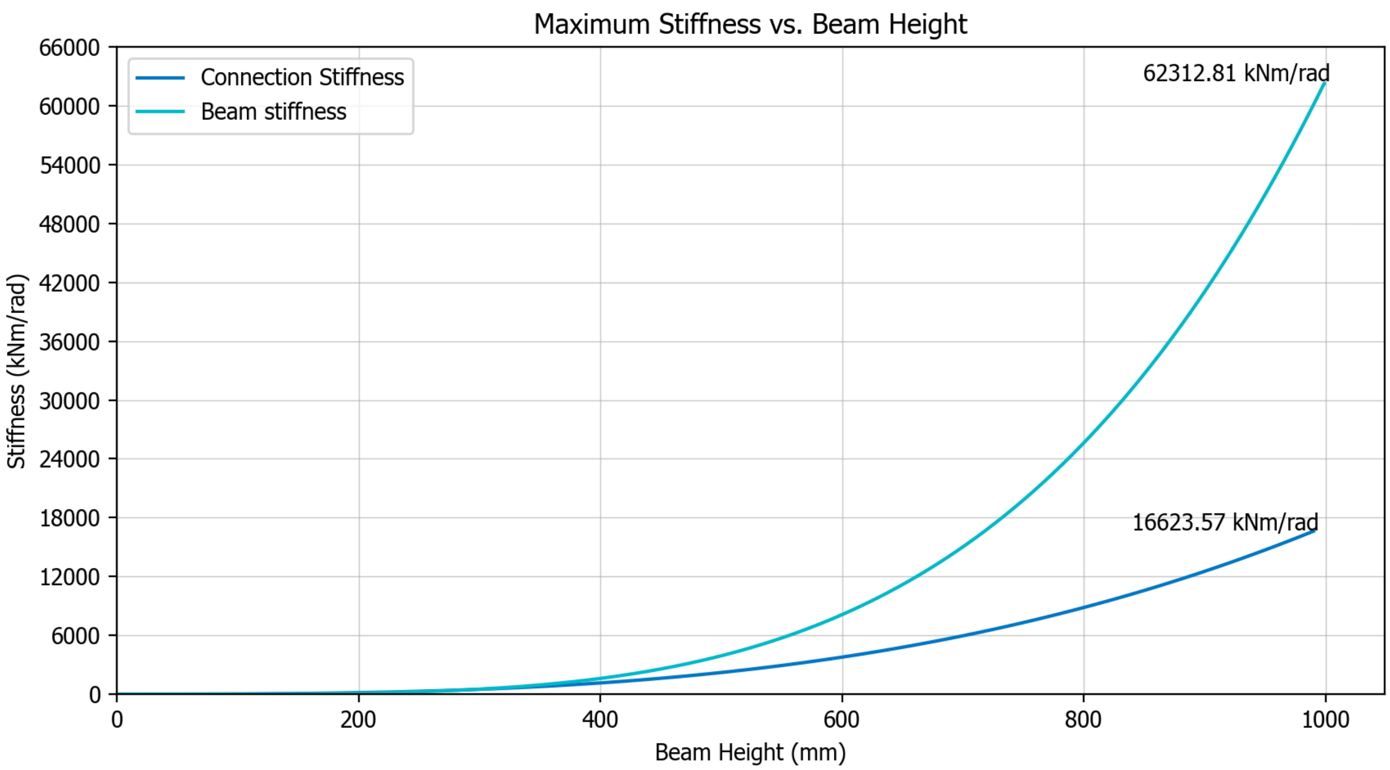

Fig. 34. Relation between connection- and beam stiffness [By author].

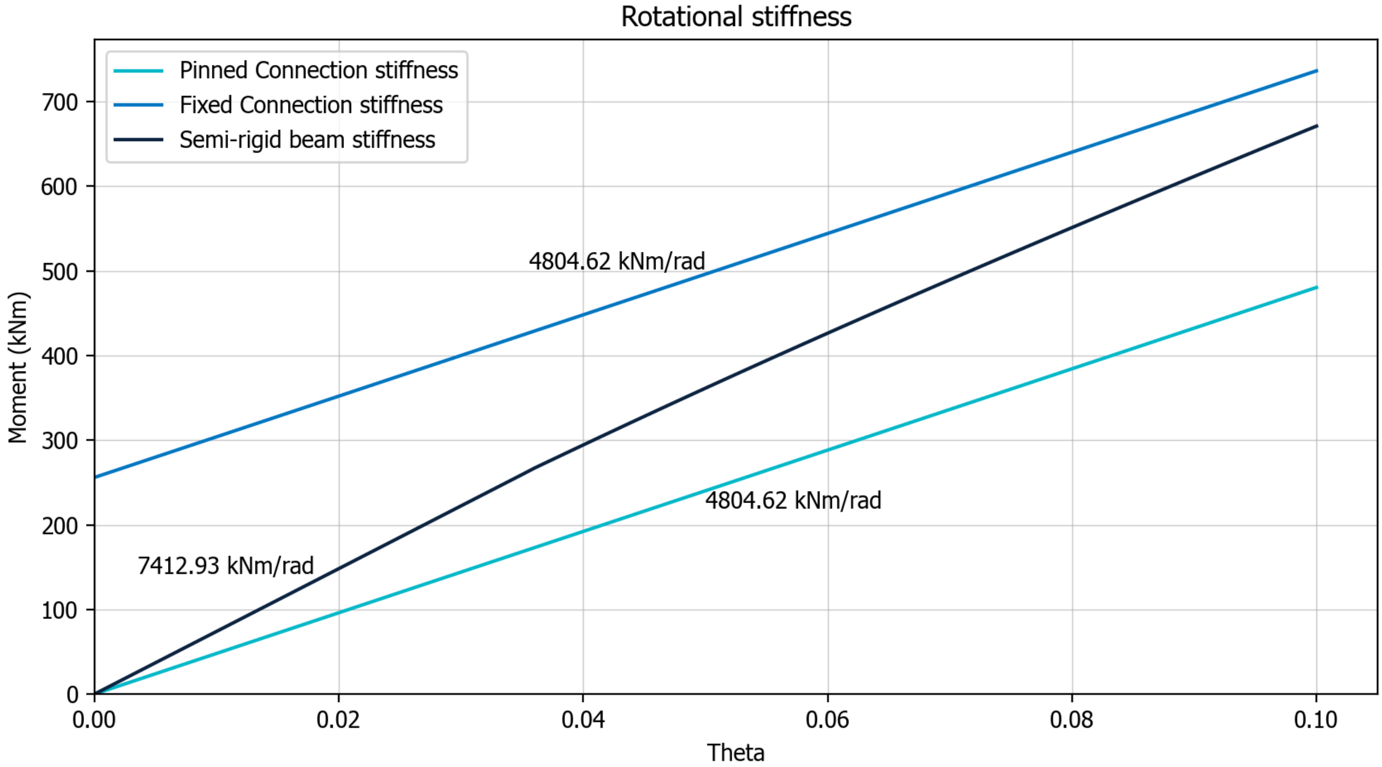

Fig. 35. Nuki joint beam stiffness larger beam size [By author].

04

Continuous joints

TU Delft Delft University of Technology

Continuous joints

In this chapter a different design approach is investigated. Based on principles more commonly seen in bridges and large steel and concrete structural frames.

4.1 Continuous connection

This approach will explore the utilization of a continuous beam. By relocating the beam-to-beam connection away from the column, following the bending moment diagram, connections experiencing solely shear force can be made, thus allowing for simpler connections. The connection then created at the intersection of the column and beam, only has to accommodate the shear forces from beam to column as the bending moment will be effectively managed by the continuity of the beam, efficiently creating a rigid connection.

Depicted in Fig. 36, where the bending moment diagram (red line) crosses the beam element at distance x, also known as the point of contraflexure, the bending moment = 0. This is the ideal point to create simple beam to beam connection. Resulting from the equations in appendix B. This point of contraflexure can defined by eq. 53 and 54, for a rigid beam with UDL.

$$x_1 = \frac{L}{2} - \frac{\sqrt{3}L}{6} \tag{53}$$

$$x_2 = \frac{L}{2} + \frac{\sqrt{3}L}{6} \tag{54}$$

With L as the beam length.
With the location of this point determined, further design aspects of this connection are not addressed.

Focussing on the "connection element" from Fig. 36, a continuous beam, using timber dry interlocking geometry is compared to multiple steel connector configurations.

To provide context for a functional interlocking geometry, an assessment of various floor configurations for different span sizes is conducted. As a result of this assessment, a decision is made defined by a balance between embodied carbon and practicality for flooring systems in both office and residential settings.

Multiple frame configurations spanning 6 meters wide, with lengths of 6, 9, and 12 meters, are compared. Floor sizes are determined using beam theory, with floor heights constrained by maximum deflection.

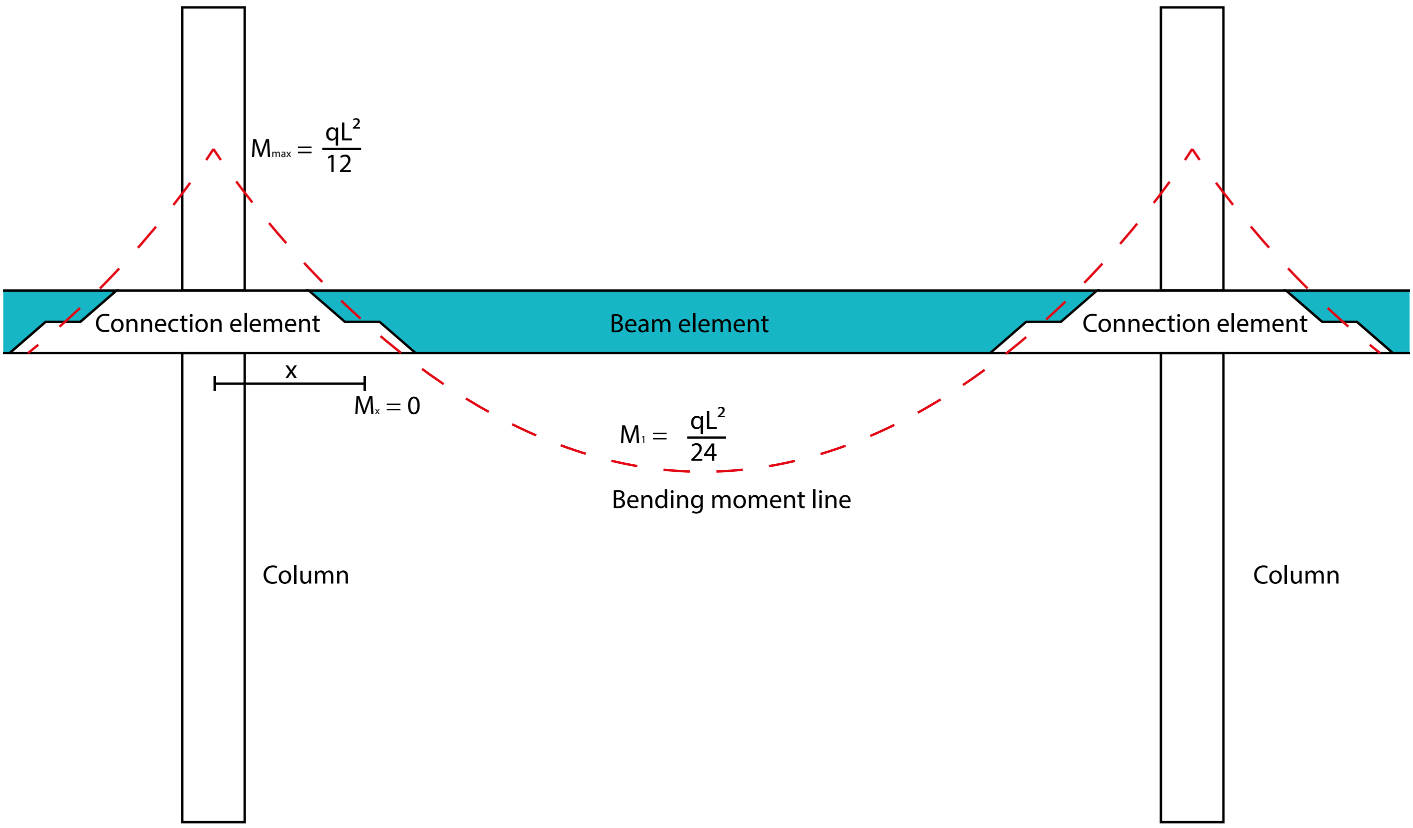

Fig. 36. Connection and bending moment diagram [By author].

4.2 Updated geometry

Taking the most effective shape from section 3.3 and making slight modifications, a new geometry principle is created. By shifting the beam elements outward from the column, the column can retain its cross-sectional area, thus preserving its strength. Maintaining the same interlocking geometry between the beams ensures that the beams are restrained in all directions. Additionally, by adding a large wooden peg to connect the beams to the column, the normal force can be transferred through the peg to the column. By orienting the peg vertically, it has enough cross-sectional area to transfer the shear forces while not significantly weakening the column, thereby maintaining an all-wooden connection.

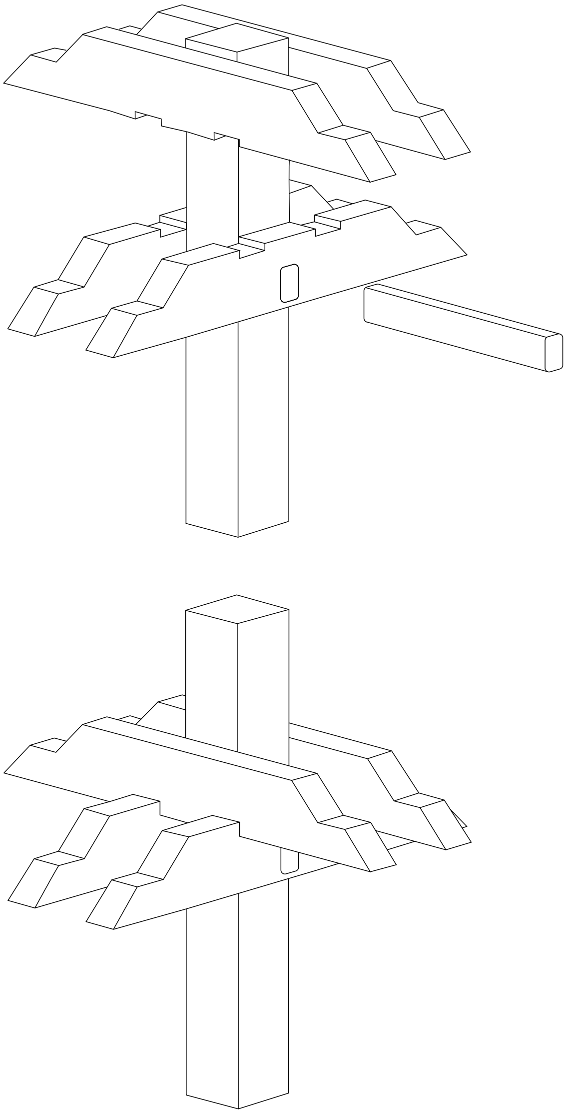

Fig. 37. Continuous design interlocking geometry [By author].

To compare this geometry with the use of steel fasteners, the second geometry reviewed is depicted in Fig. 37. The steel fasteners allow the secondary beams to be vertically aligned with the main beam, without adding extra height to the system. The main beam is connected by a set of metal bolts, tailored to the load that needs to be supported for each system, as explained in the following chapter. The functionality of these two principles is explained in depth in the subsequent chapters.

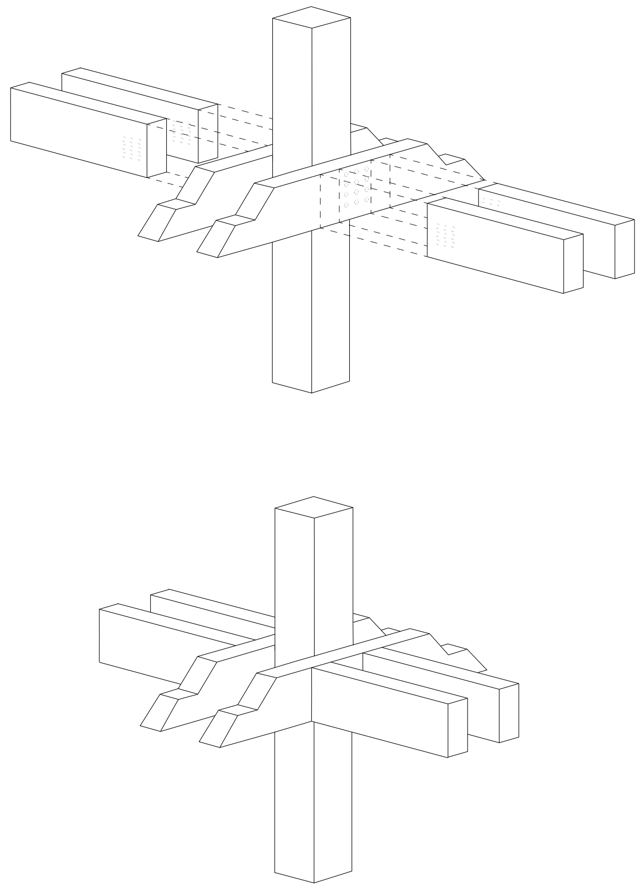

Fig. 38. Continuous design steel fasteners geometry [By author].

Table 2. Embodied carbon values [By author].

Material	Value	Source
Wood	0.8 Kg CO_2/ kg	Ansys GRANTA EduPack [49]
Steel	2.21 Kg CO_2/ kg	Ansys GRANTA EduPack [49]
Aluminium	12.3 Kg CO_2/ kg	Ansys GRANTA EduPack [49]
Façade systems	250 Kg CO_2/ m^2	From [47][48]

Table 2 contains the used values for the embodied carbon in kg CO_2 throughout the remaining chapters.

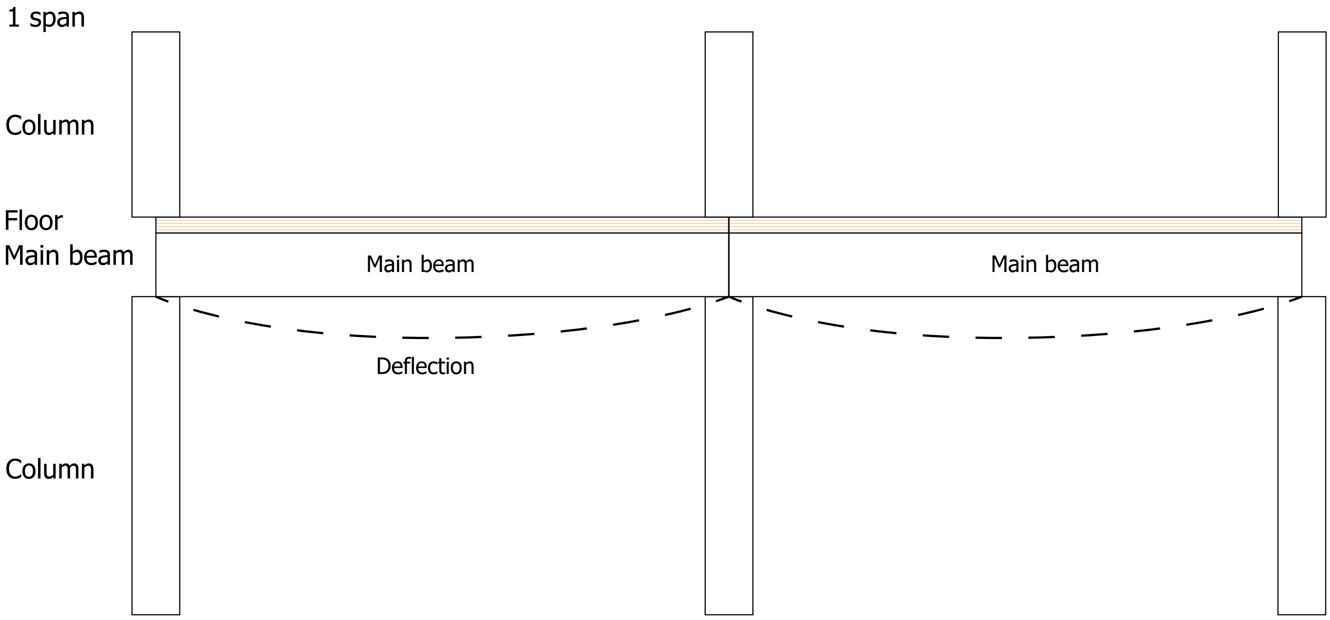

Fig. 39. Structural frame 1-span system [By author].

4.3 Multiple-span frames

1) In a single-span system, which is the most common layout for buildings, a single beam supports a floor that is simply supported, laying on top of the beam.
This layout induces a bending moment on the beam of eq 43. The resulting reaction forces are evenly distributed between the two beams. This configuration represents the simplest form.

2) The second configuration comprises a floor element spanning across three beams, forming two spans. This layout results in a larger support reaction at the centre beam (R2) and reduced reactions at R1 and R3. By connecting the next floor at R1 and R3 and splitting the beams from R2 into two beams, all loads are evenly distributed among all secondary beams. One advantage of this configuration is the reduced thickness required for the flooring system, as the spans are shorter compared to a single-span system. This leads to lower wood volumes for the floor. However, a drawback of this two-span system is the necessity for secondary beams to support the floor. These secondary beams then rest on the main beam, which is treated as a rigid beam with a centre point load in calculations, resulting in a high overall floor height needed for this system.

This vertical stacked layout is based on a timber dry system. When steel connectors are used, the secondary beams can be placed between the main beams, reducing the overall floor height.

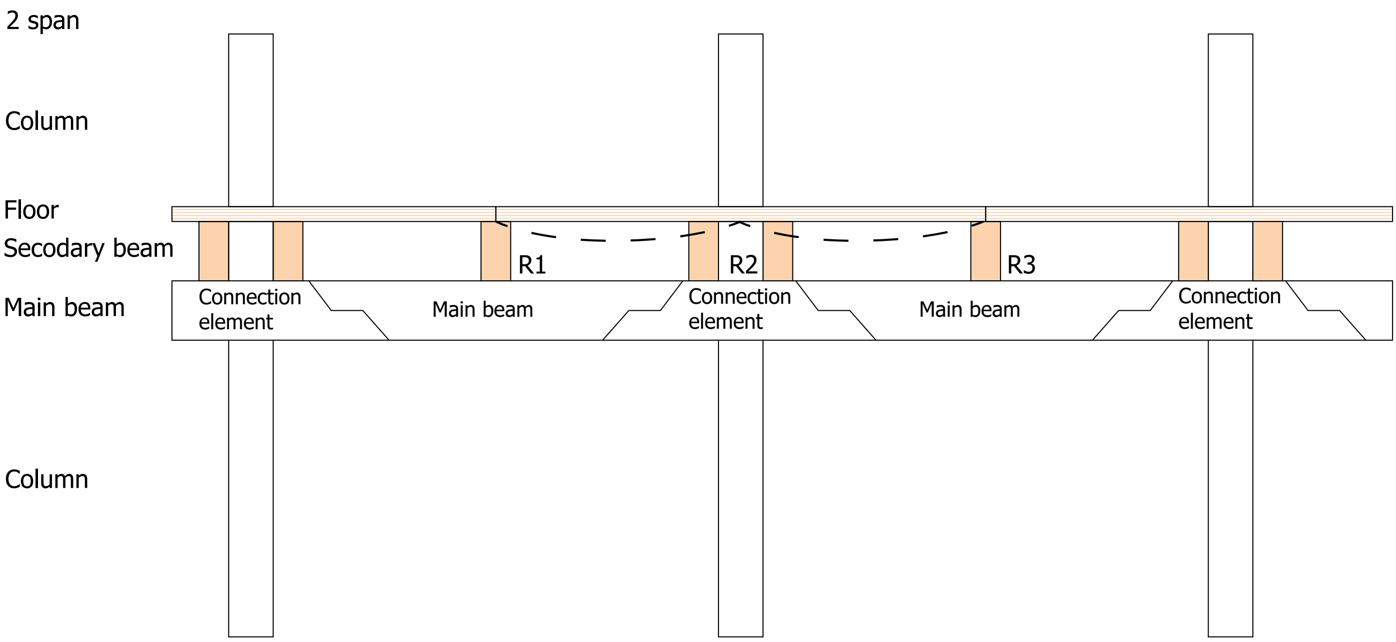

Fig. 40. Structural frame 2-span system [By author].

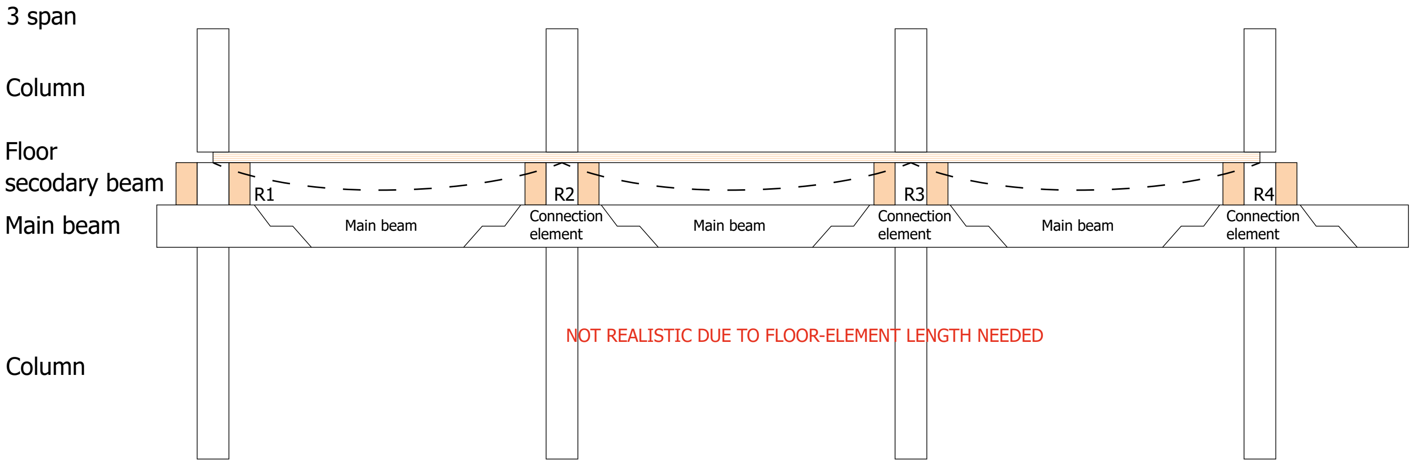

Fig. 41a. Structural frame 3-span system [By author].

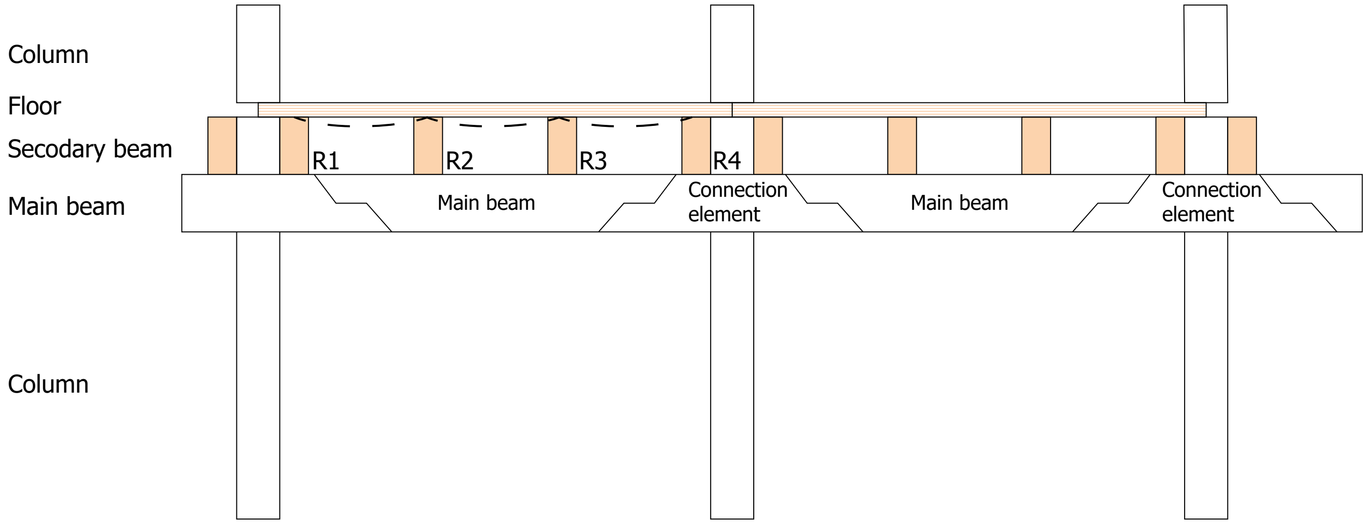

Fig. 41b. Structural frame 3-span system [By author].

3) By adding one more secondary beam, a three-span layout can be achieved. There are two configurations for this three-span system:

3a) The first configuration consists of a long flooring element spanning between four columns. Due to the long floor element required for this configuration, it is unlikely to be constructed for regular span systems of six or more meters. This configuration is only feasible for short-span systems of up to three meters.

3b) The second configuration involves two secondary beams (R2, R3) positioned between two columns, resting on the main beam, resulting in short spans. This layout leads to a thinner floor element. Once again, by connecting the new flooring element at the double beam at the column (R1, R4), all secondary beams can maintain the same height.

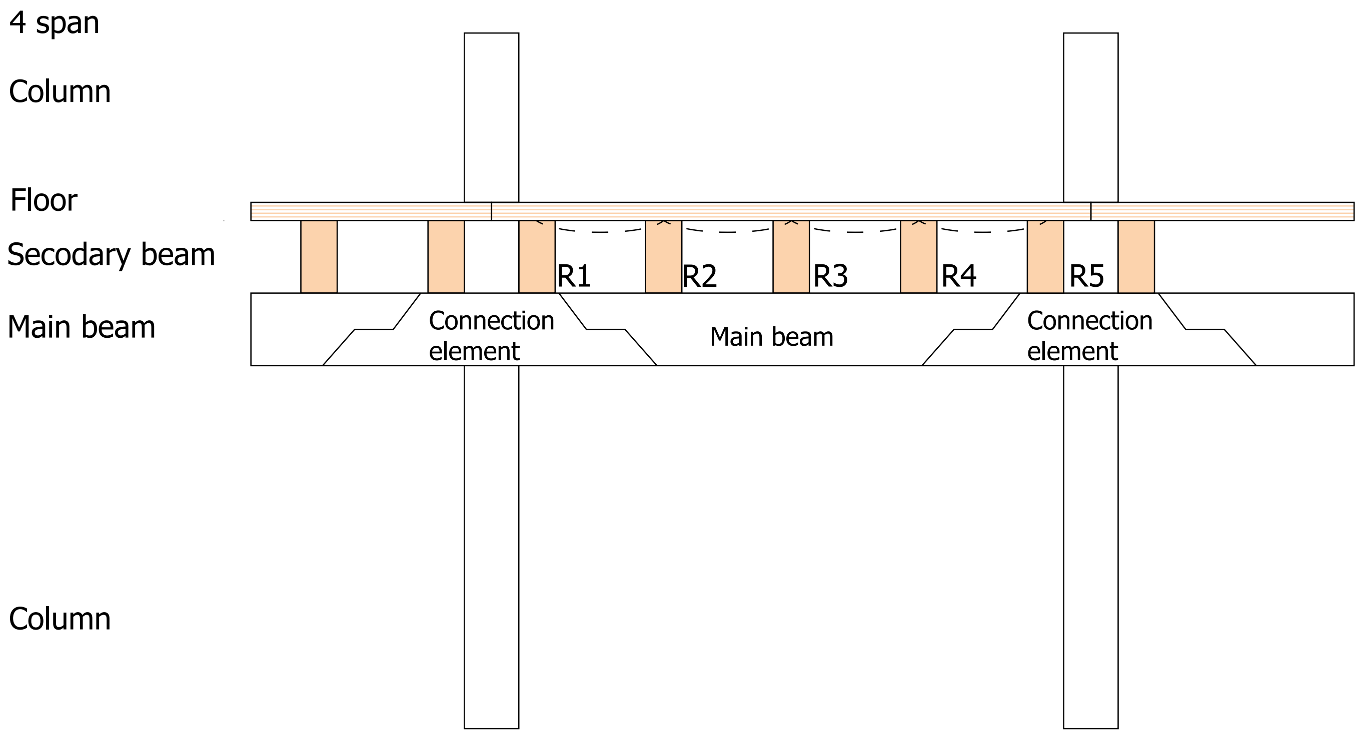

Fig. 42a. Structural frame 4-span system [By author].

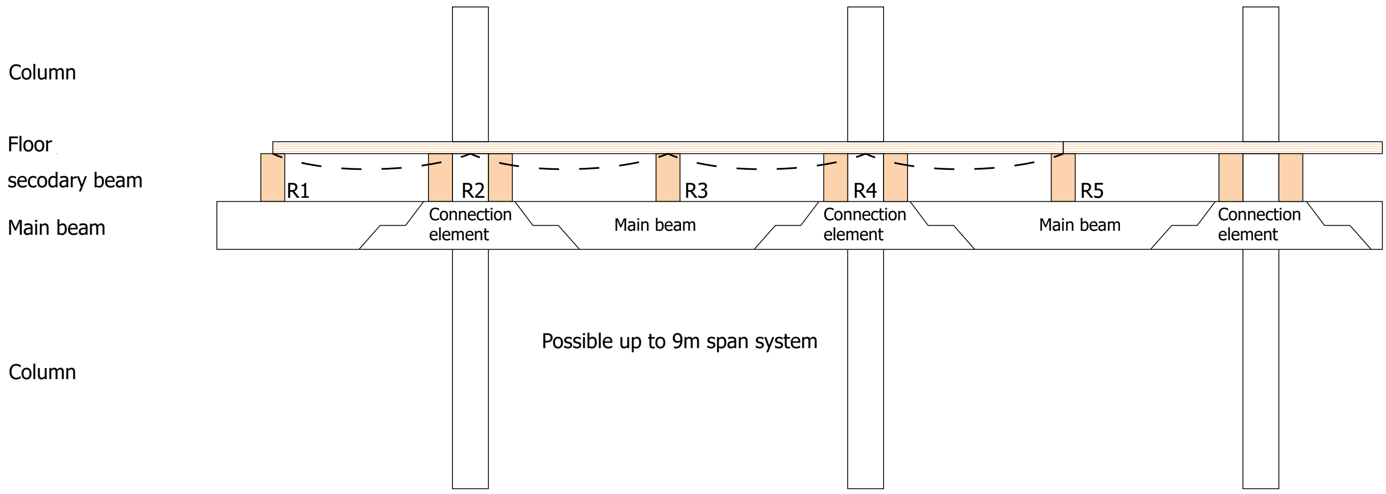

Fig. 42b. Structural frame 4-span system [By author].

The final configuration consists of a four-span system, with again two layouts available for this system.

4a) The first layout consists of three additional secondary beams (R2, R3, R4), placed between the columns, resulting in very short beam spans and consequently very thin flooring elements. For this system, the same principle applies of connecting the next flooring element at the column. Due to the load distribution, the "end" beams (R1, R5) can be thinner. However, this configuration is less than ideal for the load distribution, and that's where the following layout proves to be superior.

4b) By extending the flooring element over three columns, the heaviest loaded beams (R2, R4) are shifted to the double beams at the columns. By connecting the next floor element at R1 and R5, the load is once again evenly distributed over all the beams, resulting in nearly identical secondary beam heights. The spans experienced by the floor are identical to those in system 2, but with thinner floor elements. However, due to the length needed for the flooring element to create this system, the maximum column-to-column distance is nine meters.

05

Conventional joints

Conventional joints

In this chapter the "conventional" connection used in structural timber frames is described. These joints are used to set a baseline and enable a comparison showcasing the effect on the embodied carbon, of a structural timber frame, by implementing timber dry joints or continuous joints.

5.1 Slotted in steel plate

A "conventional" joint can be constructed using either a slotted-in steel plate, as depicted in Fig. 43a, or a metal nail plate, as shown in Fig. 43b. In the first method, a steel plate is glued into both the column and the beam, facilitating the transfer of loads between the structural elements. The bending moment experienced by the connection are calculated using eq. 42. These forces are then distributed over the bolts and subsequently transferred to the steel plate, ensuring a robust and efficient load transfer mechanism.

This method is advantageous due to the high strength material characteristics of steel. The glued-in steel plate offers stiffness and strength, making it a preferred choice for many structural applications. Additionally, the distribution of forces through the bolts to the steel plate helps in mitigating stress concentrations in the connection.

5.2 Steel nail plate

An alternative, yet functionally similar variant, is the steel nail plate. This method involves driving numerous nails into the structural elements, which are then connected by the same steel plate to create a strong connection. The extensive surface area provided by the nails ensures an effective transfer of forces, contributing to the overall strength and stability of the joint.

The steel nail plate connection offers the advantage of ease of installation and the ability to accommodate slight misalignments in the structural elements. The numerous nails provide a large contact area, which distributes the load more evenly and reduces the risk of localized failures.

5.3 Conclusion on conventional joints

The slotted-in steel plate is the most common and widely used option in contemporary large structural timber frames, this principle will be used for the calculations in the following chapters.

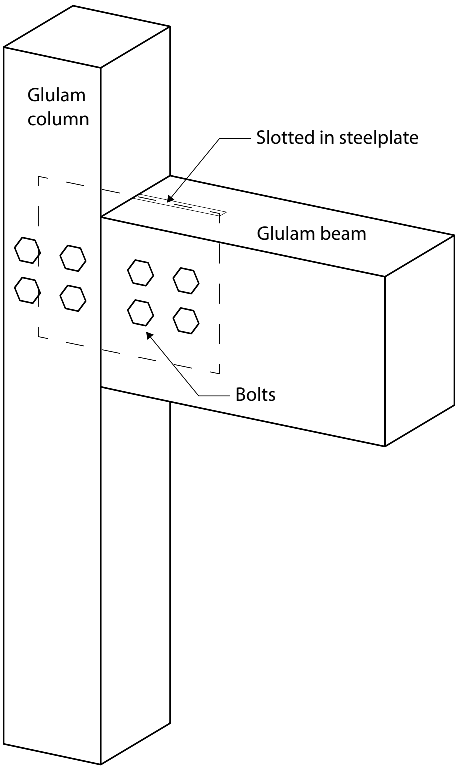

Fig. 43a. Conventional joint with slotted in steel plate [By author].

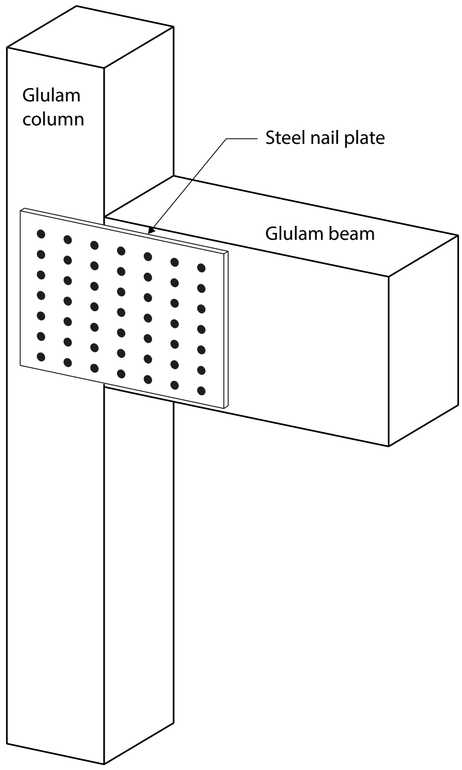

Fig. 43b. Conventional joint with steel nail plate [By author].

06

Comparison of joints

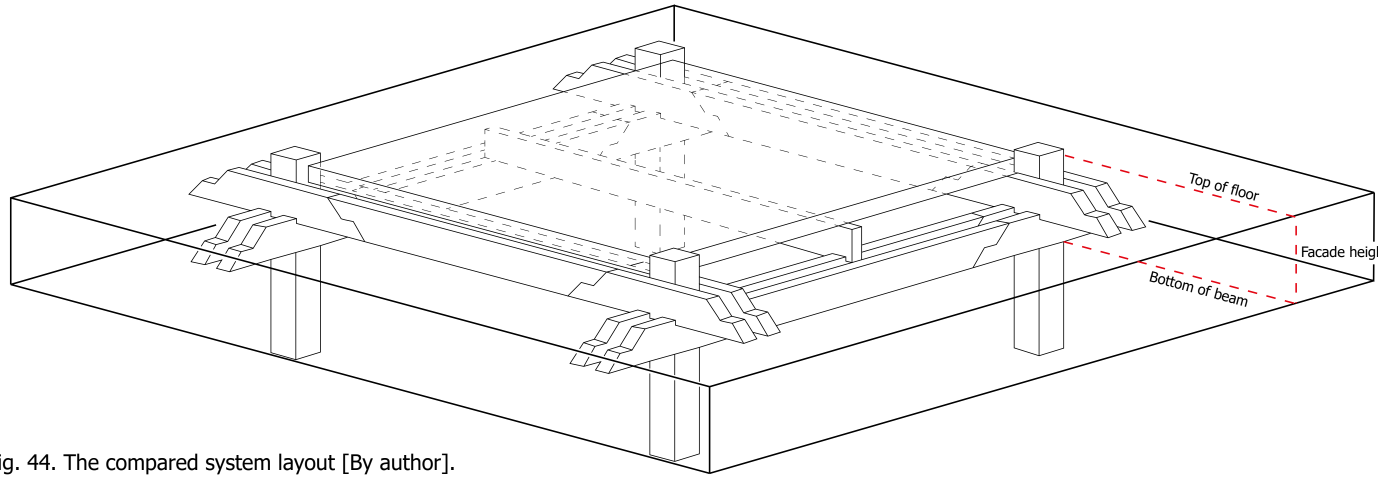

Fig. 44. The compared system layout [By author].

Comparison

In this chapter, a numerical comparison of the previously illustrated systems is presented. Comparisons between floor thickness, secondary beam height, main beam height, column sizes, wood volume per square meter, and embodied carbon per square meter are provided. Calculations are provided in Appendix C.

The calculations are based on the above configuration of a single bay with a surrounding façade. Due to the relatively large façade compared to the floor area, the influence of the façade on the embodied carbon per square meter is relatively large, which can give a distorted picture. However, on the other hand, it also emphasizes the effects of different types of systems on embodied carbon.

For consistency and comparability, calculations have been conducted using the same load case.

6.1 Dry joints efficacy

The efficacy of the different joints researched in Chapter 3 in reducing beam height and volume is illustrated here. It is evident that even the most effective joint, joint 2, in cross-section is still far from being as effective as an ideally rigidly connected beam. The dimensions of joint 2 are much closer to those of a pinned beam, as demonstrated in the graphs.

The rotational stiffness for each dry joint from chapter 3 results in beam dimensions that are closer to those of pinned beams than rigid beams. This finding is also highlighted in chapter 3, where the implications of the rotational stiffness on the overall structural performance were discussed.

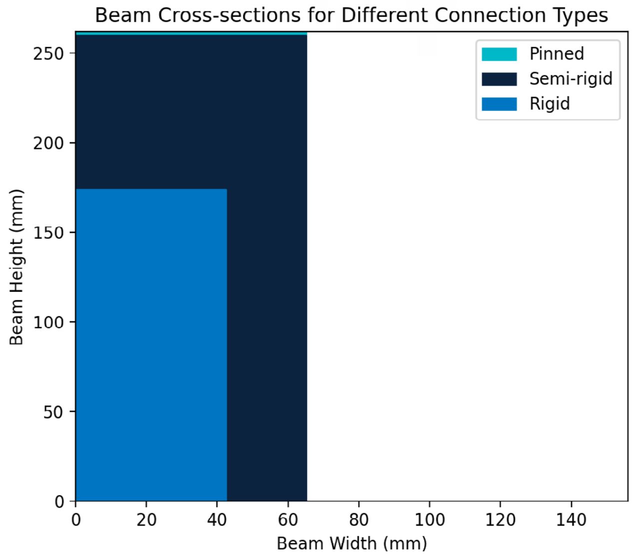

Fig. 45a. Dry joint 1 beam cross section [By author].

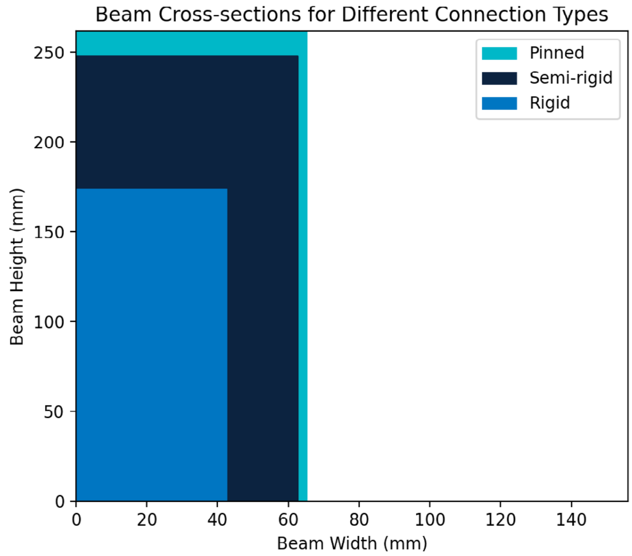

Fig. 45b. Dry joint 2 beam cross section [By author].

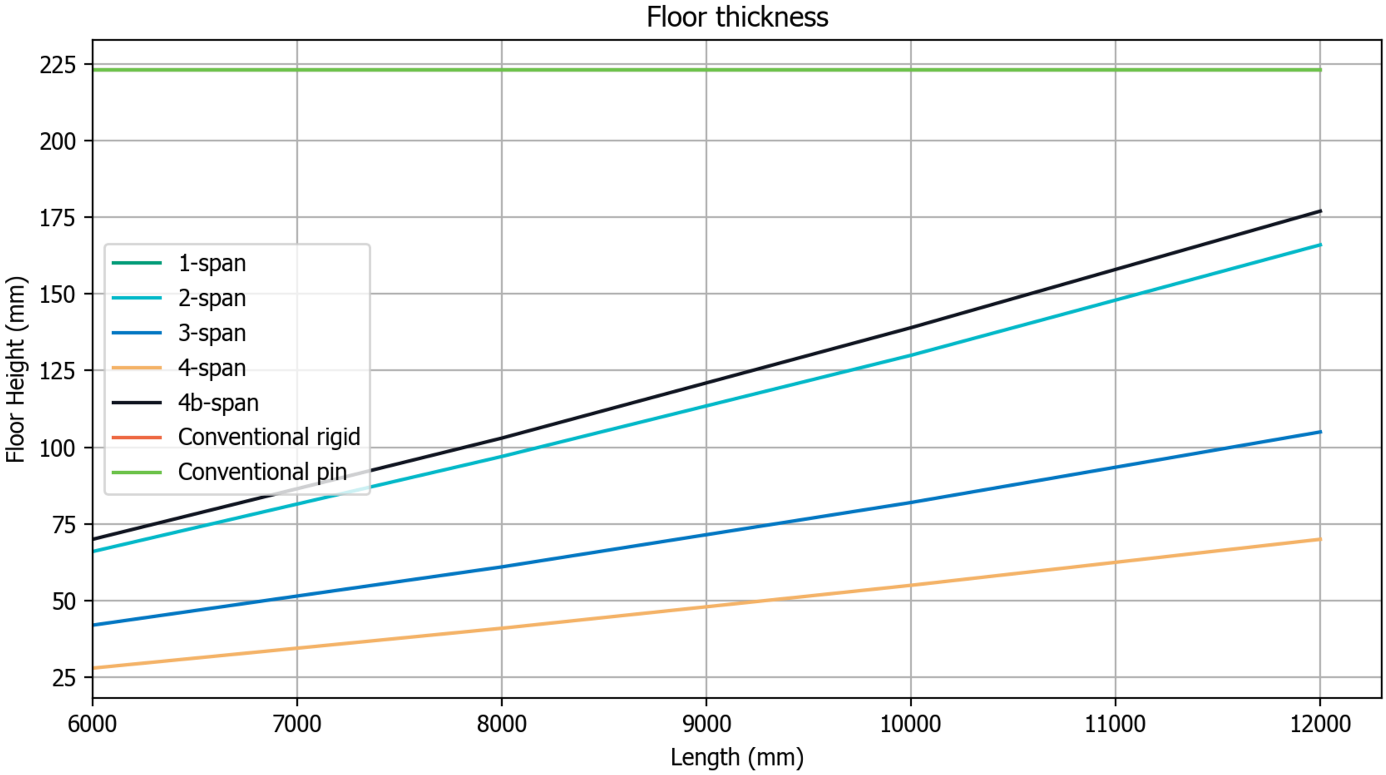

Fig. 46. Floor thickness per span configuration [By author].

6.2 Comparing multi-span frames

6.2.1 Floor thickness

In Fig. 46, the floor thickness for each different configuration and span length can be seen. The system widths for each span are consistent at six meters.

The thicknesses of the CLT floor elements clearly correlate with the span length and span system. Shorter spans result in thinner floors. The single span system has the thickest floor element, as it experiences the most deflection according to the equations, thus requiring greater height to provide adequate stiffness. The other span systems are closer in thickness, demonstrating slight differences following the logic explained in section 4.1.2. Span configurations 2 and 4b show the most promising results regarding thickness for all span lengths, having an adequate thickness considering sound transmittance and fire safety regulations. Configurations 3 and 4 have thin floor thicknesses due to their short spans, resulting in elements that are too thin considering supplier availability.

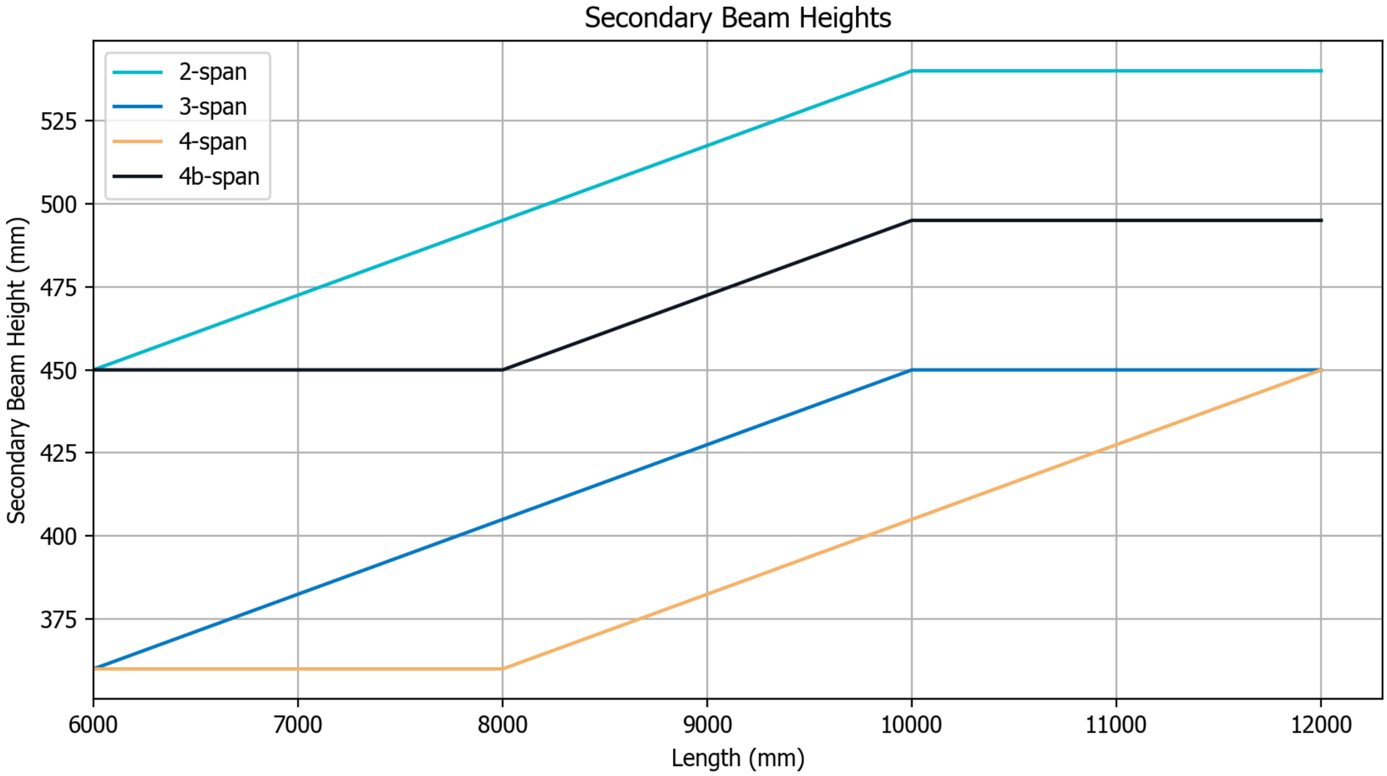

Fig. 47. Secondary beam height per span configuration [By author].

6.2.2 Secondary beam heights

Fig. 47 depicts the secondary beam height for various span systems and increasing spans. Since the width for each configuration remains consistent at six meters and the secondary beams span perpendicular to the main beams, their spans do not vary. The linear horizontal trend of the graph can be attributed to the slight differences in load on each secondary beam per span system, highlighting the maximum load and consequently the tallest secondary beam.

The linear increases are due to the beam laminae thickness being set in increments of 45mm per lamina following industry standards [46]. The 3- and 4-span systems show the same secondary beam heights, leading to an overlap in the graph. The width of each secondary beam, in the same span-system, may vary due to different loads, resulting in some beams being slightly more efficient than others, regarding their height to width ratio. However, overall, they maintain the same height, ensuring the level support required for the floor element.

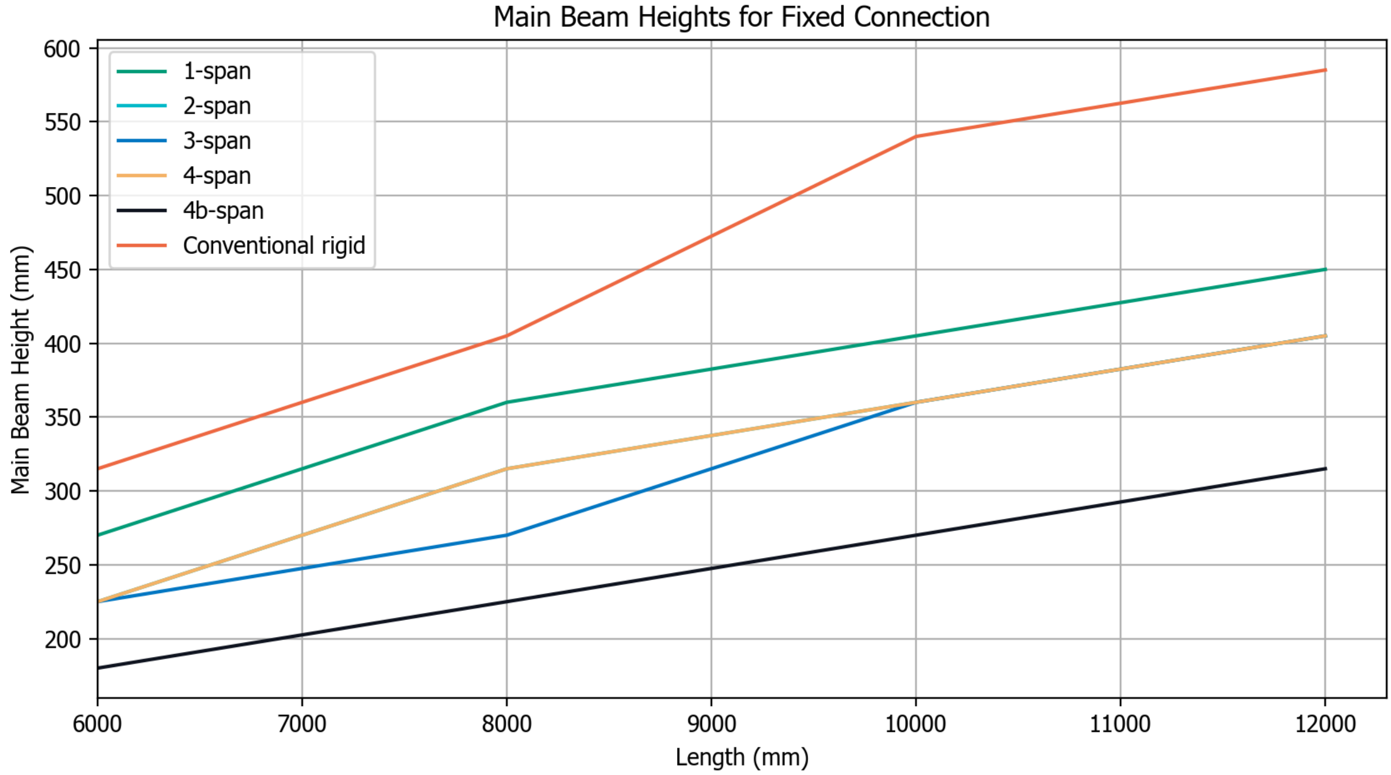

Fig. 48. Main beam height per span configuration, resulting from load caused by secondary beams, for rigid connection [By author].

6.2.3 Main beam heights

Figures 48 & 49 illustrate the beam depth of the main beams for each configuration. Systems of the 3- and 4-span are overlapping for the rigid connection, having the same values. Notably, the overall effect of the connection type on the beam height is evident, as well as its impact on the different span systems.

The smallest beam height is observed for the 4b system, exhibiting the lowest heights in both pinned and rigid configurations. For the connections and design of the timber dry joint system, only the rigid connections are taken into account, as the continuous connection can be considered rigid, as explained in chapter 4.1. Similar to figures 46 & 47, the group of 2-4 spans doesn't differ much compared to the outlier of the single span system. Since the differences between the secondary beams are 90mm for 3-4 and 2-4b, and the differences for the main beams are only 45 mm for these span systems, the depth of the secondary beam has a more significant impact on the overall structural height of the system

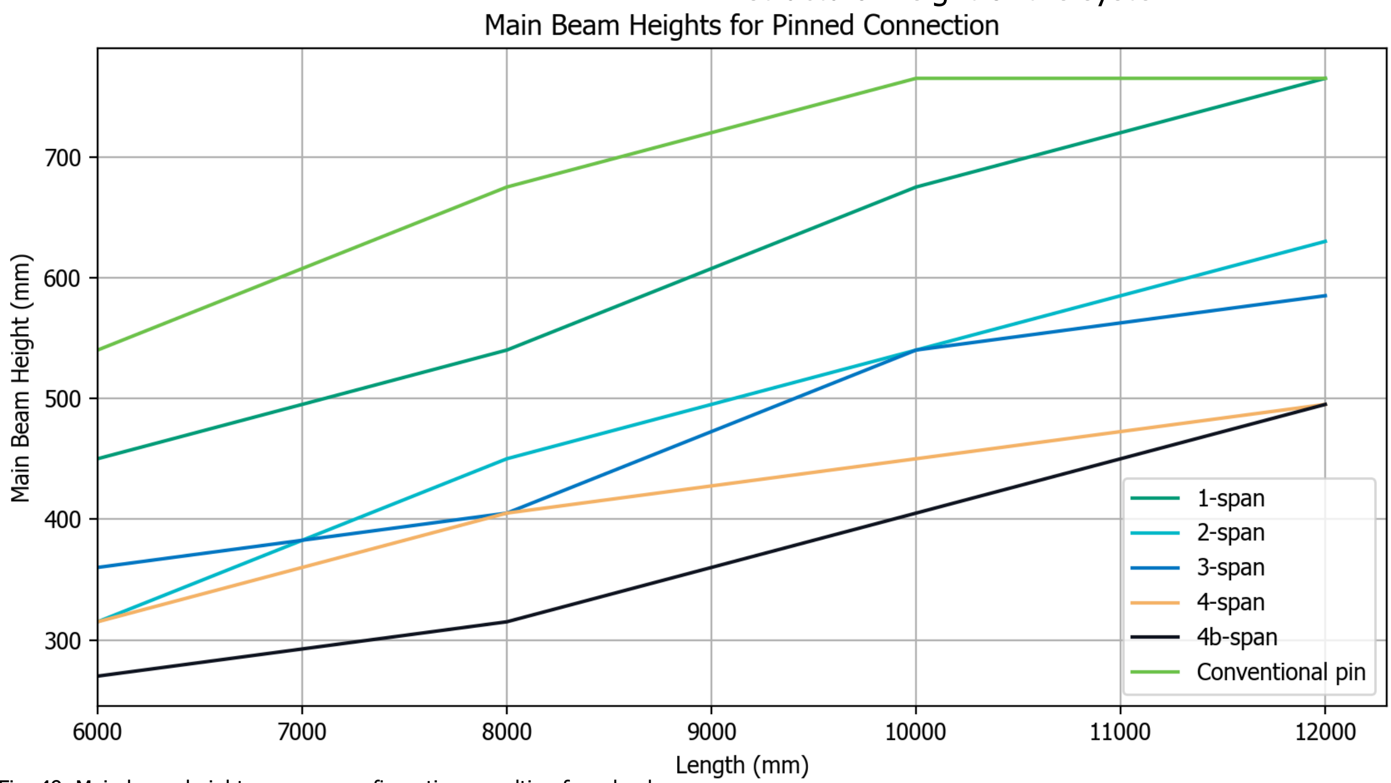

Fig. 49. Main beam height per span configuration, resulting from load caused by secondary beams, for pinned connection [By author].

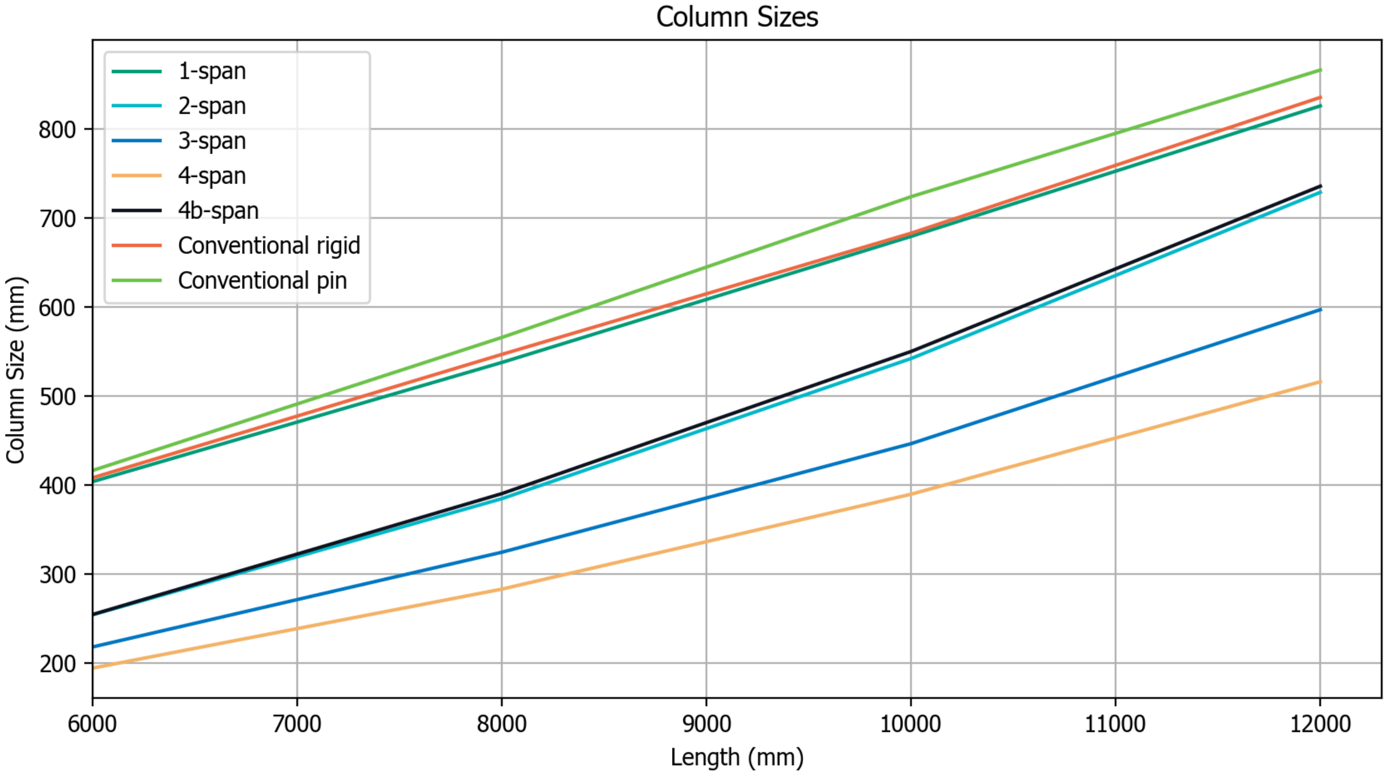

Fig. 50. Column width of square column calculated for cross-sectional area resulting from load carrying capacity for different span systems [By author].

6.2.4 Column sizes

In Fig. 50, the column widths required to support the combined load from the self-weight of the floor and beam elements are depicted, along with the variable load. The substantial floor thickness of the 1-span system is again evident in the required column sizes. Notably, the thicker floor elements in systems 2 and 4b contribute to their increased weight compared to systems 3 and 4.

Due to the thin floors of systems 3 and 4, as explained in section 4.2.1, the overall load on the columns is reduced. Therefore, a direct comparison between these systems is not equitable as these floors are unrealistically thin. The primary comparison lies between systems 2 and 4b, where 4b shows slightly larger column widths due to the thicker secondary beam. Both these systems show potential to yield the least embodied carbon outcome.

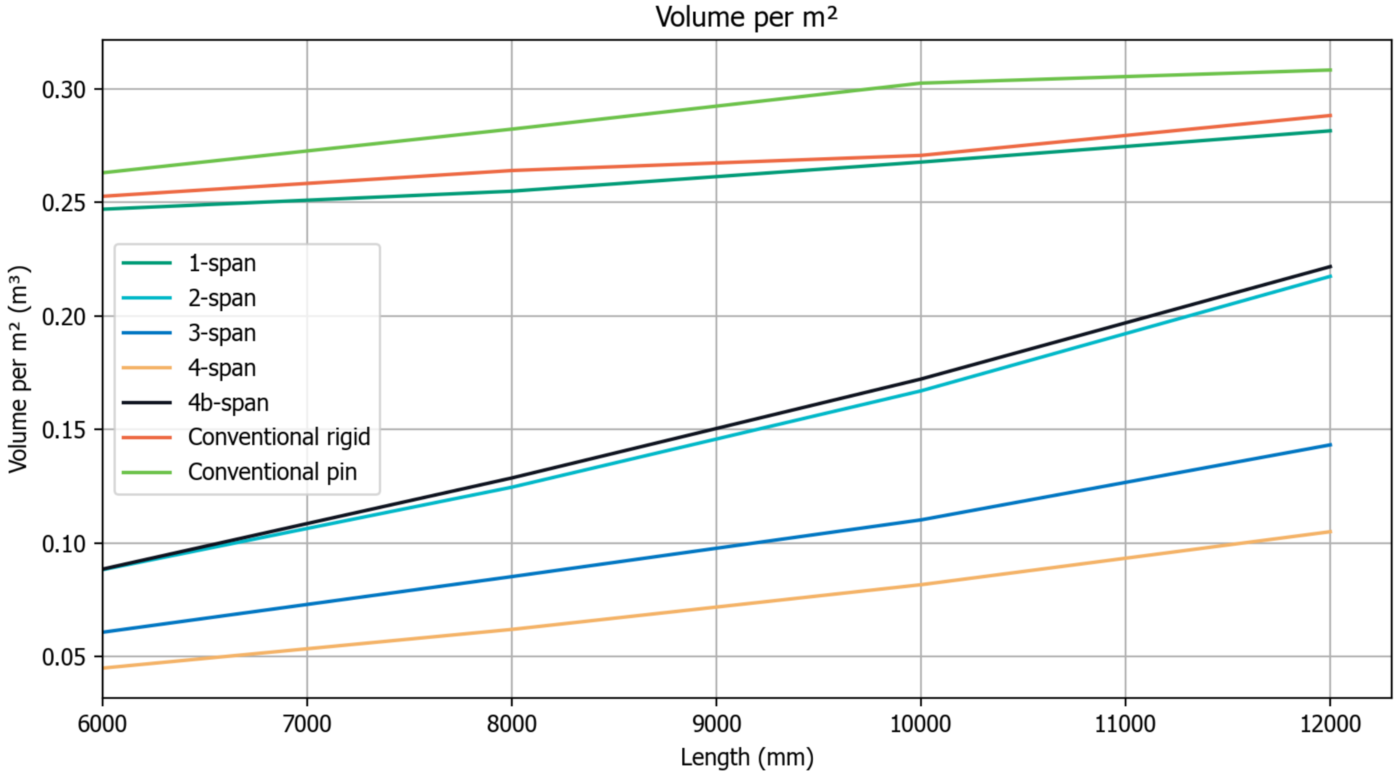

Fig. 51. Volumes per m² for different span systems including floor, beam and column elements [By author].

6.2.5 Volumes

After combining all the volumes of the floor, main and secondary beams, and the columns for each system, they are divided by the total square meters of that system to obtain a wood volume per square meter for a fair comparison. The trend of the volume closely resembles that of the columns, as the load on the columns is directly influenced by the volume of the wood.

6.2.6 Combined structural floor height

Fig. 52 illustrates the overall floor height, which combines the floor thickness, main and secondary beams, for each system. The height is based of the timber dry interlocking connection, resulting in vertically stacking all elements. Notable is the reversed trend of previous figures, where now configuration 2 and 4b are the tallest combined systems. This is due to the large secondary beam height.

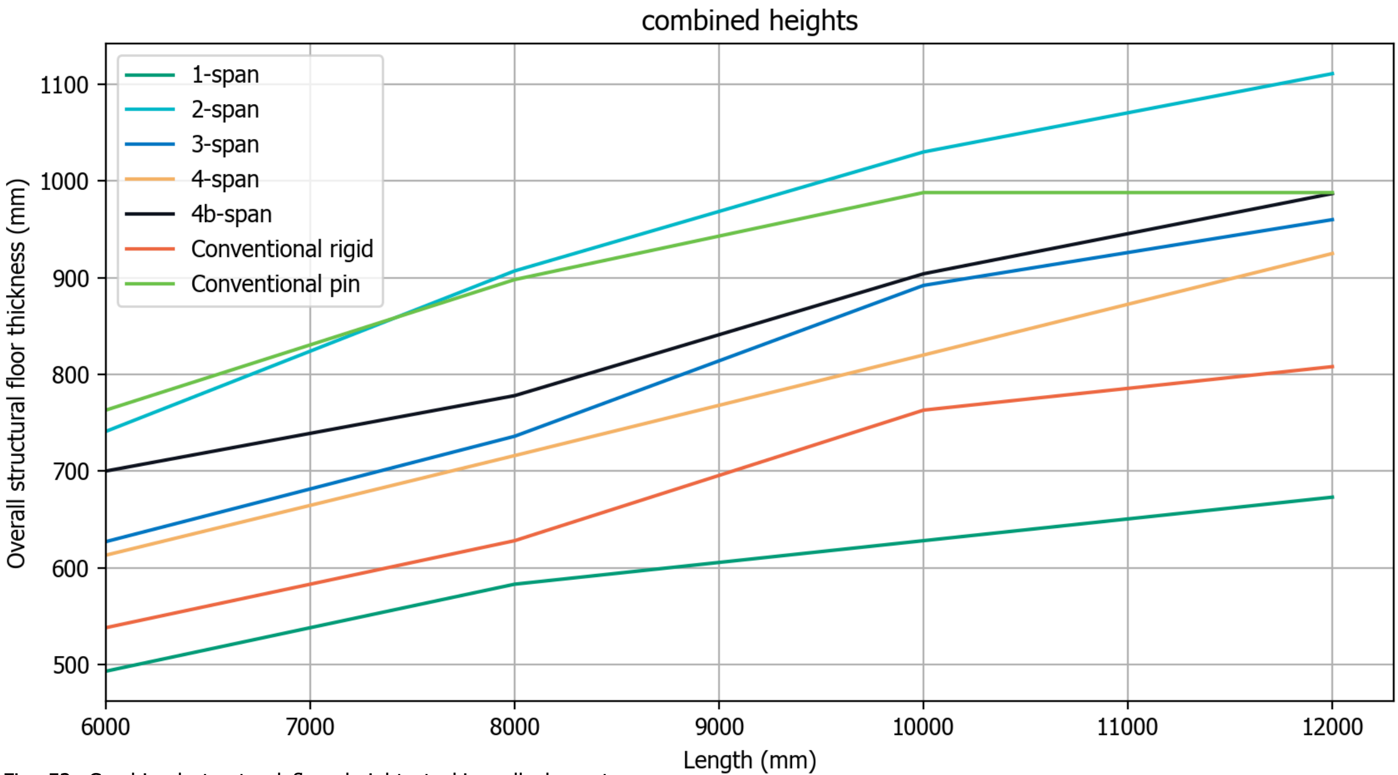

Fig. 52. Combined structural floor height stacking all elements per configuration [By author].

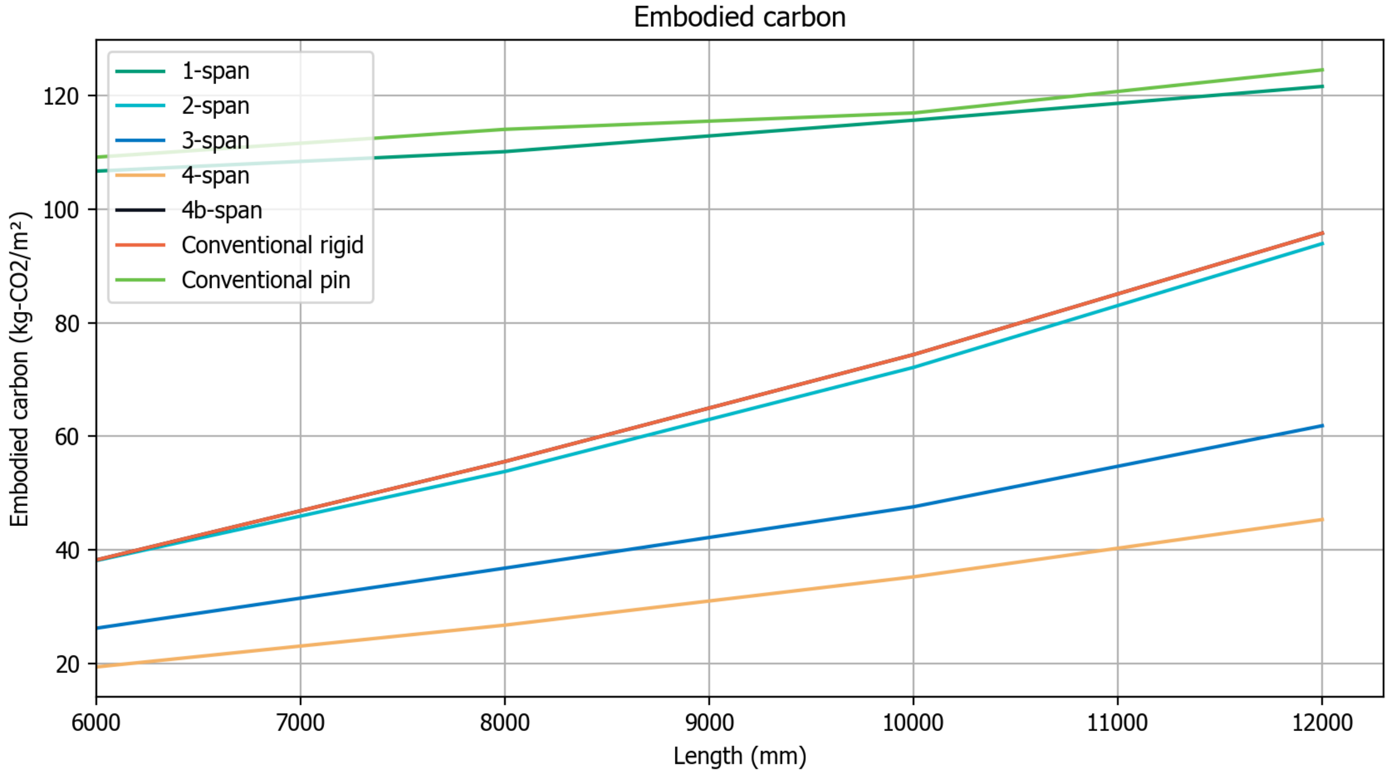

Fig. 53. Embodied carbon in kg CO_2/m² per configuration [By author].

6.2.7 Embodied carbon

Fig. 53 illustrates the embodied carbon for each configuration. The embodied carbon is calculated from the volume per m² and thus closely resembles the volume graph. The effect of adding the embodied carbon of the façade area covering the height of the structural floor system can be seen in Fig. 54. This is calculated dividing the representative structural floor height of the façade and corresponding embodied carbon, over the floor area, added together with the values of Fig. 46, resulting in a combined embodied carbon in kg CO_2/m².

Notable is the effect of the façade on the total embodied carbon in Fig. 55. By comparing this image with Fig. 54, the effect on the embodied carbon of stacking the secondary beams on top of the main beams becomes apparent. This difference of ±75 kg CO_2/m² is purely attributable to the additional height of the second beam over the main beam, resulting in extra façade area needed to cover the

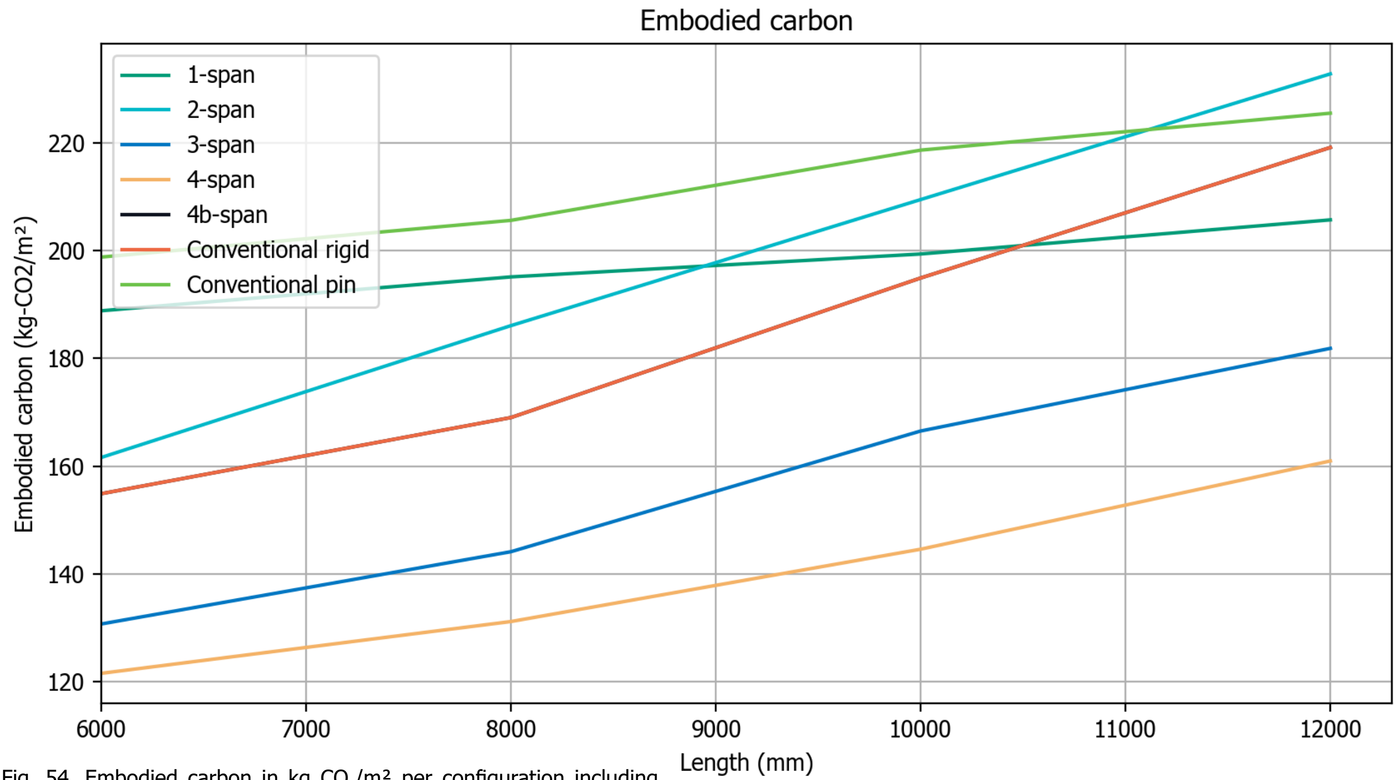

Fig. 54. Embodied carbon in kg CO_2/m² per configuration including embodied carbon of representative façade area [By author].

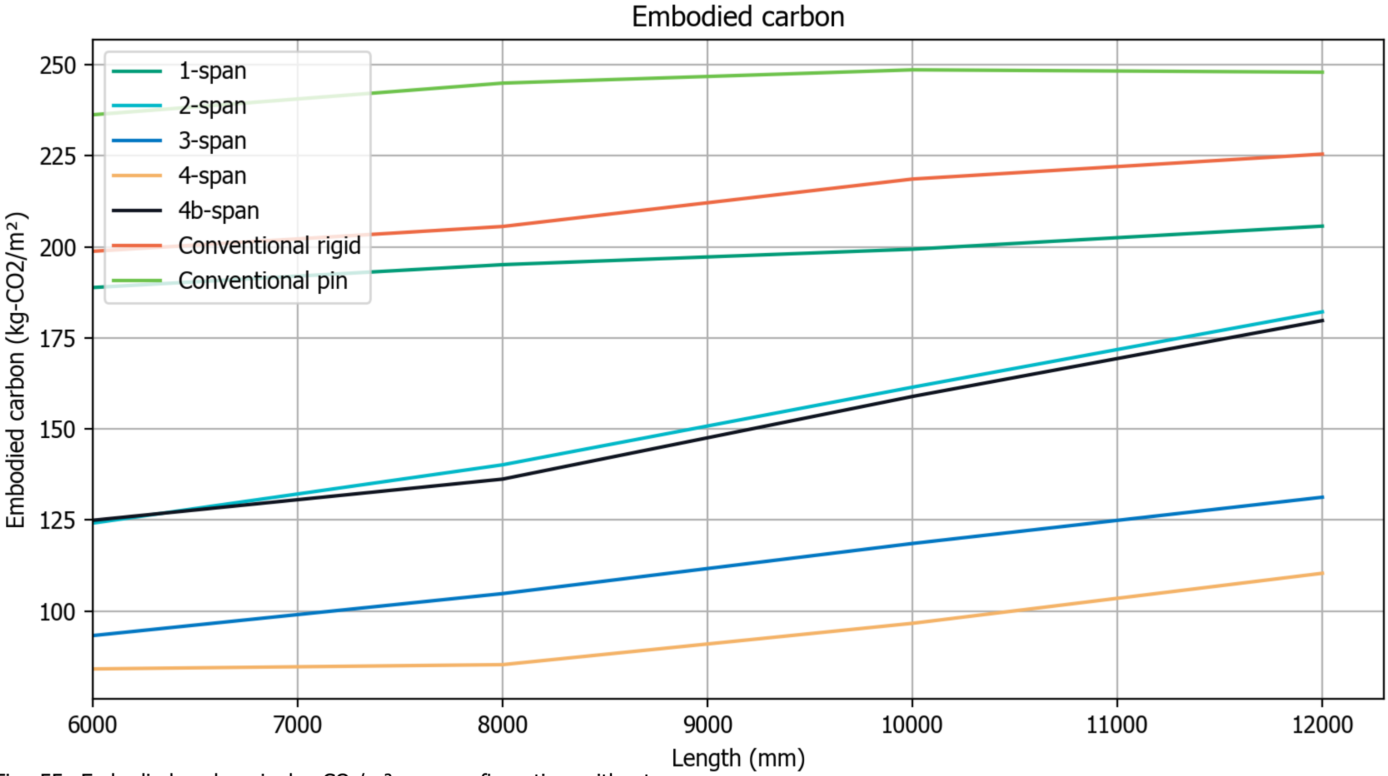

Fig. 55. Embodied carbon in kg CO_2/m² per configuration without secondary beam height, including embodied carbon of representative façade area [By author].

structural floor height, caused by the geometry of the timber dry joint.

6.3 Steel connectors

In this chapter the properties and embodied carbon of the different span systems are compared to the conventional benchmark of steel connections, for calculations regarding these steel connections, refer to Appendix D. Depicted in Fig. 56, is the effect of metal fasteners on the embodied carbon per m².

The effect of these metal fasteners is negligible, with an increment of 0,5-1 kg CO_2 per m² over the timber dry joint system. The amount of steel required to connect the beams to the columns is minimal, leading to only a slight increase in embodied carbon. Because the secondary beams can be positioned between the main beams using metal fasteners, the façade area required to cover the structural floor height is reduced, as shown in Fig. 55, for the dry joint system. Consequently, this emphasizes the importance of comparing Fig. 54 to Fig. 56.

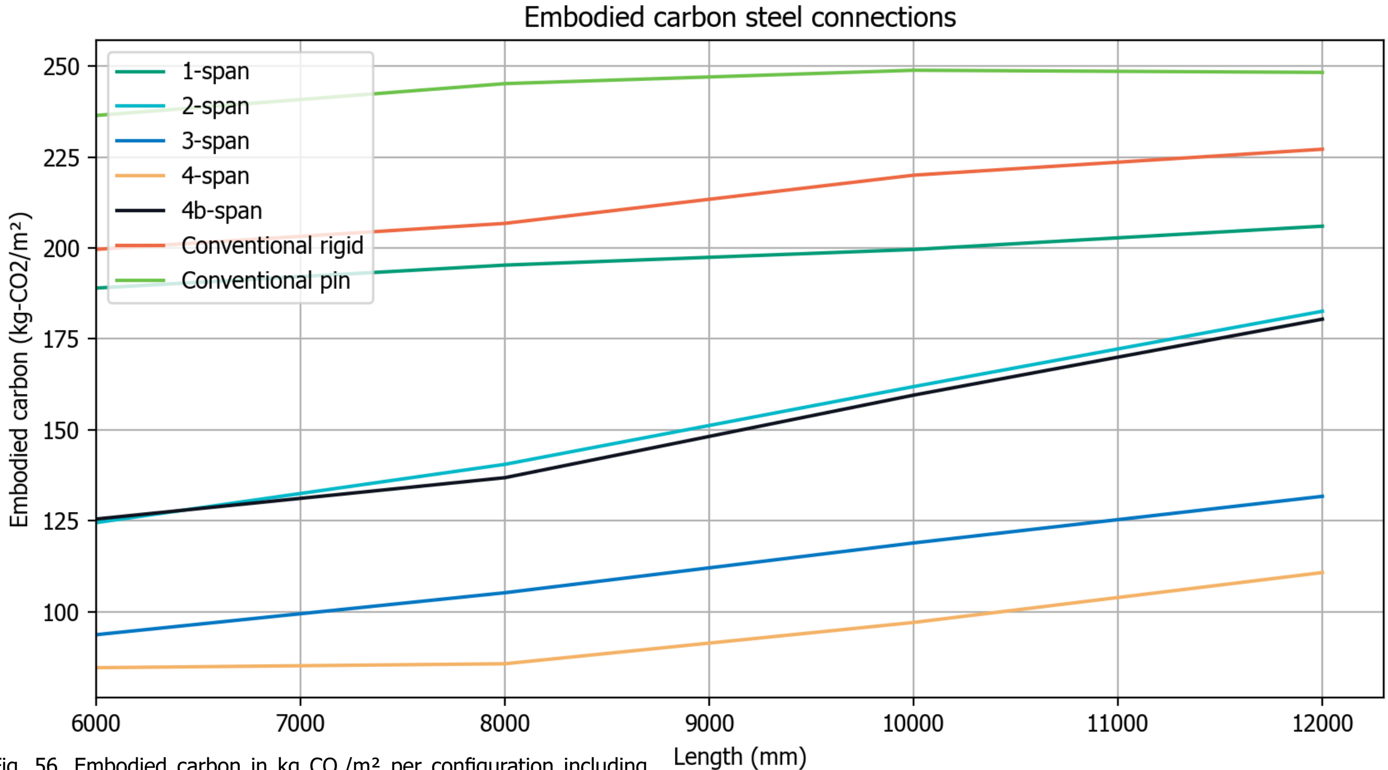

Fig. 56. Embodied carbon in kg CO_2/m² per configuration including embodied carbon of representative façade area and metal fasteners [By author].

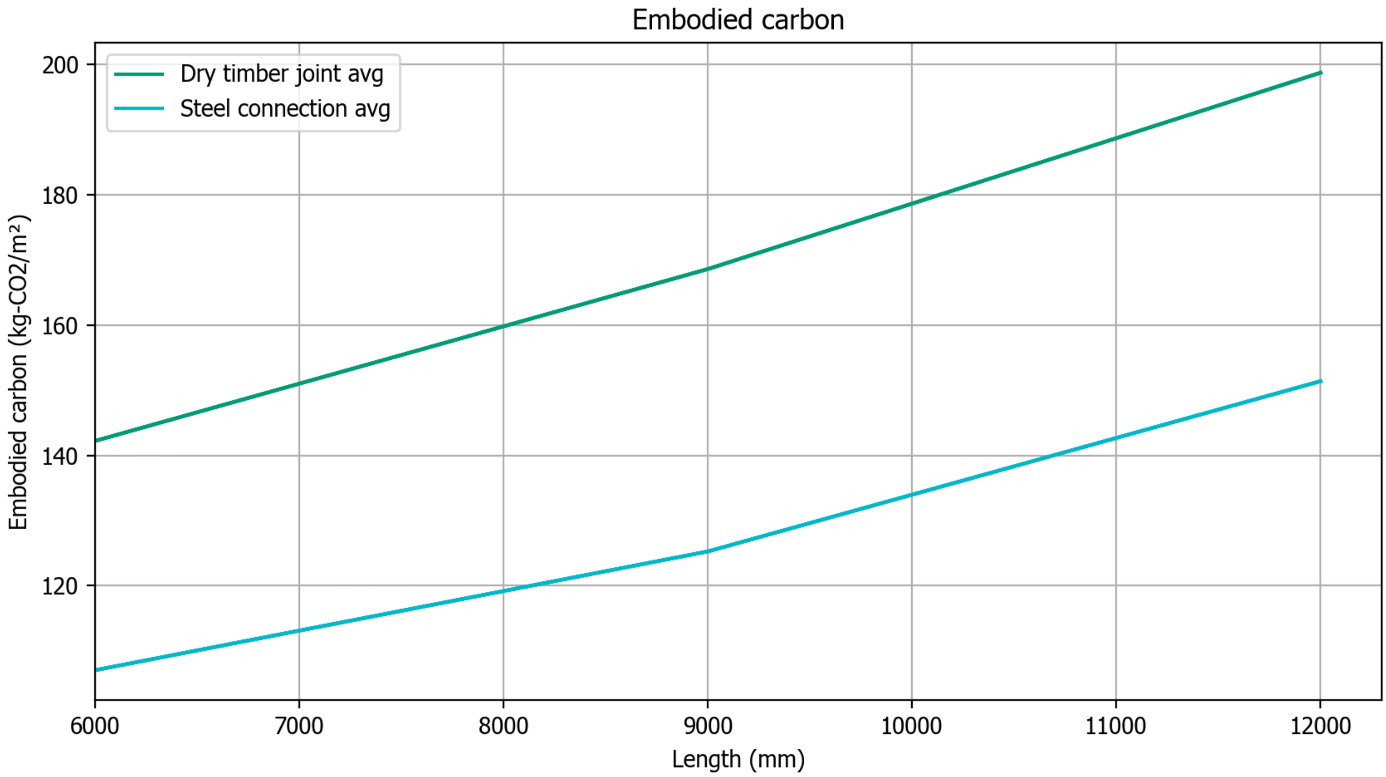

Fig. 57. Comparison of Embodied carbon in kg CO_2/m^2 between the timber dry system and the steel connector system, including embodied carbon of representative façade area and metal fasteners [By author].

Visible in Fig. 57 is difference in embodied carbon between the timber dry system and the steel connector system. Depicted are the averages of systems 2 to 4b of the two typologies. The single span system is excluded from these averages since it is the same for both systems and would distort the average. Noticeable is the difference in averages of 40 kg CO_2/m^2 between the two systems. This is due to the influence of the additional height caused by the secondary beam and the extra façade surface area it generates. Because of the small steel volume needed for the connections in this system, they have only a small contribution to the overall embodied carbon per square meter of the frame.

07

Conclusions

Conclusions

In this chapter, the main and sub research questions will be answered. Firstly, a brief overview of the context is provided. Timber building frames represent a significant advancement in reducing the embodied carbon of building structures compared to concrete or steel. However, they are not yet fully optimized. Timber building frames primarily consist of wooden floors, beams, and columns connected with metal fasteners. In the quest to further decrease the embodied carbon of these building frames, efforts have been made to reduce the embodied carbon of the connections, thus optimizing the entire frame. Where based on the literature embodied carbon savings of up to 76% could be made.

7.1 Timber dry joint design conclusions

7.1.1 Sub question I:

How to construct a timber dry joint with a rotational stiffness matching the stiffness of a rigid connection?

Reviewing the results from section 2.2 and 3.3, it is evident that the embedment length, and consequently the geometry allowing for embedment through the entire column, along with the corresponding column depth, are the primary contributors to rotational stiffness. As explored in joint 2, where the secondary beams act as additional support, effectively elongating the embedment length, the highest stiffness is observed. From a geometric standpoint, the most crucial factor is the embedment length, although factors such as timber grade and beam dimensions also play a role.

An interesting observation is the ratio between beam height and length and its impact on the added rotational stiffness of the connection. It is noted that per unit height added, the flexural rigidity of the beam increases more than the rotational stiffness. This results in a decrease in the added effect of rotational stiffness on the deflection for taller beams.

A significant drawback of the timber dry joints, both in the theoretically researched and self-designed joints, is the reduction in the cross-sectional area of the columns. This reduction can result in columns failing at the connection or being over-dimensioned, leading to inefficient designs.

7.1.2 Sub question II:

How effective are timber dry joints in reducing beam height?

When comparing the various timber dry joints against the theoretically infinite rigid connection, the conclusion is drawn that the effect of rotational embedment on increasing the stiffness of the beam is minimal. In the most effective case, as observed in joint 2 from section 3.3 a reduction in deflection from 15.4 mm for the pinned connection, to a deflection of 12.9 mm for the timber dry joint vs. a deflection of 3.4 mm for the rigid connection is observed. Resulting in a reduction of 2.5mm and showing 1/4th of the reduction of rigid connection provides. With this observation, sub question II can be answered as: Timber dry joints are not significantly effective on reducing beam height and thus timber volume.

7.1.3 Sub question III:

How can timber dry joints exhibit ductile behaviour?

Observed from the literature are the different failure modes exhibited by the specimens. It is noted that timber exhibits plastic deformation in compression, while displaying brittle failure mechanisms in tension. Designing a timber dry joint limited by compressive forces, i.e., compressive embedment from rotation, appears to be the most effective approach.

The reduction in strength of the timber from the plastic embedment causes large rotations in the connection, resulting in large deformations, providing a visual warning that the beam is excessively loaded before failing.

7.2 Continuous beam design conclusions

7.2.1 Sub question IV

What is the effect of utilizing an continuous beam on the embodied carbon?

By shifting the end of the beam away from the column and creating a connection at the point of contraflexure, a connection as rigid as the flexural rigidity of the beam is made.

This results in creating rigid connection without using additional materials, where normally this requires a lot of material and engineering. The effects of this connection, are the reduced beam dimensions needed to support the structure, lowering the embodied carbon.

7.2.1 Sub question V

What is the effect of utilizing different floor span systems on the embodied carbon?

Observable from section 6.2.1, the floor thickness significantly decreases when comparing a conventional single-span floor system to the provided multiple-span systems. This reduction is attributed to the shorter span lengths and less stringent deflection requirements for beams compared to floor elements, enabling slimmer designs using different span systems The '4-span' system proves to be the most effective, featuring the shortest spans resulting in the thinnest floor elements. However, they are so thin, they are not manufactured for the 6 meter span length in this test case.

Despite the introduction of secondary beams, the reduction of the embodied carbon ranges from 60 to 150 kg CO_2/m² from worst to best scenario, solely considering the timber volume. However, when considering additional façade area needed to cover the height of the different systems, as discussed in section 6.2.5, an average saving of approximately 75 kg CO_2/m² is achieved by choosing the multiple span systems over the single span system.

7.2.1 Sub question VI

What is the effect of timber dry joints on the embodied carbon compared to steel fasteners?

Derived from section 6.3.1, the quantity and volume of fasteners required to connect the continuous beam section to the column and the secondary beams to the main beams is so minimal that it barely contributes to the overall embodied carbon. Examining only the connections, the embodied carbon may appear larger due to the introduction of a different material than wood. However, when dividing the amount of added steel and embodied carbon over the area of the entire framing structure, only an increase in embodied carbon of 0.5 to 1 kg CO_2 /m² is observed. Resulting in a negligible effect of connecting the beams via metal fasteners or timber dry interlocking geometry.

7.3 Main conclusion

What is the effect of implementing timber dry joints on the embodied carbon of timber building frames?

Concluding from all the calculations, having a timber dry joint with an interlocking geometry does not contribute to lowering the embodied carbon of building frames.

The added height of secondary beams, as they cannot be placed between the main beams, adds more embodied carbon to the frame than the savings made from eliminating steel connections. Even systems without secondary beams still have more embodied carbon than the simplest multi-span system with steel connectors, enabling a comparison between the single span system and the multiple-span systems. The introduction of the continuous beam and corresponding multiple span systems proved to significantly reduce the embodied carbon of the structural frame.

08

Discussion and recommendations

Discussion and limitations

In this chapter, the results and conclusions presented in this thesis will be discussed, following the order of sub questions. With a comprehensive comparison, assumptions have been made that could have a significant impact on the outcomes.

8.1 Rotational Stiffness

Sub question I: *How to construct a timber dry joint with a rotational stiffness matching the stiffness of a rigid connection?*

For the calculations of the different connections, the same material values were used. Some values were derived from the literature without clear evidence that these are the correct values, as sometimes only small number of specimens were tested, leaving large room for error. However, due to the consistency in the use of these values, the comparison between the connections is valid.

Although literature proves that the established calculation method for the Nuki joint is aligned with physical tests, it cannot be said with certainty that the exact same calculation method also works for the other connections. By only theoretically testing the wooden connections and not conducting physical tests, there is a potentially wide margin of error in the rotational stiffness of the designed connections. This margin of error could mean that the stiffness is greater than calculated, which would have a positive influence on the performance, but it could also mean that the connections would be weaker in reality than the calculated values.

Sub question (II): *How effective are timber dry joints in reducing beam height?*

The calculation does not account for a construction margin between the column and beams, which would lower the stiffness, as the initial rotation cannot provide immediate rotational resistance. Thus lowering the total flexural rigidity of the beam, increasing the midspan deflection. These uncertainties in performance can be further investigated to provide clear clarification on the effectiveness of timber dry joints in decreasing beam sizes. However, it has become clear that the ambition of creating a rigid timber dry joint to decrease mid span deflections, with the investigated techniques is not feasible, showing to little rigidity.

Sub question III: *How can timber dry joints exhibit ductile behaviour?*

Theoretically, following the calculations, both the designed dry joints should exhibit ductile behaviour. However, it is not accounted for in the calculations that a certain point of failure occurs. In joint 1, the described cantilever effect is a point of concern for the potential occurrence of concentrated tensile force at point A. As known from the literature, this can lead to a brittle failure mode. Due to the lack of physical testing of the elements, this cannot be confirmed with certainty.

Concluding the discussion on the research aimed at increasing the rotational stiffness of interlocking timber dry joints, it can be stated that, with the approaches investigated, significant improvements cannot be achieved, using the calculation methods outlined in chapter 2. Nevertheless, there are still additional geometries to be explored with varying properties that may yield different results.

8.2 Continuous beam connections

For the continuous beam concepts, several assumptions have been made.

Sub question IV: *What is the effect of utilizing an continuous beam on the embodied carbon?*

Assumed is made that to utilize the continuous beam, the loads on the floor are equal over the whole floor area, resulting in an equilibrium and thus no additional rotational forces acting on the beam.

Sub question V: *What is the effect of utilizing different floor span systems on the embodied carbon?*

It is assumed that, for determining the floor heights, the floors are calculated as simply supported beams using the beam theory. Embodied carbon is calculated taking values for glulam from Edupack [49]. The deflection limit for the floor elements is set to 5mm regardless of span length. This done according to Eurocode norms.

It is also assumed that the secondary beams are simply supported, resulting in a larger beam height. This is because the beams in this system are assumed to just be laid on top of the main beams.

Sub question VI: *What is the effect of timber dry joints on the embodied carbon compared to steel fasteners?*

For the steel required in the connections, a simple calculation has been made based on the normal force of the beam divided by the shear capacity of bolts in wood class C24. More detailed calculations can be made to obtain a more specific embodied carbon value. Including calculations for additional forces such as bending moments or forces resulting from wind pressure, other than the normal force transferred from beam to column. Tuning the strength of the bolted connection to the appropriate timber class used, would further increase the accuracy of the results. Due the availability of data-sheets for timber class C24, these values are used.

For the metal connection of the secondary beams to the main beams in the metal fasteners system, connection principles as shown in appendix D are chosen to match the visual qualities as having a dry joint. The embodied carbon of the connection elements is determined by utilizing the hanger system with strength closest to the calculated load. The dimensions of this type, along with the screws required, are then multiplied by the density of aluminium and the embodied carbon per kilogram of material, as these are made from aluminium. More connection principles could have been researched and more detailed calculations can be made to more accurately calculate the embodied carbon of these connections.

Main research question: *What is the effect of implementing timber dry joints on the embodied carbon of timber building frames?*

It is assumed that the façade has the size of a single frame bay, consisting of 6 meters times the length configurations being: 6, 9, or 12 meters. This is a large façade area relative to the floor area, making the effect of the embodied carbon of the façade on the total embodied carbon per m² significant. While this ratio may not commonly occur in reality, it clearly demonstrates the trend of the effect of additional beam height on the total embodied carbon of a building.

Additionally, only the façade height covering the height of the structural floor (bottom of beams to top of floor) is considered. The CO_2/m² value of the façade is based on a single source, as the actual CO_2/m² can vary, depending on various factors. An extra comparison in Appendix E, has been added to illustrate the effect of the façade on the embodied carbon of the entire frame for different CO_2/m² values of the façade.

8.3 Recommendations

Further research could explore the effect of implementing diagonal bracings between columns and beams in timber constructions. This research should aim on finding the optimal angle and configuration of the bracing, as well as taking into account the importance of not reducing column cross-sectional area. This research could offer more potential to re-introducing timber dry joints in modern timber engineering.

Another geometry optimization to be researched is increasing the embedment length by locally increasing the column section. Optimizing the ratio between the beam and column dimensions, enhancing the rotational stiffness. Finding a balance between increasing column volume and reducing beam volume could contribute to lowering embodied carbon in structural timber frames.

More research is needed to assess the effect, potential implementation, and limitations of using continuous timber beams instead of moment-resisting connections in timber frames. Additionally, the influence of variable loads on the performance of this type of connection should be examined as imbalances could have large influences. Furthermore, the effect and feasibility of using continuous floor elements supported by (multiple) secondary beams, as this could result in a reduction in floor height, should be explored.

Another area requiring research is the effect of sound transmission between different functions distributed over the same floor element. While current standards for sound insulation are very high, it is necessary to investigate whether this could lead to comfort issues and whether applying extremely good sound insulation would result in higher embodied carbon than saved by this multi-span principle.

09

References

References

[1] Drdácký, M., Mlázovský, V., & Růžička, P. (2004). Historic Carpentry in Europe: Discoveries and Potential. In Source: APT Bulletin: The Journal of Preservation Technology (Vol. 35, Issue 3).

[2] Van Nimwegen, S. E., & Latteur, P. (2023). A state-of-the-art review of carpentry connections: from traditional designs to emerging trends in wood-wood structural joints. Journal of Building Engineering, 78, 107089. https://doi.org/10.1016/j.jobe.2023.107089

[3] Lam, F., He, M., & Yao, C. (2008). Example of traditional tall timber buildings in China - The Yingxian Pagoda. Structural Engineering International: Journal of the International Association for Bridge and Structural Engineering (IABSE), 18(2), 126–129. https://doi.org/10.2749/101686608784218743

[4] Fang, D. L. (2020). Timber joinery in modern construction: Mechanical behavior of wood-wood connections.

[5] J.L. Arlet, Innovative carpentry and hybrid joints in contemporary wooden architecture, Arts 10 (2021) 64,

[6] A. Thomson, R. Harris, P. Walker, M. Ansell. Development of non-metallic timber connections for contemporary applications, 2015.

[7] IStructE-TRADA: Manual for the design of timber building structures to Eurocode 5. IStructE, London, 2007.

[8] N. Steinhardt, Chapter 9: the Chinese building standards, in: Chinese Architecture (A History) II, Princeton University Press, 2019

[9] T. Abergel, B. Dean, J. Dulac, Towards a Zero-Emission, Efficient, and Resilient Buildings and Construction Sector: Global Status Report 2017, vol. 22, UN Environment and International Energy Agency, Paris, France, 2017.

[10] J. Shanks, P. Walker, Strength and stiffness of all-timber pegged connections, J. Mater. Civ. Eng. 21 (2009)

[11] J. Hart, F. Pomponi, More timber in construction: unanswered questions and future challenges, Sustainability 12 (2020)

[12] J. Cappellazzi, M.J. Konkler, A. Sinha, J.J. Morrell, Potential for decay in Mass Timber elements: a review of the risks and identifying possible solutions, Wood Mater. Sci. Eng. 15 (2020)

[13] J.L. Skullestad, R.A. Bohne, J. Lohne, High-rise timber buildings as a climate change mitigation measure – a comparative LCA of structural system alternatives,
Energy Proc. 96 (2016)

[14] Z. Chen, H. Gu, R.D. Bergman, S. Liang, Comparative life-cycle assessment of a high-rise Mass Timber building with an equivalent reinforced concrete alternative using the athena impact estimator for buildings, Sustainability 12 (2020)

[15]. J. Geno, J. Goosse, S. van Nimwegen, P. Latteur, Parametric design and robotic fabrication of whole timber reciprocal structures, Autom. ConStruct. 138 (2022)

[16] M.H. Ramage, H. Burridge, M. Busse-Wicher, G. Fereday, T. Reynolds, D.U. Shah, G. Wu, L. Yu, P. Fleming, D. Densley-Tingley, J. Allwood, P. Dupree, P. F. Linden, O. Scherman, The wood from the trees: the use of timber in construction, Renew. Sustain. Energy Rev. 68 (2017)

[17] A. Karolak, J. Jasie´nko, K. Raszczuk, Historical scarf and splice carpentry joints: state of the art, Herit. Sci. 8 (2020)

[18] Zwerger, K. (2021). Recognizing the similar and thus accepting the other: the European and Japanese traditions of building with wood. Journal of traditional building, architecture and urbanism, 2, 305–317. https://doi.org/10.51303/jtbau.vi2.520

[19] A.O. Feio, P.B. Lourenço, J.S. Machado, Testing and modeling of a traditional timber mortise and tenon joint, Mater. Struct. 47 (2014) 213–225, https://doi.org/10.1617/s11527-013-0056-y

[20] D.T. Burnett, P. Clouston, D.T. Damery, P. Fisette, Structural properties of pegged timber connections as affected by end distance, For. Prod. J. 53 (2003)

[21] Mueller, C. T., Fang, D., & Mueller, C. (n.d.). Joinery connections in timber frames: analytical and experimental explorations of structural behavior. https://www.researchgate.net/publication/326674720 (2018)

[22] W.-S. Chang, A. Thomson, R. Harris, P. Walker, J. Shanks, Development of all-wood connections with plywood flitch plate and oak pegs, Adv. Struct. Eng. 14 (2011)

[23] B. Kromoser, M. Braun, M. Ortner, Construction of all-wood trusses with plywood nodes and wooden pegs: a strategy towards resource-efficient timber construction, Appl. Sci. (2021)

[24] A. Rezaei Rad, H. Burton, Y. Weinand, Performance assessment of through-tenon timber joints under tension loads, Construct. Build. Mater. 207 (2019)

[25] A.C. Nguyen, P. Vestartas, Y. Weinand, Design framework for the structural analysis of free-form timber plate structures using wood-wood connections, Autom. ConStruct. 107 (2019)

[26] A. Rezaei Rad, H. Burton, N. Rogeau, P. Vestartas, Y. Weinand, A framework to automate the design of digitally-fabricated timber plate structures, Comput. Struct. 244 (2021)

[27] J. Gamerro, J.F. Bocquet, Y. Weinand, Experimental investigations on the load-carrying capacity of digitally produced wood-wood connections, Eng. Struct. 213 (2020).

[28] T.E. McLain, CDonnectors and fasteners: Research Needs and Goals, in: K.J. Fridley (Ed). Wood Engineering in the 21st Century, ASCE, Reston, VA , 1998, pp. 56-69.

[29] T. Smith, D. Moroder, F. Sarti, Stefano Pampanin, A.H. Buchanan, The reality of seismic engineering in a modern timber world. In Proceedings of INTER meeting 2015, 2015.

[30] Jorissen, A., & Fragiacomo, M. (2011). General notes on ductility in timber structures. Engineering Structures, 33(11), 2987–2997. https://doi.org/10.1016/j.engstruct.2011.07.024

[31] Trutalli, D., Marchi, L., Scotta, R., & Pozza, L. (2019). Capacity design of traditional and innovative ductile connections for earthquake-resistant CLT structures. Bulletin of earthquake engineering, 17, 2115-2136.

[32] R.Park, T. Paulay (Eds), Reinforced Concrete Structures, Wiley, 1975

[33] Hankinson, R. L. "Investigation of Crushing Strength of Spruce at Varying Angles of Grain." Air Service Information Circular 3 (259): 130. 1921

[34] Mauro's aantekeningen, bron controleren

[35] Inayama, M. (1991). Embedment theory of timber and its application (Doctoral dissertation, Ph. D. thesis, Japan, Tokyo: The University of Tokyo [in Japanese].).

[36] Roche, Stéphane Nicolas. 2017. "Semi-Rigid Moment-Resisting Behavior of Multiple Tab-and-Slot Joint for Freeform Timber Plate Structures." PhD, Lausanne, Switzerland: Ecole Polytechnique Federale de Lausanne. https://infoscience.epfl.ch/record/233607?ln=en.

[37] Fang, D., Mueller, C., Brütting, J., Fivet, C., Moradei, J. (2019). Rotational stiffness in timber joinery connections: Analytical and experimental characterizations of the Nuki joint. 229-236. 10.1201/9781315229126-28.

[38] Moradei, Julieta & Brütting, Jan & Fivet, Corentin & Sherrow-Groves, Nick & Wilson, Devon & Fischer, Aliz & Ye, Jingxian & Cañada, Javier. (2018). Structural Characterization of Traditional Moment-Resisting Timber Joinery.

[39] G. Y. Jeong, M.-J. Park, J.-S. Park and S.-J. Lee, "Predicting Moment Carrying Capacity of the "sagae" Connection Using Finite Element Method," Journal of Korean Wood Science & Technology, vol. 41, no. 5, pp. 415-424, 2013.

[40] W. Graubner, Holzverbindungen - Gegenüberstellung japanischer und europäischer Lösungen, München: Deutsche Verlags-Anstalt, 2015.

[41] E. M. Golden, Building from Tradition, London: Routledge, 2018.

[42] G. Y. Jeong, M.-J. Park, J.-S. Park and K. H. Hwang, "Predicting load-carrying capacity of dovetail connections using the stochastic finite element method," Wood and Fiber Science, vol. 44, no. 4, pp. 430-439, 2012.

[43] Chang, WS., Hsu, MF. & Komatsu, K. Rotational performance of traditional Nuki joints with gap I: theory and verification. J Wood Sci 52, 58–62 (2006). https://doi.org/10.1007/s10086-005-0734-7

[44] Wang, J., & Li, G. (2008). Simplified beam design for semi-rigid composite frames at the serviceability limit state. Tsinghua Science and Technology/Tsinghua Science and Technology, 13(5), 681–688. https://doi.org/10.1016/s1007-0214(08)70111-1

[45] Oikonomopoulou, Faidra & Bristogianni, Telesilla & Barou, Lida & Jacobs, Erwin & Frigo, Giulia & Veer, Frederic & Nijsse, Rob. (2018). Interlocking cast glass components, Exploring a demountable dry-assembly structural glass system. Heron. 63.

[46] The CLT Handbook - Swedish wood. (n.d.). Swedish Wood. https://www.swedishwood.com/publications/list_of_swedish_woods_publications/the-clt-handbook/

[47] Make. (2024, January 5). Comparing embodied carbon in façade systems. Make Architects. https://www.makearchitects.com/thinking/comparing-embodied-carbon-in-façade-systems/

[48] Patterson, T., Arup, Saint-Gobain Glass, Dodd, G., Saint-Gobain, Arup, Saint-Gobain Glass, & Bruno Mauvernay. (2021). Carbon footprint of façades: significance of glass. In Arup | Saint-Gobain Glass. https://www.arup.com/-/media/arup/files/publications/a/arup-sgg---carbon-footprint-of-façades.pdf

[49] Ansys GRANTA EduPack software, ANSYS, Inc., Cambridge, UK, 2024 v(www.ansys.com/materials).

[50] IStructE-TRADA: Manual for the design of timber building structures to Eurocode 5. IstructE, London, 2007.

[51] Pitzl. (2019). Innovative wood connection systems for highest requirements. https://www.pitzl-connectors.com/fileadmin/user_upload/dokumente/Kataloge/Katalog-2019_Verbinder-EN.pdf

10

Appendices

Table of contents

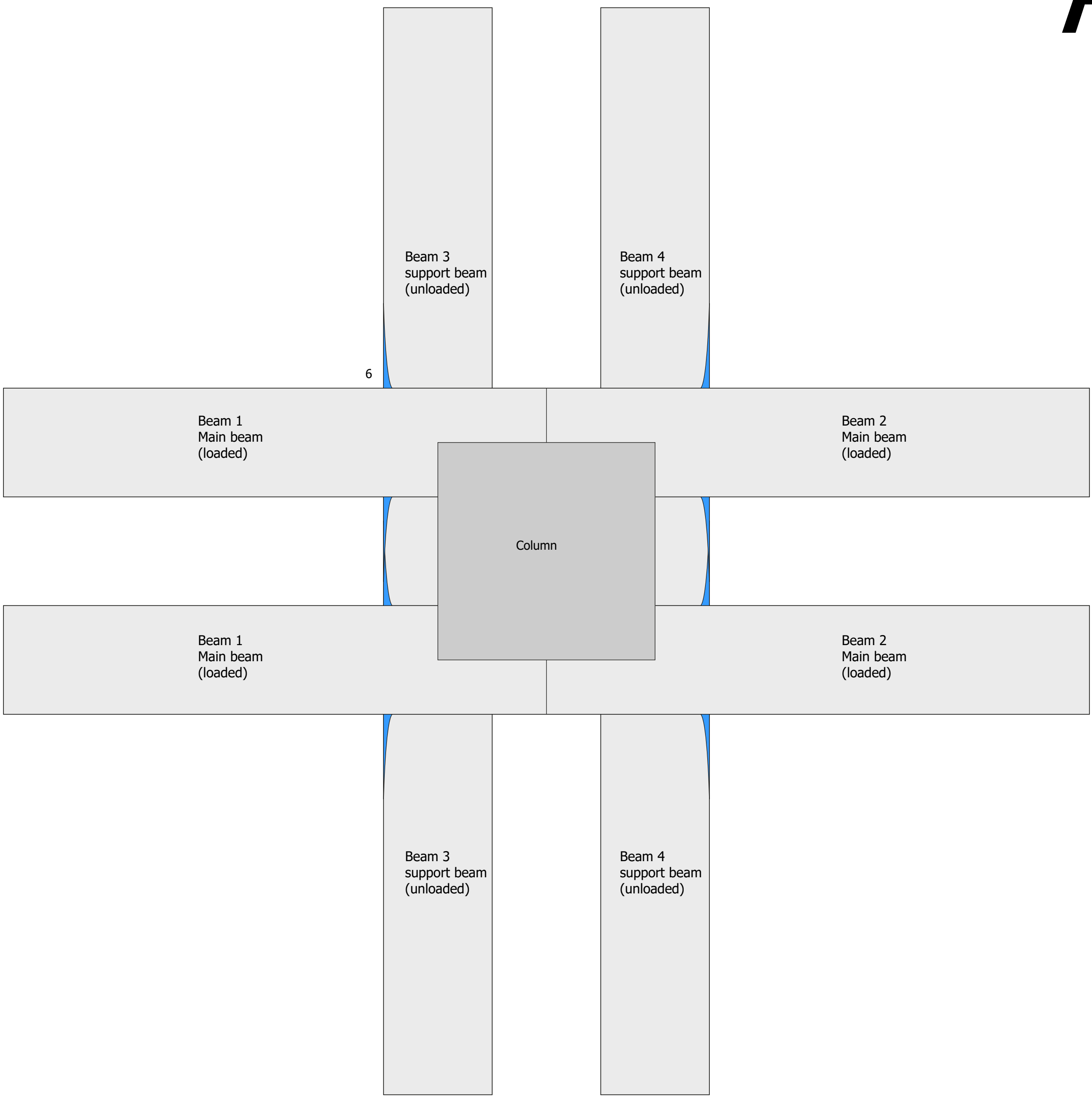

Top view of dry joint 2, blue areas are the additional embedment areas caused by the main beam embedding into the secondary beam.

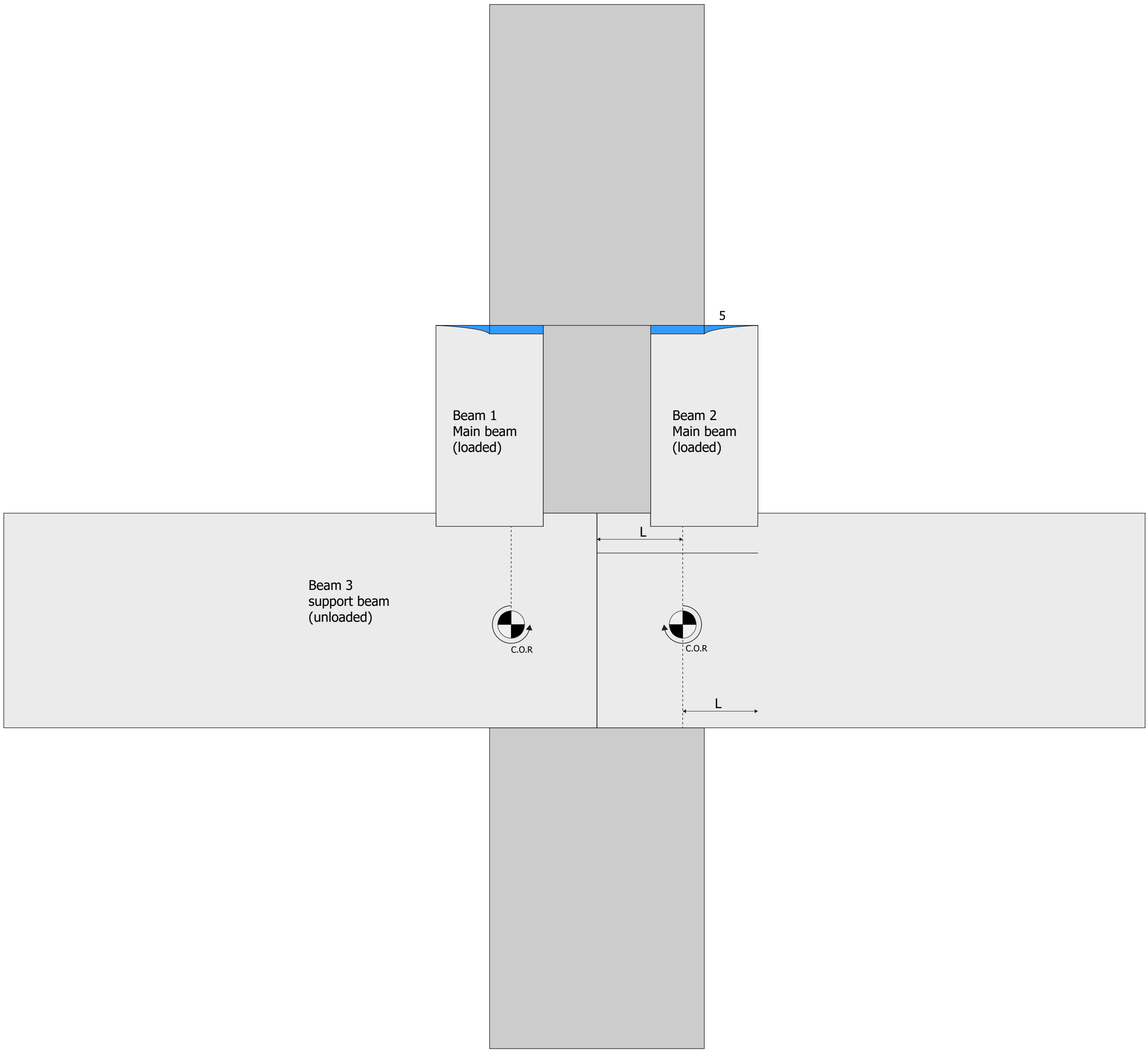

Side view of dry joint 2. The rectangular blue sections is the direct embedment from the main beam into the column, the area marked with a '5' is the additional embedment area caused by the direct embedment.

B

Defining points of contraflexure x_1 and x_2. As there are no clear equations, that are correct, available in literature. I established to create an equation myself.

Available in literature is the equation of the bending moment M_x at distance x of the connection:

$$M_x = \frac{w}{12}(6Lx - L^2 - 6x^2)$$

By setting this equation equal to 0, we can find the x where the bending moment is 0.

$$\frac{w}{12}(6Lx - L^2 - 6x^2) = 0$$

As the whole equation is between brackets, the load W can be factored out, leaving the equation to:

$$6Lx - L^2 - 6x^2 = 0$$

Rewriting to the known order of algebra:

$$-6x^2 + 6Lx - L^2 = 0$$

using the quadratic formula to find $x_{1,2}$:

$$x_{1,2} = \frac{-b \pm \sqrt{D}}{2a}$$

$$x_{1,2} = \frac{-6L \pm \sqrt{(6L)^2 - 4(-6)(-L^2)}}{2\,(-6)}$$

$$x_{1,2} = \frac{-6L \pm \sqrt{36L^2 - 24L^2}}{-12}$$

$$x_{1,2} = \frac{-6L \pm \sqrt{12L^2}}{-12}$$

$$x_{1,2} = \frac{-6L \pm 2\sqrt{3}\,L}{-12}$$

$$x_{1,2} = \frac{6L}{-12} \pm \frac{2\sqrt{3}L}{-12}$$

$$x_{1,2} = \frac{L}{2} \pm \frac{\sqrt{3}L}{6}$$

Resulting in:

$$x_1 = \frac{L}{2} - \frac{\sqrt{3}L}{6}$$

$$x_2 = \frac{L}{2} + \frac{\sqrt{3}L}{6}$$

Calculation of points of contraflexure, x_1 is the point at the left side of the beam, point x_2 is the point at the right side of the beam. With L as beam length.

C

```python
import numpy as np
import math

#ctrl + K + 0 = fold all
#ctrl + k + j = unfold all

def q_load(load, height, density):
    q = ((load + (height/1000) * density)) * 3 #N/mm = kN/m

    return q


def pin_1_way_span(q, L, E):
    # Function to calculate maximum deflection
    def d_max(L):
        return L / 300

    # Calculation for the needed I value
    I_needed = (5 * q * L**4) / (384 * (E/1000) * d_max(L))

    # Function to calculate moment of inertia
    def moment_of_inertia(b, h):
        return (b * h ** 3) / 12

    # Define the ratio range
    min_ratio = 1 / 4
    max_ratio = 1 / 2  # Default maximum ratio

    # Initialize variables to store the optimal dimensions and error
    optimal_b = 0
    optimal_h = 0
    min_error = float('inf')

    # Iterate through possible dimensions
    # Iterate through possible dimensions
    for h in range(45, 801, 45):  # Limit the height to multiples of 45mm
        min_width = max(45, int(h * min_ratio))  # Calculate the minimum width based on the height and min ratio, ensuring it's at least 45mm
        max_width = min(225, int(h * max_ratio))  # Calculate the maximum width based on the height and max ratio, ensuring it's not more than 225mm
        for b in range(min_width, max_width + 1, 5):  # Iterate through possible values of b based on the calculated width range with 5mm increments
            if (b / h) >= min_ratio and (b / h) <= max_ratio:  # Check if ratio is within bounds
                I = moment_of_inertia(b, h)
                error = abs(I - I_needed)
                if error < min_error:
                    min_error = error
                    optimal_b = round(b / 5) * 5  # Ensure optimal_b is divisible by 5
                    optimal_h = h

    return optimal_h, optimal_b

def fix_1_way_span(q, L, E):
```

```
    # Define the function to calculate maximum deflection
    def d_max(L):
        return L / 300

    # Calculation for the needed I value
    I_needed = (q * L**4) / (384 * (E/1000) * d_max(L))
    # # print("I_needed for 1 way fix = ", round(I_needed, 3), "mm^4")

    # Function to calculate moment of inertia
    def moment_of_inertia(b, h):
        return (b * h ** 3) / 12

    # Define the ratio range
    min_ratio = 1 / 4
    max_ratio = 1 / 2  # Default maximum ratio

    # Initialize variables to store the optimal dimensions and error
    optimal_b = 0
    optimal_h = 0
    min_error = float('inf')

    # Iterate through possible dimensions
    for h in range(45, 801, 45):  # Limit the height to multiples of 45mm
        min_width = max(45, int(h * min_ratio))  # Calculate the minimum width based on the height and min ratio, ensuring it's at least 45mm
        max_width = min(225, int(h * max_ratio))  # Calculate the maximum width based on the height and max ratio, ensuring it's not more than 225mm
        for b in range(min_width, max_width + 1, 5):  # Iterate through possible values of b based on the calculated width range with 5mm increments
            if (b / h) >= min_ratio and (b / h) <= max_ratio:  # Check if ratio is within bounds
                I = moment_of_inertia(b, h)
                error = abs(I - I_needed)
                if error < min_error:
                    min_error = error
                    optimal_b = round(b / 5) * 5  # Ensure optimal_b is divisible by 5
                    optimal_h = h

    return optimal_h, optimal_b


def pin_2_way_span(P, L, E):
    # Function to calculate maximum deflection
    L = L / 2
    def d_max(L):
        return L / 300

    # Calculation for the needed I value
    I_needed = ((P*2)*1000 * L**3) / (48 * (E/1000) * d_max(L))

    # Function to calculate moment of inertia
    def moment_of_inertia(b, h):
        return (b * h ** 3) / 12

    # Define the ratio range
    min_ratio = 1 / 4
    max_ratio = 1 / 2  # Default maximum ratio
```

```python

    # Initialize variables to store the optimal dimensions and error
    optimal_b = 0
    optimal_h = 0
    min_error = float('inf')

    # Iterate through possible dimensions
    # Iterate through possible dimensions
    for h in range(45, 801, 45):  # Limit the height to multiples of 45mm
        min_width = max(45, int(h * min_ratio))  # Calculate the minimum width based on the height and min ratio, ensuring it's at least 45mm
        max_width = min(225, int(h * max_ratio))  # Calculate the maximum width based on the height and max ratio, ensuring it's not more than 225mm
        for b in range(min_width, max_width + 1, 5):  # Iterate through possible values of b based on the calculated width range with 5mm increments
            if (b / h) >= min_ratio and (b / h) <= max_ratio:  # Check if ratio is within bounds
                I = moment_of_inertia(b, h)
                error = abs(I - I_needed)
                if error < min_error:
                    min_error = error
                    optimal_b = round(b / 5) * 5  # Ensure optimal_b is divisible by 5
                    optimal_h = h

    return optimal_h, optimal_b

def fix_2_way_span(P, L, E):
    # Define the function to calculate maximum deflection
    L = L / 2

    def d_max(L):
        return L / 300

    # Calculation for the needed I value
    I_needed = (P*2*1000 * L**3) / (192 * (E/1000) * d_max(L))
    # # print("I_needed = ", round(I_needed, 3), "mm^4")

    # Function to calculate moment of inertia
    def moment_of_inertia(b, h):
        return (b * h ** 3) / 12

    # Define the ratio range
    min_ratio = 1 / 4
    max_ratio = 1 / 2  # Default maximum ratio


    # Initialize variables to store the optimal dimensions and error
    optimal_b = 0
    optimal_h = 0
    min_error = float('inf')

    # Iterate through possible dimensions
    for h in range(45, 801, 45):  # Limit the height to multiples of 45mm
        min_width = max(45, int(h * min_ratio))  # Calculate the minimum width based on the height and min ratio, ensuring it's at least 45mm
        max_width = min(225, int(h * max_ratio))  # Calculate the maximum width based on the height and max ratio, ensuring it's not more than 225mm
```

```
        for b in range(min_width, max_width + 1, 5):  # Iterate through possible values of b based on the calculated width range with 5mm increments
            if (b / h) >= min_ratio and (b / h) <= max_ratio:  # Check if ratio is within bounds
                I = moment_of_inertia(b, h)
                error = abs(I - I_needed)
                if error < min_error:
                    min_error = error
                    optimal_b = round(b / 5) * 5  # Ensure optimal_b is divisible by 5
                    optimal_h = h

    return optimal_h, optimal_b


def pin_3_way_span(P, L, E):
    # Define the function to calculate maximum deflection
    def d_max(L):
        return (L / 300)


    a = L / 3

    # Calculation for the needed I value
    I_needed = (((P/2*1000) * a) / (24 * (E/1000) * d_max(L))) * ((3 * L**2) - (4 * a **2))
    # # print("I_needed 3 way span pin = ", round(I_needed, 3), "mm^4")

    # Function to calculate moment of inertia
    def moment_of_inertia(b, h):
        return (b * h ** 3) / 12

    # Define the ratio range
    min_ratio = 1 / 4
    max_ratio = 1 / 2  # Default maximum ratio

    # Initialize variables to store the optimal dimensions and error
    optimal_b = 0
    optimal_h = 0
    min_error = float('inf')

    # Iterate through possible dimensions
    for h in range(45, 801, 45):  # Limit the height to multiples of 45mm
        min_width = max(45, int(h * min_ratio))  # Calculate the minimum width based on the height and min ratio, ensuring it's at least 45mm
        max_width = min(225, int(h * max_ratio))  # Calculate the maximum width based on the height and max ratio, ensuring it's not more than 225mm
        for b in range(min_width, max_width + 1, 5):  # Iterate through possible values of b based on the calculated width range with 5mm increments
            if (b / h) >= min_ratio and (b / h) <= max_ratio:  # Check if ratio is within bounds
                I = moment_of_inertia(b, h)
                error = abs(I - I_needed)
                if error < min_error:
                    min_error = error
                    optimal_b = round(b / 5) * 5  # Ensure optimal_b is divisible by 5
                    optimal_h = h

    return optimal_h, optimal_b
```

```python

def fix_3_way_span(P, L, E,):
    # Define the function to calculate maximum deflection
    def d_max(L):
        return L / 300

    a = L / 3
    b = L - a

    # Calculation for the needed I value
    I_needed = (4 * P/2*1000 * a**3 * b**2 ) / (3 * (E/1000) * d_max(L) * (3*a + b)**2)
    # # print("I_needed 3 way fix = ", round(I_needed, 3), "mm^4")

    # Function to calculate moment of inertia
    def moment_of_inertia(b, h):
        return (b * h ** 3) / 12


    # Define the ratio range
    min_ratio = 1 / 4
    max_ratio = 1 / 2  # Default maximum ratio

    # Initialize variables to store the optimal dimensions and error
    optimal_b = 0
    optimal_h = 0
    min_error = float('inf')

    # Iterate through possible dimensions
    for h in range(45, 801, 45):  # Limit the height to multiples of 45mm
        min_width = max(45, int(h * min_ratio))  # Calculate the minimum width based on the height and min ratio, ensuring it's at least 45mm
        max_width = min(225, int(h * max_ratio))  # Calculate the maximum width based on the height and max ratio, ensuring it's not more than 225mm
        for b in range(min_width, max_width + 1, 5):  # Iterate through possible values of b based on the calculated width range with 5mm increments
            if (b / h) >= min_ratio and (b / h) <= max_ratio:  # Check if ratio is within bounds
                I = moment_of_inertia(b, h)
                error = abs(I - I_needed)
                if error < min_error:
                    min_error = error
                    optimal_b = round(b / 5) * 5  # Ensure optimal_b is divisible by 5
                    optimal_h = h

    return optimal_h, optimal_b


def pin_4_way_span_short(P1, P2, L, E):
    # Define the function to calculate maximum deflection
    def d_max(L):
        return L / 300

    a = L / 4
    b = L - a

    # Calculation for the needed I value
```

```
    I_needed = 2*(P1/2*1000 * a * b * (a + 2 * b)*(3 * a * (a + 2 * b))**(1/2)) / (27 * (E/1000) * d_max(L) * L) + (P2/2*1000 * a * b * (a + 2 * b)*(3 * a * (a + 2 * b))**(1/2)) / (27 * (E/1000) * d_max(L) * L)
    ## print("I_needed = ", round(I_needed, 3), "mm^4")

    # Function to calculate moment of inertia
    def moment_of_inertia(b, h):
        return (b * h ** 3) / 12

    # Define the ratio range
    min_ratio = 1 / 4
    max_ratio = 1 / 2  # Default maximum ratio

    # Initialize variables to store the optimal dimensions and error
    optimal_b = 0
    optimal_h = 0
    min_error = float('inf')

    # Iterate through possible dimensions
    for h in range(45, 801, 45):  # Limit the height to multiples of 45mm
        min_width = max(45, int(h * min_ratio))  # Calculate the minimum width based on the height and min ratio, ensuring it's at least 45mm
        max_width = min(225, int(h * max_ratio))  # Calculate the maximum width based on the height and max ratio, ensuring it's not more than 225mm
        for b in range(min_width, max_width + 1, 5):  # Iterate through possible values of b based on the calculated width range with 5mm increments
            if (b / h) >= min_ratio and (b / h) <= max_ratio:  # Check if ratio is within bounds
                I = moment_of_inertia(b, h)
                error = abs(I - I_needed)
                if error < min_error:
                    min_error = error
                    optimal_b = round(b / 5) * 5  # Ensure optimal_b is divisible by 5
                    optimal_h = h

    return optimal_h, optimal_b

def fix_4_way_span_short(P1, P2, L, E):
    # Define the function to calculate maximum deflection
    def d_max(L):
        return L / 300

    a = L / 4
    b = L - a

    # Calculation for the needed I value
    I_needed = 2*(4 * P1/2*1000 * a**3 * b**2 ) / (3 * (E/1000) * d_max(L) * (3* a + b)**2) + (4 * P2/2*1000 * a**3 * b**2 ) / (3 * (E/1000) * d_max(L) * (3* a + b)**2)
    ## print("I_needed = ", round(I_needed, 3), "mm^4")

    # Function to calculate moment of inertia
    def moment_of_inertia(b, h):
        return (b * h ** 3) / 12

    # Define the ratio range
    min_ratio = 1 / 4
    max_ratio = 1 / 2  # Default maximum ratio

```

```
    # Initialize variables to store the optimal dimensions and error
    optimal_b = 0
    optimal_h = 0
    min_error = float('inf')

    # Iterate through possible dimensions
    for h in range(45, 801, 45):  # Limit the height to multiples of 45mm
        min_width = max(45, int(h * min_ratio))  # Calculate the minimum width based on the height and min ratio, ensuring it's at least 45mm
        max_width = min(225, int(h * max_ratio))  # Calculate the maximum width based on the height and max ratio, ensuring it's not more than 225mm
        for b in range(min_width, max_width + 1, 5):  # Iterate through possible values of b based on the calculated width range with 5mm increments
            if (b / h) >= min_ratio and (b / h) <= max_ratio:  # Check if ratio is within bounds
                I = moment_of_inertia(b, h)
                error = abs(I - I_needed)
                if error < min_error:
                    min_error = error
                    optimal_b = round(b / 5) * 5  # Ensure optimal_b is divisible by 5
                    optimal_h = h

    return optimal_h, optimal_b

def pin_4_way_span_long(P1, L, E):
    L = L / 2
    def d_max(L):
        return L / 300

    # Calculation for the needed I value
    I_needed = ((P1)*1000 * L**3) / (48 * (E/1000) * d_max(L))
    # Function to calculate moment of inertia
    def moment_of_inertia(b, h):
        return (b * h ** 3) / 12

    # Define the ratio range
    min_ratio = 1 / 4
    max_ratio = 1 / 2  # Default maximum ratio

    # Initialize variables to store the optimal dimensions and error
    optimal_b = 0
    optimal_h = 0
    min_error = float('inf')

    # Iterate through possible dimensions
    for h in range(45, 801, 45):  # Limit the height to multiples of 45mm
        min_width = max(45, int(h * min_ratio))  # Calculate the minimum width based on the height and min ratio, ensuring it's at least 45mm
        max_width = min(225, int(h * max_ratio))  # Calculate the maximum width based on the height and max ratio, ensuring it's not more than 225mm
        for b in range(min_width, max_width + 1, 5):  # Iterate through possible values of b based on the calculated width range with 5mm increments
            if (b / h) >= min_ratio and (b / h) <= max_ratio:  # Check if ratio is within bounds
                I = moment_of_inertia(b, h)
                error = abs(I - I_needed)
                if error < min_error:
                    min_error = error
```

```
                    optimal_b = round(b / 5) * 5  # Ensure optimal_b is divisible by 5
                    optimal_h = h

    return optimal_h, optimal_b

def fix_4_way_span_long(P1, L, E):
    L = L / 2
    def d_max(L):
        return L / 300

    # Calculation for the needed I value
    I_needed = ((P1)*1000 * L**3) / (192 * (E/1000) * d_max(L))

    # Function to calculate moment of inertia
    def moment_of_inertia(b, h):
        return (b * h ** 3) / 12

    # Define the ratio range
    min_ratio = 1 / 4
    max_ratio = 1 / 2  # Default maximum ratio

    # Initialize variables to store the optimal dimensions and error
    optimal_b = 0
    optimal_h = 0
    min_error = float('inf')

    # Iterate through possible dimensions
    for h in range(45, 801, 45):  # Limit the height to multiples of 45mm
        min_width = max(45, int(h * min_ratio))  # Calculate the minimum width based on the height and min ratio, ensuring it's at least 45mm
        max_width = min(225, int(h * max_ratio))  # Calculate the maximum width based on the height and max ratio, ensuring it's not more than 225mm
        for b in range(min_width, max_width + 1, 5):  # Iterate through possible values of b based on the calculated width range with 5mm increments
            if (b / h) >= min_ratio and (b / h) <= max_ratio:  # Check if ratio is within bounds
                I = moment_of_inertia(b, h)
                error = abs(I - I_needed)
                if error < min_error:
                    min_error = error
                    optimal_b = round(b / 5) * 5  # Ensure optimal_b is divisible by 5
                    optimal_h = h

    return optimal_h, optimal_b



def secundairy_beam(w, E):
    # Define the function to calculate maximum deflection
    d_max = 6000 / 300


    # Calculation for the needed I value
    I_needed = (5 * w * (6000 ** 4)) / (384 * (E/1000) * d_max)
    ## print("I_needed = ", round(I_needed, 3), "mm^4")

    # Function to calculate moment of inertia
```

```python
    def moment_of_inertia(b, h):
        return (b * h ** 3) / 12

    # Define the ratio range
    min_ratio = 1 / 4
    max_ratio = 1 / 2  # Default maximum ratio

    # Initialize variables to store the optimal dimensions and error
    optimal_b = 0
    optimal_h = 0
    min_error = float('inf')

    # Iterate through possible dimensions
    for h in range(45, 801, 45):  # Limit the height to multiples of 45mm
        min_width = max(45, int(h * min_ratio))  # Calculate the minimum width based on the height and min ratio, ensuring it's at least 45mm
        max_width = min(225, int(h * max_ratio))  # Calculate the maximum width based on the height and max ratio, ensuring it's not more than 225mm
        for b in range(min_width, max_width + 1, 5):  # Iterate through possible values of b based on the calculated width range with 5mm increments
            if (b / h) >= min_ratio and (b / h) <= max_ratio:  # Check if ratio is within bounds
                I = moment_of_inertia(b, h)
                error = abs(I - I_needed)
                if error < min_error:
                    min_error = error
                    optimal_b = round(b / 5) * 5  # Ensure optimal_b is divisible by 5
                    optimal_h = h


    return optimal_h, optimal_b

def volume(floor, sec, main, L, width):
    Vf = floor / 1000 #per m²
    Vs = sec[0] * sec[1] / 1000000 #area m²
    Vm = main[0] * main[1] / 1000000 #area m²

    volume = (Vf * (L/1000) * (width/1000)) + Vs * (width/1000) + (Vm * L/1000) * 2 # Floorfield, two main beams and 2 second beams

    return volume

def volume_1_span(floor, length, main, width):
    Vm = main[0] * main[1] / 1000000

    volume_1 = (floor/1000)* (length/1000) * (width) + ((length/1000) * Vm * 2)  # Floorfield, two main beams and 2 second beams

    return volume_1


def rel_volume(floor, sec, main, L, width, column):
    Vf = floor / 1000 #per m²
    Vs = sec[0] * sec[1] / 1000000 #area m²
    Vm = main[0] * main[1] / 1000000 #area m²
    vc = (column * column / 1000000) * 3 #volume in m3 for 1 column

```

```
    volume = ((Vf * (L/1000) * (width/1000)) + Vs * (width/1000) + (Vm * L/1000) * 2 + vc) / (L/1000 * width/1000)  # volume per m2

    return volume

def rel_volume_1(floor, length, main, width, column):
    Vm = main[0] * main[1] / 1000000
    vc = (column * column / 1000000) * 3 #volume in m3 for 1 column

    volume = ((floor/1000)* (length/1000) * (width) + ((length/1000) * Vm * 2) + vc) / (length/1000 * width)  # Floorfield, two main beams and 2 second beams

    return volume


def column_size(load, volume, density, L , Width):
    ### COLUMN CALCULATION ###
    #Axial force
    N = ((load) *1000) + volume * density #Newtons
    Kmod = 0.6
    Kc = 1
    fc0k = 21 #mpa
    Ym = 1.2

    #Design strength
    Fcd = Kmod * Kc *(fc0k / Ym) #MPa

    #number of stories on column
    stories = 1

    #column area needed
    A_needed_C = (N * (L/1000) * (Width/1000) * stories) / Fcd  #mm²

    #Column dimensions
    C_width = np.sqrt(A_needed_C)

    return C_width


def mbnf(load, floor, main, density, Width, L, sec,): #main beam normal force on connection to column
    N = load
    Vf = floor / 1000  # per m²
    Vm = main[0] * main[1] / 1000000  # area m²
    if sec:  # Check if secondary beam dimensions are provided
        Vs = sec[0] * sec[1] / 1000000  # area m²
    else:
        Vs = 0  # Set secondary beam area to 0 if not provided

    Normal_force = (Vf * ((Width / 1000 * L / 1000) / 4)) + (Vm * (L / 1000 / 2) * density + Vs * (L / 1000 / 2)) * density + N * ((Width / 1000 * L / 1000) / 4)  # kN

    return Normal_force


def overallheight_1(floor, main):
    height = floor + main[0]
```

```python
    return height

def overallheight(floor, main, sec):
    height = floor + main[0] + sec[0]
    return height

def overallheight_2(floor, main, sec):
    height = floor + main[0] #+ sec[0]
    return height


def CO2(volume, height, L, width, co):
    co2_volume = volume * 432
    co2_height = ((2* (L/1000) + 2* width) * height/1000 * co) / ((L/1000) * width) # omtrek (2 lange + 2 korte zijde) * hoogte in m = m² gevel * co2/m² = kg co2

    co2 = co2_volume  + co2_height

    return co2


def shearforce(load):
    A = load*1000 / 3.8 # mm² needed for shear force
    return A

def pointload(w, system_width):
    point = w * system_width/2
    return point

def pointload_2(w, system_width, L):
    r1 = r3 =  (3*w)/8 * (L/1000)/2 * system_width
    r2 = (10*w)/8 * (L/1000)/2 * system_width

    return r1,r2, r3


#reaction forces 3 spans (4 supports)
def pointload_3(w,system_width, L):
    r1 = r4 =  0.4 * w * (L/1000)/3 * system_width
    r2 = r3 =  1.1 * w * (L/1000)/3 * system_width

    return r1,r2, r3, r4

#reaction forces 4 spans (5 supports)
def pointload_4(w,system_width, L):
    r1 = r5 =  0.393 * w * (L/1000)/4 * system_width
    r2 = r4 =  1.143 * w * (L/1000)/4* system_width
    r3 = 0.928 * w * (L/1000)/4

    return r1,r2, r3, r4, r5

#reaction forces 4 spans (5 supports)
def pointload_4b(w,system_width, L):
    r1 = r5 =  0.393 * w * (L/1000)/2 * system_width
    r2 = r4 =  1.143 * w * (L/1000)/2 * system_width
    r3 = 0.928 * w * (L/1000)/2 * system_width
```

```python

    return r1,r2, r3, r4, r5



def calculate_bolts(beam_height, column_width, normal_force, options):
    # Initialize variables to track the best option
    best_option = None
    min_steel = float('inf')

    for bolt_size, bolt_strength in options:
        # Calculate the space required for each bolt
        bolt_radius = bolt_size / 2
        bolt_spacing = 4 * bolt_size
        distance_to_top = 4 * bolt_size
        distance_to_side = 3 * bolt_size

        # Calculate the total number of bolts needed based on normal force and bolt strength
        bolts_needed = math.ceil(normal_force / bolt_strength)

        # Check if bolts_needed is a prime number
        if bolts_needed > 1:
            prime = True
            for i in range(2, int(math.sqrt(bolts_needed)) + 1):
                if bolts_needed % i == 0:
                    prime = False
                    break
            if prime:
                bolts_needed += 1

        # Calculate the maximum number of bolts that can fit horizontally and vertically
        max_horizontal_bolts = math.floor((column_width - 2 * distance_to_side) / bolt_spacing)
        max_vertical_bolts = math.floor((beam_height - distance_to_top) / bolt_spacing)

        # Calculate the maximum number of bolts that can fit in the given area
        max_total_bolts = max_horizontal_bolts * max_vertical_bolts

        # Ensure that the number of bolts needed does not exceed the maximum possible
        total_bolts = min(bolts_needed, max_total_bolts)

        # Find the pair of factors closest to each other
        factors = []
        for i in range(1, total_bolts + 1):
            if total_bolts % i == 0:
                factors.append((i, total_bolts // i))

        # Select the pair of factors that are closest to each other
        min_difference = float('inf')
        selected_factors = (1, total_bolts)
        for factor_pair in factors:
            difference = abs(factor_pair[0] - factor_pair[1])
            if difference < min_difference:
                min_difference = difference
                selected_factors = factor_pair

```

```
        rows, columns = selected_factors

        # Calculate the number of bolts per row
        bolts_per_row = math.ceil(total_bolts / rows)

        # Calculate the distance between the bolts
        distance_between_bolts = bolt_spacing

        # Calculate the amount of steel required
        steel = total_bolts * math.pi * bolt_radius**2

        # Check if this option results in the minimum amount of steel
        if steel < min_steel:
            min_steel = steel
            best_option = (bolt_size, bolt_strength, total_bolts, rows, columns, bolts_per_row, round(steel))

    return best_option


def sec_beam_co2(*point_loads, L):
    # Define the matrix
    matrix = [
        (0.000072, 18, 19.6, 60),
        (0.0001008, 24, 31.4, 60),
        (0.0001728, 34, 47.1, 60),
        (0.0002112, 44, 62.7, 60),
        (0.000072, 18, 32.3, 100),
        (0.0001008, 24, 51.7, 100),
        (0.0001728, 34, 77.5, 100),
        (0.0002112, 44, 103.3, 100)
    ]

    total_co2 = 0

    for point_load in point_loads:
        # print("\nCalculating for point load:", point_load)

        # Find the closest capacity to the point load
        closest_capacity = min(matrix, key=lambda x: abs(x[2] - point_load))[2]
        # print("Closest cpacity:", closest_capacity)

       # Find the closest match based on both point load and capacity
        closest_match = min((row for row in matrix if row[2] == closest_capacity), key=lambda x: abs(x[0] - point_load))
        # print("Closest match:", closest_match)

        # Choose the screws length based on the selected column
        screw_length = closest_match[3]
        # print("Screw length:", screw_length)

        # Calculate CO2 emissions
        volume = closest_match[0]
        number_of_screws = closest_match[1]
        # print("Volume:", volume)
        # print("Number of screws:", number_of_screws)

```

```
        # Calculate the volume of screws (cylindrical shape) in m³
        screw_volume = (math.pi * ((5/2)**2) * screw_length * number_of_screws) / (10**9)  # Convert mm³ to m³
        # print("Screw volume (m³):", screw_volume)

        material_density = 2700  # kg/m³
        co2_per_kg = 12  # kg CO2 per kg material

        # Calculate CO2 emissions from volume and screws
        co2_volume = volume * material_density * co2_per_kg
        # print("CO2 emissions from volume:", co2_volume, "kg")

        # Calculate CO2 emissions from screws
        co2_screws = screw_volume * material_density * co2_per_kg
        # print("CO2 emissions from screws:", co2_screws, "kg")

        total_co2 += co2_volume + co2_screws
        co2_m2 = total_co2 / ((L/1000) * 6)

    return round(co2_m2,2)

```

D

```
def bolt_CO2(bolt_area, beam_width, column_width):
    volume = bolt_area/1000000 * (beam_width/1000 * 2 + column_width/1000)
    CO2 = volume * 7800 * 2.21 # volume m³* density kg/m³ * kg co2/kg weight.
    return CO2

def bolt_CO2_m2(CO2,L):
    result = CO2 / (L/1000 * 6)
    return result



# # Example usage:
# beam_height = 270  # in units
# column_width = 531  # in units
# normal_force = 63  # in units
# options = [
#     (8, 3.5),
#     (8, 3.94),
#     (8, 3.94),
#     (10, 4.19),
#     (10, 5.62),
#     (10, 5.83),
#     (12, 4.82),
#     (12, 6.64),
#     (12, 7.93),
#     (16, 5.9),
#     (16, 7.91),
#     (16, 12.18)
# ]

# best_option = calculate_bolts_and_area(beam_height, column_width, normal_force, options)
# if best_option:
#     bolt_size, bolt_strength, total_bolts = best_option
#     # print("Total bolts needed:", total_bolts)
#     # print("Total steel required:", total_bolts * math.pi * (bolt_size/2)**2)
# else:
#     # print("No suitable option found.")
```

Calculations of Bolts needed for connecting main beam to column. Values derived from: see next page

For loading perpendicular to the grain:

$$F_{v,Rd,\ 0} = k_{mod} \times \frac{1}{k_{90}} \times n \times \frac{F_{v,Rk,\ 0}}{\gamma_m}$$

where k_{90} is the modification factor that accounts for the weaker bearing strength when loading perpendicular to the grain as follows:

k_{90} = (1.35 + 0.015*f*) for softwood
= (1.30 + 0.015*f*) for LVL
= (0.9 + 0.015*f*) for hardwood

Characteristic lateral load capacity $F_{v,Rk}$ for selected fasteners :

Fastener		Assumed	Minimum	Minimum	Load parallel to the grain				Load perpendicular to the grain			
					Single shear		Double shear		Single shear		Double shear	
					Load capacity		Load capacity		Load capacity		Load capacity	
Diameter mm	Reference	Effective diameter (mm)	Timber thickness (mm)	Fastener length (mm)	C16 (kN)	C24 (kN)	C16 (kN)	C24 (kN)	C16 (kN)	C24 (kN)	C16 (kN)	C24 (kN)
Nails												
3.0	swg 11	1.3	36	72	0.73	0.78	–	–	0.62	0.67	–	–
3.4	swg 10	1.5	41	82	0.89	0.97	–	–	0.77	0.83	–	–
4.5	swg 7	4.5	54	108	1.43	1.55	–	–	1.22	1.32	–	–
5.5	swg 5	5.5	66	132	2.01	2.17	–	–	1.71	1.85	–	–
Small wood screws												
3.48	no. 6	2.6	28	84	0.79	0.84	–	–	0.61	0.68	–	–
4.17	no. 8	3.1	33	100	0.94	1.03	–	–	0.71	0.80	–	–
4.88	no. 10	3.6	39	117	1.27	1.41	–	–	0.99	1.09	–	–
5.59	no. 12	4.1	45	134	1.59	1.68	–	–	1.35	1.43	–	–
Large wood screws												
6.3	no.14	4.6	50	101	2.57	2.74	–	–	1.93	2.17	–	–
7.01	no. 16	5.1	84	112	3.09	3.29	–	–	2.61	2.78	–	–
7.93	8 mm coach	7.9	47	94	3.46	3.89	–	–	2.45	2.76	–	–
7.93	8 mm coach	7.9	63	126	3.51	3.89	–	–	2.66	2.92	–	–
9.52	10 mm coach	9.5	47	94	4.56	5.02	–	–	3.47	3.83	–	–
9.52	10 mm coach	9.5	63	126	5.24	5.58	–	–	3.83	4.31	–	–
12.5	12 mm coach	12.5	47	94	6.57	7.19	–	–	4.97	5.54	–	–
12.5	12 mm coach	12.5	97	194	8.40	8.96	–	–	6.15	6.78	–	–
Bolts												
8	M8	–	47	110	4.30	4.62	8.60	9.24	3.10	3.50	5.98	6.75
8		–	63	142	4.30	4.62	8.60	9.24	3.66	3.94	7.33	7.88
8		–	97	210	4.30	4.62	8.60	9.24	3.66	3.94	7.33	7.88
10	M10	–	47	114	6.41	6.89	10.75	12.14	3.71	4.19	7.17	8.09
10		–	63	146	6.41	6.89	12.83	13.78	4.97	5.62	9.61	10.85
10		–	97	214	6.41	6.89	12.83	13.78	5.43	5.83	10.85	11.66
12	M12	–	47	118	6.53	7.37	12.62	14.24	4.27	4.82	8.25	9.31
12		–	63	150	8.50	9.54	16.91	19.08	5.72	6.46	11.05	12.48
12		-	97	218	8.87	9.54	17.75	19.08	7.46	7.93	14.92	15.85
16	M16	–	47	126	8.31	9.39	16.06	18.13	5.23	5.90	10.10	11.40
16		–	63	158	11.14	12.58	21.52	24.30	7.01	7.91	13.54	15.28
16		–	97	226	14.76	15.88	29.52	31.75	10.79	12.18	20.84	23.53

Notes:
[a] Minimum headside thickness is 12*d* for nails and 4*d* for screws.
[b] Minimum coach screw pointside penetration is 6*d*.
[c] Assumed fastener strength, f_{uk} = 540 N/mm².
[d] Predrilling allowances made for large screws only.
[e] Values for service classes 1 and 2.
[f] Minimum spacings based on simplified rules.
[g] Round smooth shank nails/screws.
[h] Joint capacity = $F_{v,Rk}$ × number of shear planes × (effective) number of fasteners/γ_m, where typically γ_m = 1.3 for connections (except metal punched plates).

Spacing rules for nails

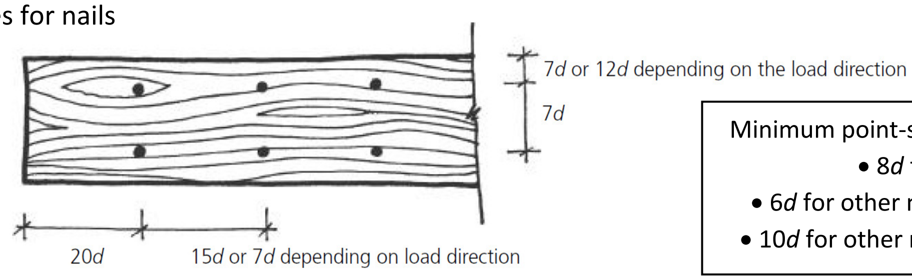

Minimum point-side penetration:

- 8*d* for smooth nails,
- 6*d* for other nails in side grain
- 10*d* for other nails in end grain

Spacing for screws $\phi \leqslant$ 6mm

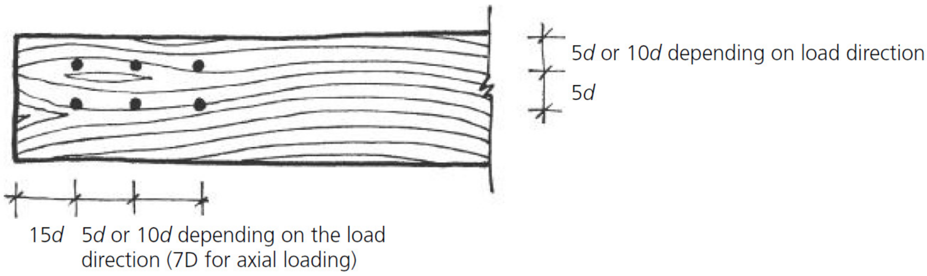

Spacing for bolts and large screws $\phi >$ 6mm

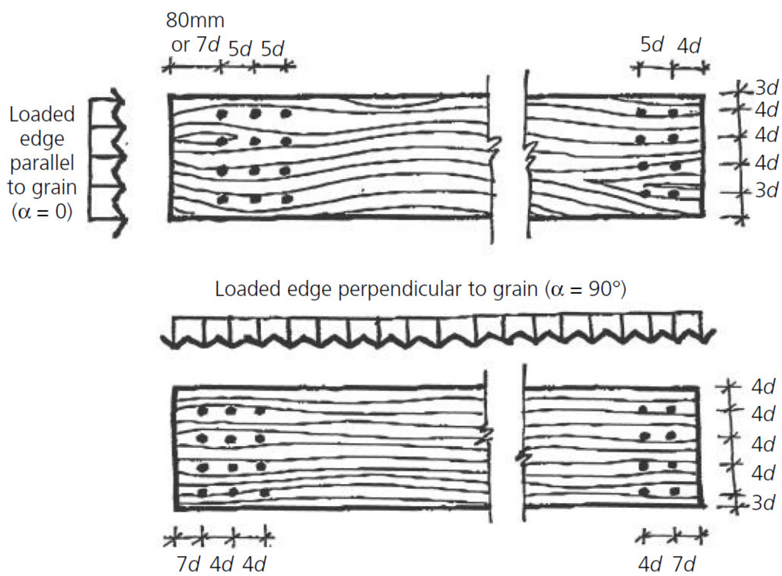

88210.0000

88214.0000

88318.0000

88322.0000

Productgroup	Screws size	Packing unit	CE
88___.0000	Ø 5 x 60 - 100	10	*

Art-No.	Dimensions w x h x d (mm)	Number of screws	Minimal timber section with screws Ø 5 x 60 (mm)		Characteristic load capacity*	
			Header	Joist	Ø 5 x 60	Ø 5 x 100
88210.0000	60 x 100 x 12	18	70 x 120	80 x 120	19,6	32,3
88214.0000	60 x 140 x 12	24	70 x 160	80 x 160	31,4	51,7
88318.0000	80 x 180 x 12	34	70 x 200	100 x 200	47,1	77,5
88322.0000	80 x 220 x 12	44	70 x 240	100 x 240	62,7	103,3

* $F_{2,Rk}$ (kN) for GL24h with fully threaded screws: Ø 5 x 60 with effective thread length of 54 mm and Ø 5 x 100 with effective thread length of 94 mm. For other screws and thread lengths or wood based materials: cf. design manual.

Also available

Connectors of the series 882 - 884 in double version (on page 13). Double width for double load capacity. The perfect connection for square timber sections or wide beams with low height.

Uplift protection

Alternatively the Pitzl HVP series 88004.0000 to 88322.0000 can be ordered with uplift-protection.

Option uplift protection:
With uplift protection: „.1000“
Order example: 88214.1000

Included in delivery:
Series 880 1 drilled hole + 1 self-tapping screw Ø 4 x 10 mm
Series 881 883 2 threaded drilled holes + 2 screws Ø 5 x 20 mm + 1 uplift protection flat steel

[51]

Make projects
Facade embodied carbon comparison

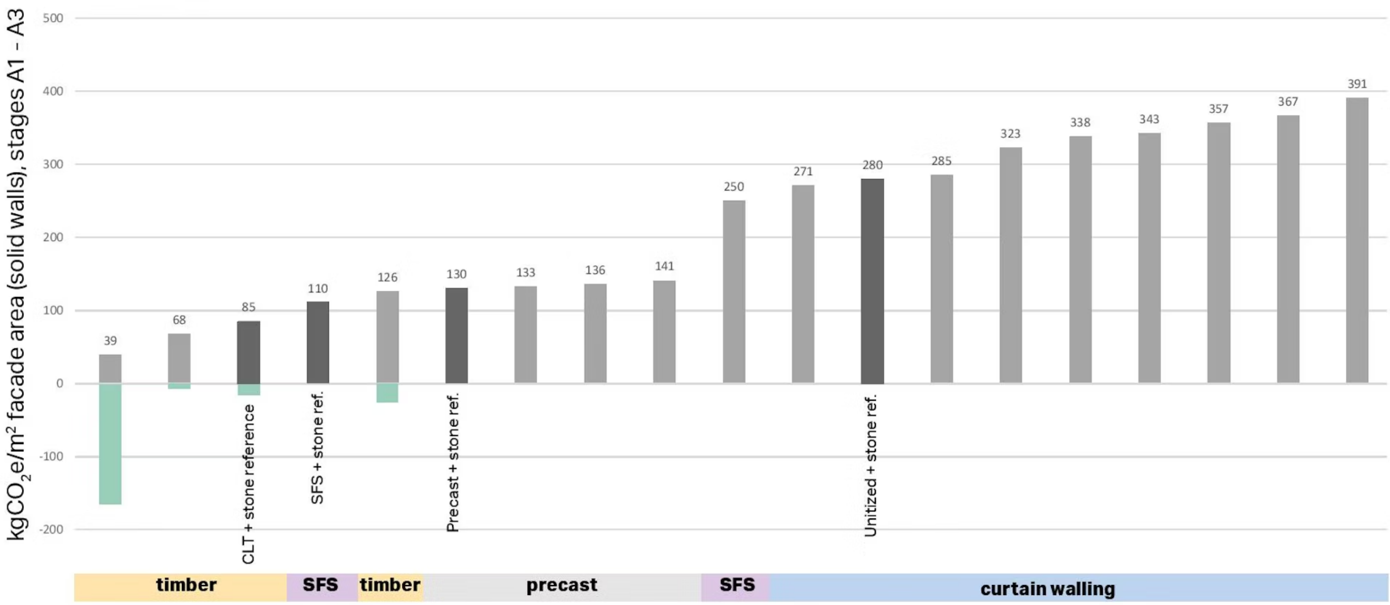

[47]

Facade systems comparison

Embodied carbon over façade life cycle

The diagram on the right shows the total embodied carbon for each façade system from cradle-to-grave (stages A to C) over a 60 year lifetime, in terms of each LCA stage.

The embodied carbon of a façade will vary significantly depending on the system type and design. For the 16 facades studied, the embodied carbon (A1 – A5, B4 and C1 – C4) ranged from 160 to 520 $kgCO_2e/m^2$ of façade.

The cradle-to-gate stages (A1 – A3) represent the majority contribution to the embodied carbon of the façade. The second largest contribution is stage B4, which represents the replacement of the glazing after 30 years in service, as is the typical LCA assumption. WT-10 (Deep cavity Double Skin Facade, 100% Single + DGU) had the largest overall cradle-to-grave embodied carbon, followed by WT-11 (Narrow cavity double skin façade, 100% Single + DGU) and WT-01 (Aluminium Unitised Curtain Wall, 100% DGU).

Over the page, we see 3D projection of the same data, with each façade typology sorted into a band of thermal ('U-value') and solar ('solar gains') performance. This can be used to give an indication of the way in which these facades may perform in operation.

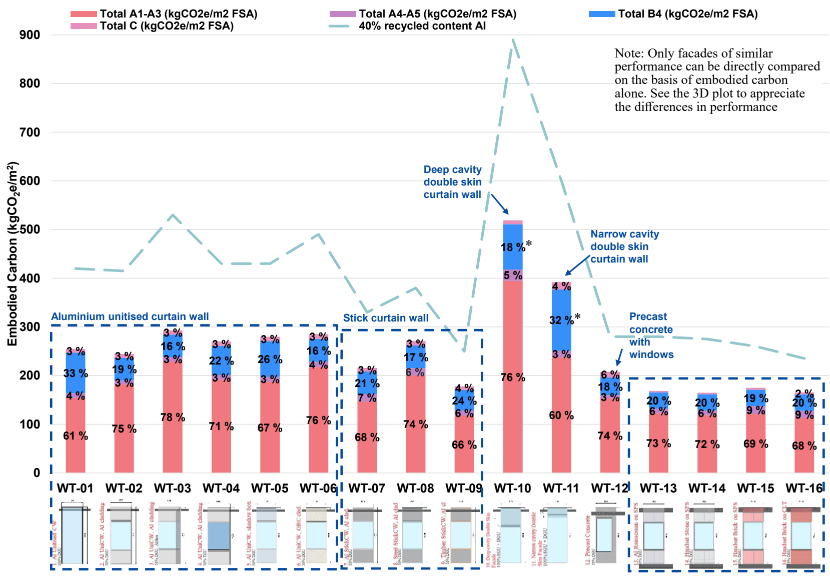

Embodied carbon by stage

A1-A5, B4, C ($kgCO_2e/m^2$) – 78% pre-consumer recycled content Aluminium
* The service life of the inner double glazed unit and outer laminated pane was defined as 30 years. If detailed to enable replacement of the inner IGU without affecting the outer laminate, the service life of the laminate could potentially be extended to 60 years, reducing the overall carbon impact during the B4 stage.

Carbon footprint of façades: significance of glass   Arup | Saint-Gobain Glass   18

[48]

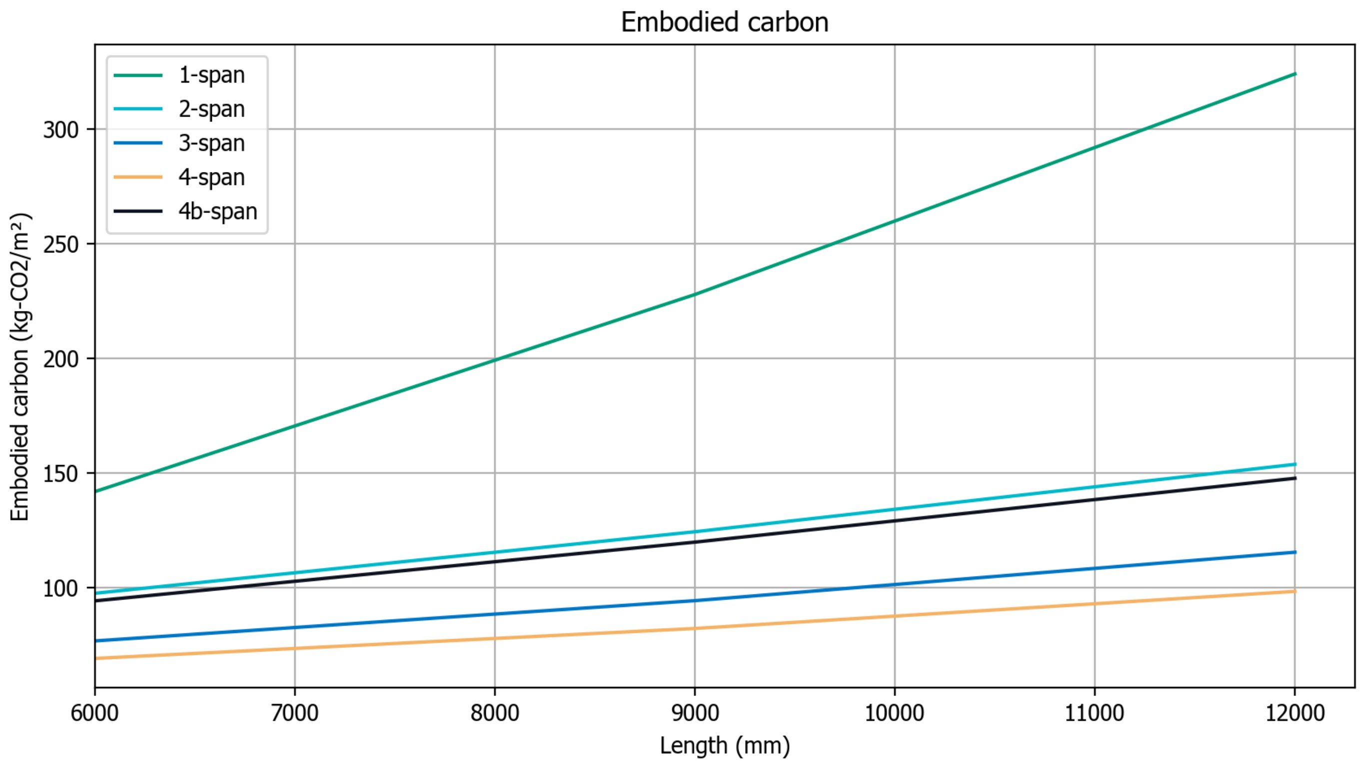

Depicted above are the values if the façade has an embodied carbon value of 100 kg CO_2/m². Depicted below are the values of the façade has an embodied carbon value of 800 kg CO_2/m².

800 kg CO_2 /m² is a substantial amount of CO_2 for a façade system, but an increase of 8 times the amount of CO_2 /m² increases the effect on the embodied carbon per m² of the whole structural system by about six times. Showing the effect of the façade on this floor area. However, as floor area increases, the effect of the façade will lessen.

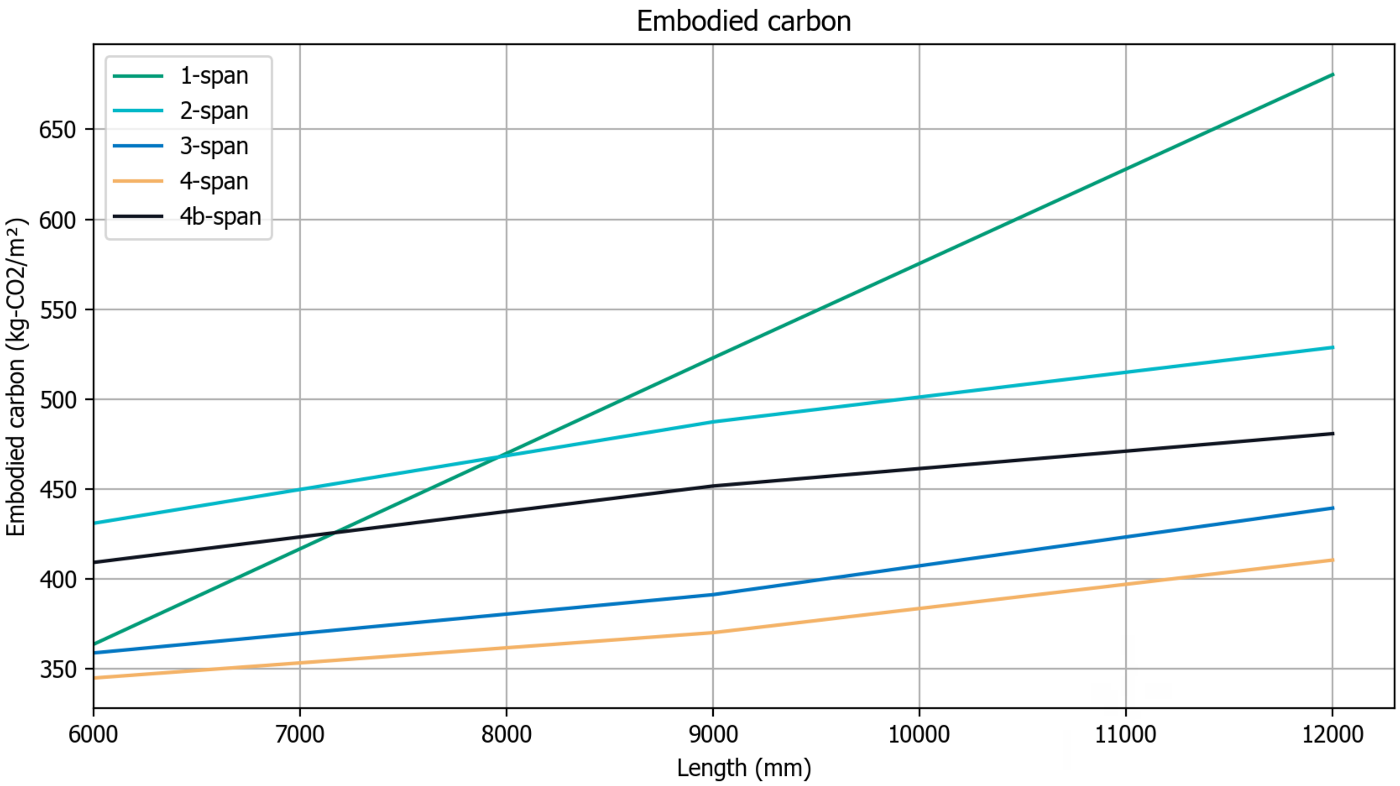

R.D.H. (Bob) Post
Studentnr: 5674298

Reflection

Beforehand, I had aimed to make groundbreaking inventions that could revolutionize modern timber construction. However, in hindsight, this ambition might have been overly optimistic given the limited time frame. Looking back, while I didn't achieve this goal, I believe the research and geometry principles developed during the project have laid the groundwork for new ideas and proposals to further optimize modern timber construction. However, these concepts require further research and validation before being implemented or proven effective.

1. What is the relation between your graduation project topic, your master track (A, U, BT, LA, MBE), and your master programme (MSc AUBS)?

By combining architectural design with innovative technical solutions to promote sustainable construction, my project aimed to develop an efficient timber construction system where various aspects such as structure, usability, and user experience were present. This aligns well with the Building Technology track, although the aspect of user experience was less emphasized in my project, which primarily focused on structural efficiency.

2. How did your research influence your design/recommendations and how did the design/recommendations influence your research?

The research has mainly focused solely on the behaviour of existing timber dry joints regarding rotational stiffness; none of the studies have really looked at the impact on a large scale and at the building level. Almost all connections do not consider the forces passing through the column. The comparisons made in some studies are biased by using everything in favour of the connection being studied and using unfavourable values for other situations. This initially gave me false hope that this could really make a big difference. What became clear to me during the research is why there was little information on two-way connections. One reason is that there are few frames where the forces are evenly distributed in two directions, and the other reason is that working out these connections is very complicated. What has influenced the design during the research is that I have looked further into what other tactics we can use to make wooden frames more efficient, since the theory and tactics for strengthening timber dry joints do not seem to work and are not efficient. This has collectively led me to propose a new construction concept where the floors are laid on multiple beams and the beams are efficiently connected to the column. There are still many challenges to this concept, and much research needs to be done to demonstrate that it can be used in real timber frames and is not just theoretically viable. So, due to the developments during the design of dry wood connections, a different direction has ultimately been taken.

3. How do you assess the value of your way of working (your approach, your used methods, used methodology)?

I believe I have been precise in my search for understanding the theories behind dry wood connections and overall structural mechanics. By reading various papers with different approaches and grasping the fundamentals, the theoretical basis for the research has been strong and comprehensive. However, I could have earlier noted the effect of these connections on the column cross-section and overall force distribution in structural frames. This could have led me to consider alternative design approaches sooner.

Furthermore, I have attempted to conduct a wide range of comparisons and remain objective by not making favourable or unfavourable assumptions. I believe this approach has been valuable and effective, although not as extensive as I would have liked due to time constraints. This is because I spent too long in the phase after P2, persistently trying to find and develop the ideal dry joint, resulting in a few weeks of no progress. I understand that this is part of the process, but in hindsight, I should have realized earlier that this wasn't the way to proceed and should have explored alternatives sooner.

During meetings, it was suggested earlier whether I should consider proving that this system doesn't work. I resisted this idea for too long because I was so eager to make that connection work. However, I eventually realized that proving something doesn't work can also be a valuable thesis topic and can lead to new insights.

4. How do you assess the academic and societal value, scope, and implication of your graduation project, including ethical aspects?

By not favouring or dismissing certain options and maintaining an objective standpoint, my thesis has contributed to insights in the academic field that not all developments or applications from the past, which were highly effective with the techniques available at the time, need to remain valuable in contemporary developments. On the other hand, it also highlights that established contemporary methods are not necessarily the only ones that can work, and that concepts from other industries can also improve modern construction.

The societal contribution primarily lies in the use of less material, thereby directly reducing CO_2 emissions. Additionally, by using less wood in a single building, multiple wooden buildings can be constructed since there isn't enough wood available to make everything from wood alone. This allows for multiple users to work or live in more sustainable buildings. Furthermore, with more wood available by lowering volumes used per building, it can lead to lower construction costs, resulting in more affordable homes.

5. How do you assess the value of the transferability of your project results?

I believe my project results offer insights into the effectiveness of different joints and structural systems. By closely following my design steps and reasoning, the project facilitates new ideas building upon my research to be explored.

6. Reflection summary

So, in summary, I believe my approach has worked well in understanding what to consider when developing dry joints. This has provided me with clear insights into the potential strengths and weaknesses of these types of connections. Thanks to the feedback to explore a different direction, I have introduced new ideas for further optimizing timber frames. This feedback was valuable in encouraging me to look beyond just finding that one idealized connection and to consider the bigger picture. It significantly improved my project. What I have personally learned from this is to zoom out more often from what you're working on to not lose sight of the larger goal and to learn to accept that even if you really want something, it may not be the right direction.